Tunnel Ionization in Strong Fields in atoms and molecules and its applications

by

Ryan Murray

A thesis
presented to the University of Waterloo
in fulfillment of the
thesis requirement for the degree of
Doctor of Philosophy
in
Physics

Waterloo, Ontario, Canada, 2011

I hereby declare that I am the sole author of this thesis. This is a true copy of the thesis, including any required final revisions, as accepted by my examiners.

I understand that my thesis may be made electronically available to the public.

Abstract

We look at the theory of ionization of atoms and molecules in the presence of a strong laser field. The history of ionization of atoms is reviewed and the methods used to calculate the ionization rates are examined in detail. In particular the quasi-classical methods used to solve for atomic rates are examined in detail. Early work on the ionization of molecules is also examined. A new method of calculating ionization rates is developed which allows for clear, analytic descriptions of atoms and molecules in intense light fields. The results and implications of this new theory are also examined in both atoms and molecules. The results are compared against known analytic results in the case of atoms and against numerical computation for molecules. Finally, applications of the study of atoms and molecules in intense fields are examined. We show how processes such as high harmonic generation and laser induced electron diffraction occur in strong fields and give an overview of the current state of the art and likely goals for the future. The process of laser induced electron diffraction is given close examination and ways of optimizing the diffraction patterns are discussed. The use of two-color orthogonal fields is shown to greatly increase contrast and efficiency when the carrier phases are tuned correctly.

Acknowledgements

I wanted to write a big, moving thank you to the people who are most responsible for making sure this thesis was complete, but unfortunately I am have a terrible way with words; so I will keep it simple. First and most important is my wife Cortney, who by all accounts is a saint for putting up with me. Her continual support has been the main reason I have these pages written. Countless motivational talks and constantly making sure I don't starve or run myself ragged are only the begining of what she has done for me. I can't thank her enough, though I will try. Next is my supervisor, Misha Ivanov. My mentor, and the person who is responsible for focusing my effort. His guidance is what has kept my random and inexperienced wanderings from going to far and he has always pulled me back to the path to interesting and physically relevant work. Everything I accomplish in the future will be a result of the lessons I have learned from him. Finally I would like to thank my friends and co-workers who have given me countless ideas, stimulating conversations and great times. In no particular order: Serguei Patchkovskii, Michael Spanner, Olga Smirnova, Denys Bondar, David Villeneuve, Josh Mutus, Helmut Satzger, Fraser Turner, Jean-Paul Brichta, Luke Chipperfield, David Hoffmann and many others who I have momentarily forgotten. My experiences with them are what has shaped me and my work. I am very grateful to have studied at three institutions during my Ph.D.: University of Waterloo, National Research Council of Canada, and Imperial College London. The experiences and people at these three institutes will never be forgotten.

Dedication

This is dedicated to my parents, who's continual support and encouragement is what has made this work possible.

Table of Contents

List of Figures

Chapter 1

Introduction

The invention of the laser over fifty years ago[1] has had a profound effect on the way we live our lives. It has sparked revolutions in the fields of medicine and technology. Though the invention of the laser is in itself a fantastic scientific step, the real revolution was caused by the study of laser light interacting with matter. Without understanding the interaction of light with matter the laser would be little more than a novelty.

Now that lasers are an every day item that can fit into small packages like laser pointers and DVD players the attention of fundamental research has turned increasingly to 'extreme' lasers. The word 'extreme' here refers to ultra-short and ultra-strong.

Over the past several decades the duration of lasers pulses has dropped from on the order of picoseconds (10^{-12}s) to femtoseconds and recently to the attosecond (10^{-18}s)[2] regime. Pulse length is now on the order of electronic motion in atoms, which gives unprecedented opportunities to observe electron dynamics in 'real-time'.

Along with the exponential decrease in pulse duration there has been a similar increase in pulse strength. Focused intensities now typically range from 10^{13} to greater than 10^{20} W/cm^2, depending on the source. The strength of these pulses are strong enough to exceed the fields binding electrons to atoms and to drive free electrons at relativistic speeds, Figure 1.1.

The extreme conditions created by the new generation of lasers open up a whole new regime of light-matter interaction, along with many fundamental applications. The time and spatial resolution which can be achieved using these new sources to image systems provides the possibility of creating the molecular movie[4], among the most sought after goals of light-matter interaction.

Before the molecular movie can be filmed though we must first understand the effect of such short and intense fields on matter. Two things are likely to happen to matter in an

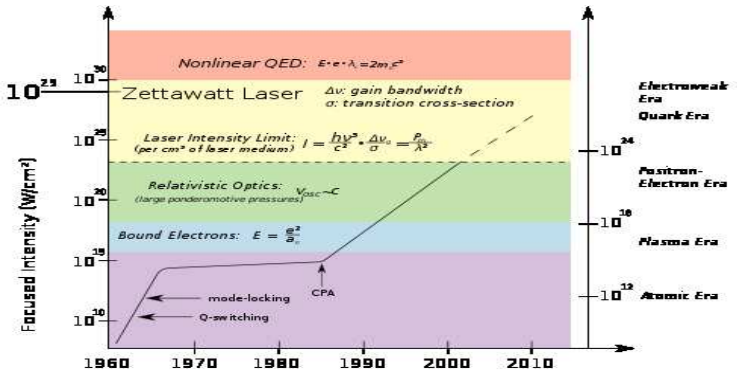

Figure 1.1: Progress of peak laser intensity as a function of time, with important regimes and innovations. Taken from: [3]

intense field: excitation and ionization. These two processes account for nearly all damage and photo-chemical processes in matter. The most interesting of these two processes, from the perspective of the strong field physics researcher, is ionization. The photo-ionization of matter has been known for over a century[5] and it is this process that is the focus of this work.

The contents of this work are mainly confined to the effects of lasers in the infrared(0.7 - 300 μm) consequentially we are concerned mainly with multi-photon ionization and more specifically the regime where multi-photon ionization can be viewed as tunneling in an oscillating laser field. This can occur when the light field suppresses the atomic or molecular potential in such a way as to allow an electron to escape through tunneling. There are several exciting processes that can occur through this mechanism which will be explored in greater detail later.

Prior to discussing applications of tunneling ionization to further dynamics, in particular to making a molecular movie, the tunneling process must first be understood. Tunneling rates have been calculated in atoms for at least fifty years and have been well understood for forty. Chapter 2 will be focused on reviewing these results and putting them into a modern context. There is also a modern derivation which sets the stage for work on larger systems in 3. The content in Chapter 3 is the original work of the author, while the work in Chapter 2 is an in depth review of the work of others in the field.

The ionization of complex systems such as molecules is complicated by the molecular structure, extended electronic orbitals and multiple electrons. We use the semi-classical ideas described in chapter 4 to derive many simple and intuitive results which give great insight into the tunneling process in molecules. The work in this chapter also provides a place to start for even more complex multi-electron theories which could be applied to

laser-induced tunnel ionization in larger molecules. The theory presented in this chapter is the sole work of the author.

Once the process of tunneling in strong fields is understood we turn our attention to its uses. Chapter 5 deals with the processes that occur in strong fields after ionization. High harmonic generation, laser induced electron diffraction, and non-sequential double ionization each show separate and important aspects of the interaction between light and matter. These processes are some of the tools which will be used in making the molecular movie. High harmonic generation allows for superb, though controversial, imaging of molecular orbitals and electron dynamics in ions. Laser induced electron diffraction is at the outset an extremely daunting task, but promise of sub-angstrom and sub-femtosecond resolution of single molecules is too strong to dismiss the idea entirely. The content of this chapter is split between the authors work and a review of the work of others. The author is responsible for the content on laser induced electron diffraction.

Finally, we conclude with a summary of our work and some ideas for future work in the field.

Chapter 2

Strong Field Ionization of Atoms

2.1 Introduction: basic tunneling theory

The process of tunneling is among the most fundamental quantum processes; the concepts of wave-particle duality and other intrinsically quantum ideas must be invoked to understand and picture tunneling. The fundamental nature of tunneling means it is of central importance in a variety of fields including solid state physics (scanning tunneling microscope, various semiconductor devices), cosmology, nuclear physics, biophysics, and atomic and molecular optical physics. There has been a large body of work dedicated to understanding tunneling; though in complex systems it is a very non-trivial subject. See for example [6, 7] for a good review of the state of the art.

We will focus strictly on tunneling processes in strong laser fields. The problem is simplified by the addition of a strong field though it is still quite difficult. The goal of this chapter is to survey the body of work on the problem of atomic ionization in the presence of a laser field with particular interest on tunnel ionization. Prior to tackling atomic ionization a theoretical groundwork must be laid. I will start by deriving quantum tunneling in the most simple case of a plane wave tunneling through a square potential barrier. Then I will introduce the Wentzel-Kramers-Brillouin(WKB) approximation, a vitally important and sadly under studied analytic method of solving partial differential equations and a key to solving tunneling problems in a general and often semi-analytic way.

Upon completion of the theoretical framework needed to understand tunneling in strong fields I will give a historical review of theoretical efforts in tunneling. This starts with a simple derivation by Landau. The work of Perelomov, Popov and Terent'ev(PPT) is the next important piece of work, followed by some modern advancements and a new derivation of strong field atomic ionization which paves the way for the molecular ionization studies in the next chapter.

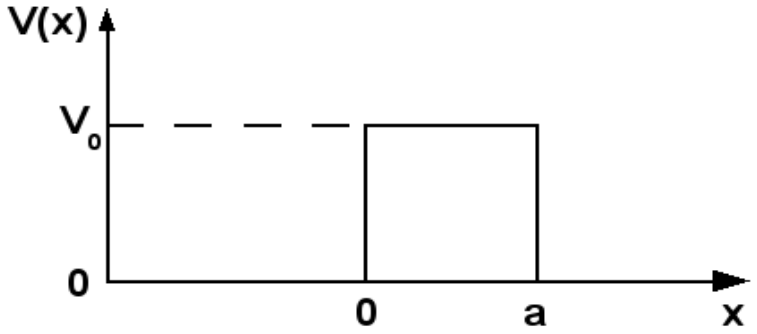

Figure 2.1: A Square potential barrier with height V_0. Taken from: [12]

2.2 Tunneling and the WKB Approximation

2.2.1 Tunneling through a square potential barrier

The most basic form of tunneling is that which occurs when a plane wave is incident on a square potential barrier. This simple problem is seen in nearly every text on quantum mechanics[8, 9, 10, 11]. The system under consideration is shown in Figure 2.1, here the square barrier is from the origin to $x = a$ and at a height of V_0.

The Hamiltonian for a particle incident on the square well potential is as follows:

$$\begin{aligned} H &= -\frac{\hbar^2}{2m}\frac{d^2}{dx^2} + V(x) \\ V(x) &= V_0[\Theta(x) - \Theta(x-a)] \end{aligned} \tag{2.1}$$

where $\Theta(x)$ is the Heaviside step function. I wish to solve the time independent Schrödinger equation for the Hamiltonian in equation 2.1. The barrier divides the solution space into three parts: left of the barrier, right of the barrier and the barrier. In each of these regions the particle is free or under a constant force and therefore quasi-free. The solution in each of these regions can then be written as a superposition of incoming and outgoing plane waves.

$$\begin{aligned} \Psi_L &= A_1 e^{ikx} + A_2 e^{-ikx} \\ \Psi_B &= A_3 e^{\kappa x} + A_4 e^{-\kappa x} \\ \Psi_R &= A_5 e^{ikx} + A_6 e^{-ikx} \end{aligned} \tag{2.2}$$

The wave numbers are $k = \sqrt{2mE/\hbar^2}$ and $\kappa = \sqrt{2m(E - V_0)/\hbar^2}$.

What is interesting here is that even for $E < V_0$ the wave function can exist inside the barrier. In this case κ would be an imaginary number and the wave function would exponentially decrease. This is contrasted to the classical case when the particle would fly over the barrier for $E > V_0$ and be fully reflected for $E < V_0$.

The quantum case will not be fully transmitting or reflecting. To see how the quantum case behaves I derive a transmission amplitude (the amplitude of the forward moving particle on the right side of the barrier,A_5) and a reflection amplitude (the amplitude of the backward propagating particle on the left side of the barrier, A_2).

To derive these amplitudes I need to specify boundary conditions. First the wave functions must match at $x = 0$ and $x = a$ and its derivative must also be continuous at those points.

$$\Psi_L(0) = \Psi_B(0), \frac{d\Psi_L(0)}{dx} = \frac{d\Psi_B(0)}{dx} \tag{2.3}$$

$$\Psi_B(a) = \Psi_R(a), \frac{d\Psi_B(a)}{dx} = \frac{d\Psi_R(a)}{dx} \tag{2.4}$$

Inserting equations 2.2 into the above conditions I arrive at relations between the six normalization constants. I also assume that the particle is incident from the left (A_1=1), and there is no particle incident from the right (A_6=0). I call A_2 the amplitude of reflection, and A_5 is the amplitude of transmission. To solve for the amplitudes I have a system of four equations and four unknowns, I eliminate A_3 and A_4 to obtain equations for the transmission and reflection amplitudes.

$$A_2 = \frac{4k\kappa e^{-ia(k-\kappa)}}{(k+\kappa)^2 - e^{2ia\kappa}(k-\kappa)^2} \tag{2.5}$$

$$A_5 = \frac{(k^2-\kappa^2)\sin(a\kappa)}{2ik\kappa\cos(a\kappa) + (k^2+\kappa^2)\sin(a\kappa)} \tag{2.6}$$

The above equations can now be used to calculate the transmission and reflection for various values of V_0. For $E > V_0$ the transmission amplitude is not 1, but an oscillating function of κa and there is a finite chance of reflection.

$$T = |A_5|^2 = \frac{1}{1 + \frac{V_0^2 \sin^2(\kappa a)}{4E(E-V_0)}} \tag{2.7}$$

$$R = 1 - T \tag{2.8}$$

This result is quite surprising when compared to the classical case. A classical particle would be 100% transmitted with the same energy.

For a particle of energy $E < V_0$ there is an exponentially decreasing chance that the particle will tunnel through the barrier and emerge on the other side. This is the phenomenon of quantum tunneling. There is a finite chance that the transmission will be

non-zero. For the limiting case of a very high or wide barrier the transmission approaches zero.

$$T = |A_5|^2 = \frac{1}{1 + \frac{V_0^2 \sinh^2(\kappa a)}{1+4E(V_0-E)}} \tag{2.9}$$

The simple fact that quantum particles can be found in classically forbidden regions leads to much of the physics discussed below. The square barrier is a special case in that I can actually calculate tunneling amplitudes analytically and exactly. For nearly all other systems one must use clever approximate techniques to obtain tunneling amplitudes and rates. I will discuss several of those techniques below. It is interesting that most of the methods we present to calculate tunneling are rooted in classical pictures and explicitly use classical mechanics to calculate tunneling rates which is an intrinsically quantum effect.

2.2.2 The WKB approximation

The Wentzel-Kramers-Brillouin (WKB) approximation, also known as the semi-classical or quasi-classical approximation, is the most common method for approximating tunneling rates in complex systems. A large portion of work has been devoted to expanding and extending the WKB approximation to cover more and more complex systems[13, 14]. The WKB theory was originally a 1-dimensional theory. A large body of the work cited above has been devoted to either extending the WKB to n-dimensional systems or applying a 'trick' to make the problem one dimensional. Currently no complete theory exists for more than one dimension though there are several theoretical efforts.

The WKB approximation can be traced back to Liouville[15] and Green[16] and is sometimes known as the LG method. The modern version was created in 1926 jointly, and independently, by Wentzel[17], Kramers[18], and Brillouin[19] as a method of solving the Schrödinger equation. The method they use is to assume an exponential as the solution to the time independent Schrödinger equation(TISE).

$$\Psi(x) = e^{-iS(x)/\hbar} \tag{2.10}$$

The argument of the exponent is expanded in a series in powers of $\hbar$. The reduced Plank constant is considered a small parameter in the quasi-classic case. Let us first begin with the TISE for the one-dimensional motion of a single particle.

$$-\frac{\hbar}{2m}\frac{d^2}{dx^2}\Psi(x) = (E - V(x))\Psi(x) \tag{2.11}$$

We make the substitution $\Psi(x) = e^{-iS(x)/\hbar}$ and obtain the following equation for S.

$$\frac{1}{2m}\left(\frac{dS}{dx}\right)^2 - \frac{i\hbar}{2m}\frac{d^2S}{dx^2} = E - V(x) \tag{2.12}$$

The function S is expanded in a series in powers of $\hbar$.

$$S(x) = S_0 + \frac{\hbar}{i} S_1 + \left(\frac{\hbar}{i}\right)^2 S_2 + ... \tag{2.13}$$

In the first approximation I drop all terms containing $\hbar$ and insert equation 2.13 into 2.12:

$$\frac{1}{2m}\left(\frac{dS_0}{dx}\right)^2 = E - V(x) \tag{2.14}$$

Equation 2.14 is known as the Hamilton-Jacobi equation and can be solved for S_0. The result is the time independent part of the classical action.

$$S_0 = \pm \int \sqrt{2m(E - V(x))} dx = \pm \int p(x) dx \tag{2.15}$$

The integrand is simply the classical momentum $p(x)$. Lets take a look at the conditions under which the approximation in equation 2.14 remains valid. This is the case when the second term in equation 2.13 is much smaller than the first.

$$\hbar \left| \frac{S''}{S'^2} \right| = \left| \frac{d(\hbar/S')}{dx} \right| \ll 1 \tag{2.16}$$

Where primes indicate differentiation with respect to x. From equation 2.15 I know that $S' = p(x)$, so I can rewrite the above as:

$$\left| \frac{d\hbar/p(x)}{dx} \right| = \left| \frac{d(\lambda/2\pi)}{dx} \right| \ll 1 \tag{2.17}$$

Here λ is the de Broglie wave length of the particle. For the first order term to be valid the wavelength of the particle must vary slowly over distances of order of itself. This is the condition for quasi-classical motion. The above condition can be rewritten as follows

$$\frac{m\hbar|F|}{p^3} \ll 1 \tag{2.18}$$

Where F is the force on the particle. This shows that the 1st order WKB is not valid near turning points, points where the momentum of the particle is zero as it reverses direction.

We now can derive the term to first order in $\hbar$ from Eqns 2.13 and 2.12 in the same was as I found the zeroth order term. The first order term is as follows,

$$S_0' S_1' + \frac{1}{2} S_0'' = 0 \tag{2.19}$$

The solution to which is,

$$S_1 = -\frac{1}{2}\log p(x) \tag{2.20}$$

We now substitute this term and the zero-order term into the original guess for the wave function to arrive at the following result.

$$\Psi = \frac{C_1}{\sqrt{p(x)}} e^{i\int^x p(x')dx'/\hbar} + \frac{C_2}{\sqrt{p(x)}} e^{-i\int^x p(x')dx'/\hbar} \tag{2.21}$$

The above equation is for a particle in a classically allowed region. In classically forbidden regions the momentum is imaginary so that the exponentials in equation 2.21 become real and exponentially decreasing or increasing. This is the same result as the exponential dependence of tunneling in the square barrier case.

$$\Psi = \frac{C_1}{\sqrt{p(x)}} e^{\int p(x)dx/\hbar} + \frac{C_2}{\sqrt{p(x)}} e^{-\int p(x)dx/\hbar} \tag{2.22}$$

These two equations describe a quasi-classical particle in a potential in two different regions, they need to be connected at the boundaries: the turning points. First I consider the WKB wave function on both sides of the turning point. For the classically allowed region,

$$\Psi = \frac{A}{\sqrt{p(x)}} e^{i\int_a^x p(x)dx/\hbar} + \frac{B}{\sqrt{p(x)}} e^{-i\int_a^x p(x)dx/\hbar}, x < a \tag{2.23}$$

and for the classically forbidden region,

$$\Psi = \frac{C}{\sqrt{|p(x)|}} e^{-\int_x^a p(x)dx/\hbar}, x > a \tag{2.24}$$

We have made the assumption that the turning point is at $x = a$ and to the left of the turning point is classically allowed, see figure 2.2. The wave function on the left side only has the damped solution as the exponentially increasing solution is unphysical. Equations 2.24 and 2.23 are valid only sufficiently far away from $x = a$. At values of x close to a I can find an exact solution to the Schrödinger equation provided I am close enough to assume that the potential is constant across the turning point. In that case the solution to the Schrödinger equation is known and is given by[9] an Airy function,

$$\Psi(x) = CAi(-(2F)^{1/3}(x + E/F)) \tag{2.25}$$

The Airy function has a well known asymptotic form for large argument.

$$Ai(x) = \frac{1}{2|x|^{1/4}} \exp(-\frac{2}{3}|x|^{3/2}), |x| << 1 \tag{2.26}$$

$$Ai(x) = \frac{1}{x^{1/4}} \sin(\frac{2}{3}x^{3/2} + \pi/4), |x| >> 1 \tag{2.27}$$

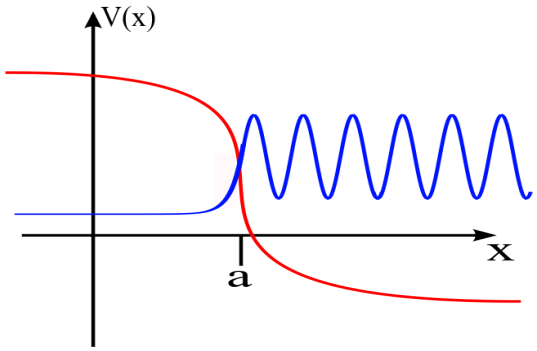

Figure 2.2: The WKB wave function incident on a barrier at $x = a$ to the left is the exponentially damped solution and to the right is the oscillating solution. They are matched at $x = a$ with the exact solution to Schrödingers equation.

By comparing equations (2.26) and (2.27) to equations (2.24) and (2.23) I can deduce that the momentum is given by:

$$p(x) = \sqrt{2mF(x-a)} \tag{2.28}$$

$$F = -\frac{dV(x)}{dx} \tag{2.29}$$

Finally, the momentum for $x < a$ is imaginary so the constant in the WKB wave function under the barrier gets a phase added to it from the $i^{1/2} = e^{i\pi/4}$ term.

$$C = Be^{i\pi/4} = Ae^{-i\pi/4} \tag{2.30}$$

The full WKB wave function is thus:

$$\frac{C}{2\sqrt{|p(x)|}} e^{-\frac{1}{\hbar}|\int_a^x p(x)dx|} \rightarrow \frac{C}{\sqrt{p(x)}} \cos\left(\frac{1}{\hbar}|\int_a^x p(x)dx| - \frac{\pi}{4}\right) \tag{2.31}$$

This can be summed up as: when the particle passes through the barrier it acquires a phase of $\pi/4$. The WKB wave function is thus known everywhere that the quasi-classical approximation is valid.

2.3 Review of tunneling theories

The case of oscillating laser field is far less trivial than of a DC field, and although the tunnel ionization of an atom has been under study for more than fifty years, it has proven to be a stubborn problem. Figure 2.3 illustrates the idea behind tunnel ionization. When an electric field is applied to an atom the atomic potential is skewed. If the field is strong enough it can suppress the potential so much that it creates a barrier under which the electron can tunnel.

The following sections will detail some of the major work on tunnel ionization in the past fifty years. I will start with a derivation for the ionization rate of ground-state atomic Hydrogen, put forth by Landau[9]. This derivation makes use of the quasi-classical approximation and parabolic coordinates. The next key advancement was by Perelomov et al.[20, 21, 22] who extended the work of Landau to general atomic states and oscillating electric fields. Finally we review some recent advances in the detailed understanding of ionization in atoms[23, 24].

2.3.1 Three dimensional static tunneling in atoms

The derivation used by Landau[9] is a straight-forward application of the quasi-classical WKB approximation to the tunneling problem in a Hydrogen atom. The basic premise is

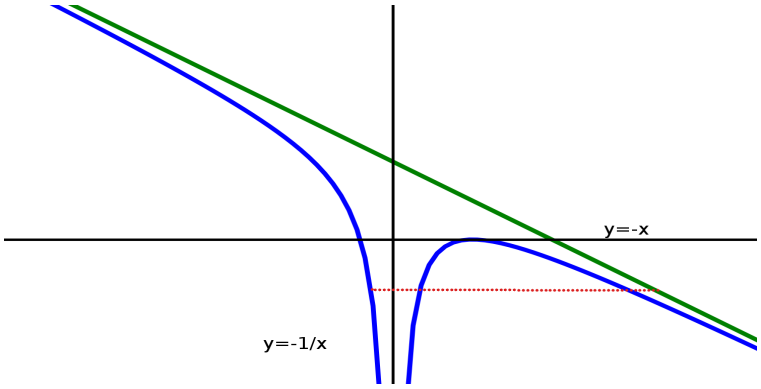

Figure 2.3: Schematic of tunnel ionization. The atomic potential, in blue, is deformed by the electric field, in green. The dotted red line represents the tunnel formed at a particular energy.

to match the atomic wave function to an outgoing WKB solution and then calculate the rate as the flux at the exit of the barrier. This is all done in parabolic coordinates. Before I proceed with the derivation we will briefly introduce cylindrical parabolic coordinates.

The parabolic coordinates η,ξ,ϕ are defined by the following formulae

$$x = \sqrt{\eta\xi}\cos\phi, y = \sqrt{\eta\xi}\sin\phi, z = \frac{1}{2}(\xi - \eta)$$
$$r = \frac{1}{2}(\eta + \xi) \tag{2.32}$$

or conversely

$$\xi = r + z, \eta = r - z, \phi = \tan^{-1}(y/x) \tag{2.33}$$

Here η and ξ vary from 0 to ∞ and ϕ from 0 to 2π. The surface of constant ξ,η is a paraboloid along the z axis. This set of coordinates is very convenient for describing a central potential in which there is a dominant direction: ionization along the z-axis. For more detail on the properties of the cylindrical parabolic coordinates see[9, 25]. The final important thing to mention is what the Hydrogen atomic wave function and potential look like in parabolic coordinates. This is key to what follows. The wave function for the 1-s state of Hydrogen is:

$$\Psi = \frac{1}{\sqrt{\pi}}e^{-(\xi+\eta)/2} \tag{2.34}$$

and the potential,

$$V(\eta, \xi, \phi) = -\frac{2}{\eta + \xi} \tag{2.35}$$

When considering an electron being ionized along the negative z-axis then, for large z, $\eta = -2z$ and $\xi = 0$. The ionization along the z-axis is then equivalent to movement only along the η axis in parabolic coordinates.

We wish to calculate the rate of ionization of a Hydrogen atom in a static electric field. The WKB approximation in equation2.31 can be employed to accomplish this. This is done by matching the wave function in equation 2.34 with the WKB solution for the electron under the barrier. The ionization corresponds to the electron moving in one dimension along the η direction so I match at a point η_0 which is much less than the exit point $\eta_0 \ll \eta_1 = 1/F$ where F is the field strength. The WKB solution is then propagated to the exit point, where the rate is calculated. The WKB wave function at the exit point is,

$$\Psi = \sqrt{\frac{p_0}{\pi p}} e^{-\frac{\xi+\eta_0}{2} + \int_{\eta_0}^{\eta_1} p d\eta + i\frac{\pi}{4}} \tag{2.36}$$

Here $p = \sqrt{F\eta/4 + 1/4\eta^2 + 1/2\eta - 1/4}$ is the classical momentum and p_0 is the momentum at η_0. The first term in the exponent is from the initial wave function, the second and third are from the WKB approximation. We are interested in the amplitude square of the wave function, so the phase is unimportant.

$$|\Psi|^2 = \frac{|p_0|}{p\pi} e^{-\xi} e^{-2\int_{\eta_0}^{\eta_1} p d\eta - \eta_0} \tag{2.37}$$

Since the electron is far away along the η direction I can assume that $\eta \gg 1$ and make the following expansion

$$p = \frac{1}{2}\sqrt{F\eta - 1} - \frac{1}{2\eta\sqrt{1 - F\eta}} + ... \tag{2.38}$$

The first term in the above equation is enough for the p in the prefactor but the second term should be kept in the exponential. The wave function then becomes:

$$|\Psi|^2 = \frac{1}{\pi\sqrt{F\eta - 1}} e^{-\xi} e^{-\int_{\eta_0}^{\eta_1} \sqrt{F\eta - 1} d\eta + \int_{\eta_0}^{\eta_1} \frac{1}{\eta\sqrt{F\eta - 1}} d\eta - \eta_0} \tag{2.39}$$

The second term in the exponent is commonly known as the eikonal The integrals above are straightforward and the result is,

$$|\Psi|^2 = \frac{4}{\pi\eta_0 F} e^{-\xi - 2/3F} \frac{1}{\sqrt{F\eta - 1}} \tag{2.40}$$

With this I can now calculate the rate. The rate is defined as the probability current through a plane perpendicular to the z-axis at the exit point.

$$\Gamma = 2\pi \int_0^\infty |\Psi|^2 v_z \rho d\rho \tag{2.41}$$

Where ρ is the normal cylindrical polar coordinate. For large η the integral is simple and the rate is finally

$$\Gamma = \frac{4}{F} e^{-2/3F} \tag{2.42}$$

This simple result gives the ionization rate of a Hydrogen atom in its ground state as a function of field strength. This result holds for field strengths $F \ll 1$. The rate derived above is the basis for all other rate equations. The exponential factor is common to nearly all tunnel ionization rates. The equation shows that for low field strength ionization is low and it exponentially increases as the field strength grows until the 'over the barrier' region is reached and the electron is no longer bound by the barrier. This method can be extended to handle time dependent fields and any atomic state by the methods of PPT. There is an alternative derivation of the general time dependent case put forth by Keldysh. This derivation, while very important for the field will not be covered here. I wish to focus on the WKB based approaches and their consequences. For a detailed review of Keldysh, see his original paper[26] and a review[27].

2.3.2 Three dimensional time-dependent tunneling in atoms

The extension of the work above to time dependent fields was first done by Perelomov, Popov and Ter'entev in a series of three papers[20, 21, 22]. They applied the WKB theory to the time dependent case and invented what is now called the imaginary time method used for solving the Hamilton-Jacobi equation in the time dependent case[28, 29, 30, 31, 32, 33].

The derivation is similar to what is presented above, the major differences are that the action is defined by the time dependent Hamilton-Jacobi equation and the calculation is done in regular Cartesian coordinates. The eikonal approximation[9] is used to include the Coulomb core perturbatively and the zero-range potential problem is solved exactly. I start by defining the bound wavefunction in the asymptotic region.

$$\Psi(x, y, z) = C_{\kappa l} \kappa^{3/2} e^{-\kappa z} \tag{2.43}$$

Here $\kappa = \sqrt{2I_p}$ is the characteristic momentum of the bound state and I_p is the ionization potential of the bound state. This will be matched with the standard WKB wavefunction at some point z_0. The matched WKB wavefunction is then propagated to the exit point z_e where it is:

$$\Psi(z_e) = C_{\kappa l} \kappa^{3/2} \frac{|p_z(z_0)|}{|p_z(z_e)|} e^{-\kappa z + iS(z_0, t_0; z_e, 0) + \int_{t_0}^{t} V(t')dt'} \tag{2.44}$$

For the case of $z_0 << z_e$ I can approximate $p_z(z_0) \approx \kappa$. The first term in the exponential is due to the Coulomb asymptote, the second is the action from the point z_0 to z_e and the

third term is the Coulomb correction due to the eikonal approximation, see [21, 34, 35]. The function $V(z')$ is the atomic potential. The action in equation 2.44 is defined by the Hamilton-Jacobi equation as follows:

$$-\frac{dS}{dt} = \frac{1}{2}\left(\frac{dS}{dz}\right)^2 + F(t)z \tag{2.45}$$

The field $F(t) = F\cos\omega t$ is a linear, monochromatic laser field. The Hamilton-Jacobi equation is non-trivial to solve in this form but as it is identical to Newton's equation I can solve those and calculate the action directly. Newton's equation and the initial conditions are (dots represent time differentiation):

$$\ddot{z} = F\cos\omega t \tag{2.46}$$

$$z(t_0) = z_0, \dot{z}(t_0) = i(\kappa^2 + p_\perp^2)^{1/2} = i\kappa' \tag{2.47}$$

This ordinary differential equation is trivial to solve and its solution is given below.

$$z(t) = z_0 + p_z(t - t_0) - \frac{F}{\omega^2}(\cos\omega t - \cos\omega t_0) \tag{2.48}$$

$$\dot{z}(t) = p_z + \frac{F}{\omega}\sin\omega t \tag{2.49}$$

where $p_z = i\kappa' - \frac{F}{\omega}\sin\omega t_0$ is the canonical momentum of the electron, a conserved quantity. Knowing that the trajectory starts tunneling at t_0 and emerges at the peak of the field $t = 0$ I can use the canonical momentum to find the value t_0.

$$\sin\omega t_0 = \frac{\omega}{F}(i\kappa' - p_x) \tag{2.50}$$

which when simplified is:

$$\left(p_z + \frac{F}{\omega}\sin\omega t_0\right)^2 + p_\perp^2 = -\kappa^2 \tag{2.51}$$

We will only consider the most probable trajectory, which emerges from under the barrier at the peak of the field with $p_z = p_\perp = 0$, in this case the above equation simplifies to $\omega t_0 = i\sinh^{-1}\gamma$. Where $\gamma = \frac{\kappa\omega}{F}$ is the Keldysh parameter. Here I can see that the tunneling time t_0 is purely imaginary. It is useful to introduce the imaginary time $\tau = it$, this makes the motion under the barrier quite clear and the derivation more intuitive. The trajectory and velocity are now

$$z(\tau) = z_0 + \frac{F}{\omega^2}(\cosh\omega\tau_0 - \cosh\omega\tau), \dot{z}(\tau) = -\frac{F}{\omega}\sinh\omega\tau \tag{2.52}$$

The tunneling time τ_0 is then the following

$$\tau_0 = \tau_C \frac{\sinh^{-1}\gamma}{\gamma} \approx \tau_C \begin{cases} 1-\gamma^2/6, \gamma \ll 1 \\ \log\gamma/\gamma, \gamma \gg 1 \end{cases} \tag{2.53}$$

Here τ_C is the tunneling time in the adiabatic limit. The tunneling time is given for both limits of the Keldysh parameter. The adiabatic tunneling limit $\gamma \ll 1$ where the barrier is near stationary during the tunneling, and the multi-photon limit $\gamma > 1$ where the ionization is 'vertical' in energy. For a discussion on these limits and their applicability see eg [26, 23, 24].

Knowing the above form for the trajectory I can easily calculate the action as the time integral of the Lagrangian($L = T - V$)[36].

$$S(0,t_0) = \int_{t_0}^{0} dt' L(t') \tag{2.54}$$

$$S(0,t_0) = \int_{t_0}^{0} dt' \left[\frac{1}{2}\dot{z}^2 + Fx(t')\cos\omega t' - \frac{\kappa^2}{2}\right] \tag{2.55}$$

$$= -i\kappa z_0 + i\frac{I_p}{\omega}\left[(1+\frac{1}{2\gamma^2})\sinh^{-1}\gamma - \frac{\sqrt{1+\gamma^2}}{2\gamma}\right] \tag{2.56}$$

This expression for the action leads to the well known atomic ionization rates used by Keldysh, PPT et al. when in the adiabatic regime the Keldysh parameter approaches zero and in this limit the action returns to the standard expression for a static field $S = \frac{i\kappa^3}{3F}$.

Before I insert equation (2.56) into the equation for the wave function and calculate the rate I will derive the Coulomb correction using the eikonal approximation. The correction to the action from the Coulomb core is

$$\Delta S = \int_{t_0}^{t} dt' V(z(t')) \tag{2.57}$$

Indeed, it is seen that the characteristic perpendicular momentum is $p_\perp \sim \sqrt{F/\kappa} \ll \kappa$ (as long as $F \ll 1$). Hence, tunneling proceeds along the z-axis, with $x, y \ll z$ in the asymptotic region $z > z_0$. This allows one to set x, y to zero in the above equation. The integral in equation (2.57) is straightforward when the Coulomb potential is used $V(z) = Q/z$.

$$\Delta S = \frac{iQ\gamma}{\kappa}\ln\left(\frac{\tanh\omega t_0/2 + \tanh\omega t/2}{\tanh\omega t_0/2 - \tanh\omega t/2}\right) \tag{2.58}$$

We now perform an asymptotic expansion on Eqn. (2.58). Such an expansion is just as important for the Coulomb correction as for the zero-order contribution (i.e. corresponding

to the short-range potential). The Coulomb correction simplifies to

$$\Delta S = -i\frac{Q}{\kappa}\ln\frac{2\kappa^2}{Fz_0} \tag{2.59}$$

Now I can insert equations (2.56,2.59) into equation (2.44) and calculate the rate

$$\Psi(z_e) = C_{\kappa l}\kappa^{3/2}\frac{\kappa}{\sqrt{|p_z(z_e)|}}e^{-\kappa z_e+\kappa z_e-\frac{I_p}{\omega}\left[(1+\frac{1}{2\gamma^2})\sinh^{-1}\gamma-\frac{\sqrt{1+\gamma^2}}{2\gamma}\right]+\frac{Q}{\kappa}\ln\frac{2\kappa^2}{Fz_0}} \tag{2.60}$$

Which gives the following rate

$$\Gamma(F,\omega) \propto \int |\Psi|^2 p_z(z_e)dp_\perp \tag{2.61}$$

$$= \left(\frac{2\kappa^3}{F}\right)^{2Q/\kappa-m-1} e^{-\frac{2I_p}{\omega}f(\gamma)} \tag{2.62}$$

Where $f(\gamma) = (1+\frac{1}{2\gamma^2}\sinh^{-1}\gamma - \frac{\sqrt{1+\gamma^2}}{2\gamma})$. This is the key result of the PPT theory for oscillating fields and is what appears in the ADK theory[37].

In this chapter I considered solutions to several problems in the ionization of atomic targets. The solutions for any atom in a constant field and in an oscillating laser field were found. The method used to solve these problems is related to the WKB approximation and the method of trajectories. In particular the method of trajectories, or the imaginary time method, makes a clear connection between the DC case and the oscillating case, and the derivation for the latter is very similar to the former. Once the DC case is known it is simply a matter of finding a different trajectory to compute the case of an oscillating field.

The next chapter introduces a new approach to the problems discussed here. This approach gives results that are identical to the PPT results but are done in a much simpler way. The simple method considered below allows for generalization to arbitrary systems. Only the DC case is considered because generalizing to oscillating fields is done in the same manner as above, just by changing the trajectory.

Chapter 3

New partial Fourier transform based approach

The tunnel ionization of an electron from an atom or molecule is at the core of nearly every process in strong laser fields. It is the first step in the famous three-step model [38, 39, 40] of strong-field dynamics, and is a key ingredient in high-harmonic generation(HHG), laser induced electron diffraction(LIED) and non-sequential double ionization(NSDI). For a review of these processes and their applications see (e.g. [41]). The ionization of atoms has been under investigation for over forty years and is well understood theoretically [26, 20, 21, 22, 37, 23, 42, 43, 44, 45] and experimentally[46, 47, 48]. The famous work of Keldysh [26] ignited the field and Perelomov, Popov and Terent'ev (PPT) [20, 21, 22] found a general theory of tunneling from atoms in an oscillating electric field based on the quasi-classical approximation. While many other studies have been done, PPT remains the most widely used tunneling theory for atoms.

The PPT theory is an asymptotic theory that, in the case of a static electric field, matches the field-free bound wave function to the WKB (Wentzel-Kramers-Brillouin approximation) solution for a free electron in the static field. The ionic potential is included in this WKB solution via the perturbation theory in action, effectively in the eikonal approximation, inside the classically forbidden region. Importantly, the two wave functions are generally of different symmetry, and one of them (the bound wave function) does not include the external electric field. Consequently, the matching is not exact and must be done analytically, with care to ensure cancellation of errors (see e.g. [49] for a recent discussion). The matching is done in the classically forbidden region, sufficiently far from both the entrance and the exit points of the tunneling trajectory. In the atomic case, the use of analytic wave functions allows one to remove the dependence on the matching point, giving accurate ionization rates.

Though the atomic case is well studied, only in the past decade have there been detailed

experimental studies of tunneling in molecules. Most early studies focused on un-aligned samples and comparing molecular rates to 'companion' atoms [50, 51, 52, 53] and are based on the idea that molecular ionization rates may be comparable to those of atoms with similar ionization potentials. Unsurprisingly, both theoretical and experimental studies have shown there is little correlation between atoms and molecules with similar ionization potentials [50, 54, 55, 56]. Recent experiments on aligned samples have produced angular dependent rates allowing for detailed study of the effect of molecular orbitals [57, 58, 59, 60]. These studies give great insight into the dynamics of molecules in strong laser fields. The theory needed to describe these studies must be done very carefully and currently there is no theory as powerful as the atomic theories. The most common approaches in use today are Molecular ADK(MO-ADK) [55] and molecular strong field approximation(MO-SFA). The first approach relies on a single-center expansion of the ionizing molecular orbital in a series of spherical harmonics, also assuming purely single-center Coulombic interaction of the outgoing electron with the molecular core. This method has several limitations: for large multi-center systems and delocalized orbitals with complex nodal structure the expansion contains many terms and results lose physical transparency. The use of a purely Coulomb potential is another important limitation. I also note a technical drawback of the original derivation [55], related to rotations of the molecule relative to the direction of the electric field. Such rotation mixes different m-components of the same angular momentum state l, and the contributions of different m have to be added at the level of amplitudes and not probabilities. For an atomic system there is a single m and this is not an issue but in a molecule there are many m states contributing a single orbital and the m dependent phase factors must be added coherently. The second common analytical model is the molecular strong field approximation (MOSFA)(see e.g. [56]), which is based on the Keldysh-Faisal-Reiss theory[43, 44, 45]. This method also has important limitations. The first is the absence of the Coulomb potential – this drawback is corrected a-posteriori, again assuming single-center Coulomb interaction with the core. The second problem is gauge non-invariance.

A recent proposal by Fabrikant[49] aims to fix most of the problems common among the current analytical theories by using a PPT-like method on molecular systems. The authors use the imaginary time method[29] to derive analytical ionization rates for atoms and small molecules in a strong field. The only issue with this method is a consequence of using complex initial conditions on the particles classical trajectory, making the method difficult for practical computation if the wave function is not known analytically, but is given on the real-space grid.

Purely numerical approaches are very demanding computationally and are often hard to interpret physically. Recently, breakthrough fully correlated calculations have been done[61, 62] for H_2. Extensions to larger systems rely on time-dependent density functional theory (TD-DFT) or single active electron(SAE) type approximations[63]. These numerical

studies provide important foundations for testing approximate analytical theories.

In this chapter I propose a simple and physically transparent analytical method applicable for atoms and molecules. Our approach resolves many of the problems outlined above while maintaining an intuitive physical interpretation. The key aim (and advantage) of our approach is that it can be generalized for arbitrary wave functions and arbitrary potentials given on a numerical grid. Consequently, it avoids the use of imaginary time and, more importantly, complex-valued trajectories. This property makes it directly adaptable to fast numerical calculations for arbitrary wave functions and arbitrary potentials.

By drawing on the work of Maslov's multi-dimensional WKB theory[14] I have found an algorithm based on partial Fourier transforms that allows for separation of variables, as long as the (arbitrary) core potential is included in the eikonal approximation. The method allows one to maintain the physical transparency of our results for arbitrary wave function and arbitrary core potential. In this chapter, I show that our approach allows one to reproduce all analytical results of the PPT theory for the atomic case while avoiding any need for a single-center expansion in the spherical harmonics. This makes our approach naturally applicable to a general multi-center wave function and an arbitrary multi-center potential. I also discuss straightforward generalization of the method, which avoids uncertainty associated with the matching procedure, and what alternative calculations and approximations it requires in this case. The method is broadly applicable to general wave functions and arbitrary molecular potentials. The route to its generalization for oscillating electric fields is discussed in the following chapter.

3.1 Description of the method

We will now develop an algorithm that is suitable for calculating both analytic and computational ionization rates. I shall begin the discussion with the zero-range potential, which always serves as a starting point for the eikonal-like treatment of an arbitrary core potential.

We wish to solve the time-independent Schrödinger equation(TISE) for an electron in a static electric field. The length-gauge Hamiltonian for such a system is as follows (atomic system of units are used throughout):

$$\begin{aligned} \hat{H}_{LG} &= \frac{\hat{\mathbf{p}}^2}{2} - Fz, \\ \Psi(z_0) &= \Psi_0(z_0) \end{aligned} \tag{3.1}$$

Here $\mathbf{p}$ is the kinetic momentum, which in atomic units is equal to the electron velocity, F is the field strength and z is the direction of the field. The boundary condition states that

at some point z_0 the WKB wave function must match with the wave function of the bound system. I now introduce the mixed representation wave-function (a tool used by Maslov[14] to express the WKB wave function near a caustic). I shall show that using this representation allows one to reproduce all known results while retaining physical transparency. I write the bound wave function as

$$\Psi(x,y,z) = \frac{1}{2\pi}\int dp_x \int dp_y e^{ixp_x+iyp_y}\Phi(p_x,p_y,z) \tag{3.2}$$

where,

$$\Phi(p_x,p_y,z) = \frac{1}{2\pi}\int dx \int dy e^{-ixp_x-iyp_y}\Psi(x,y,z) \tag{3.3}$$

The physical motivation for this representation is that I can now derive the WKB solution that reflects the symmetry of the tunneling process along the direction z of the external field and matches the component $\Phi(p_x,p_y,z)$ of the total wave function $\Psi(x,y,z)$. Mixed representation makes such matching straightforward irrespective of the symmetry or complexity of $\Psi(x,y,z)$. For a short-range potential with the boundary condition $\Phi(p_x,p_y,z)$, tunneling becomes a straightforward 1D problem. Another key feature of Eqn. 3.2 is that the Fourier transform relates closely to the important physical picture associated with the strong field approximation (SFA).

Equation (3.2) is now inserted into the Schrödinger equation $-I_p\Psi(x,y,z) = \hat{H}_{LG}\Psi(x,y,z)$, where I_p is the ionization potential – the binding energy of the bound state. Note that in the presence of the electric field the spectrum is, strictly speaking, continuous and all energies are allowed. For a short-range potential, the 3D equation is reduced to a single dimension:

$$-\frac{\partial^2\Phi(p_x,p_y,z)}{\partial z^2} = 2(E'+Fz)\Phi(p_x,p_y,z) \tag{3.4}$$

Here $E' = I_p + p_x^2/2 + p_y^2/2$. That is, the perpendicular momentum increases the effective ionization potential, making it harder to tunnel. Tunneling in the perpendicular direction is exponentially suppressed; this is important for future approximations as tunneling can be considered to occur predominately along the electric field, i.e. in the z direction. The field-free motion in the x-y plane is separated from the motion in the z plane and the regular 1D WKB approximation can be applied to eqn (3.4):

$$\Phi(p_x,p_y,z) = \frac{C}{\sqrt{p_z(z)}}e^{iS(p_x,p_y,z)/\hbar} \tag{3.5}$$

Here $p_z(z) = |\partial S(p_x,p_y,z)/\partial z|$ is the kinetic momentum (equal to the electron velocity in atomic units) in the z direction and $S(p_x,p_y,z)$ is the classical action. In the classically

forbidden region both the action and the electron velocity are imaginary, which is why the absolute value is used for $p_z(z)$. This WKB solution is now matched to the initial wave function at z_0, determining the constant C and giving the following expression for the mixed representation wave-function:

$$\Phi(p_x, p_y, z) = \Phi(p_x, p_y, z_0)\sqrt{\frac{p_z(z_0)}{p_z(z)}}\exp\left(\frac{i}{\hbar}(S(p_x, p_y, z) - S(p_x, p_y, z_0))\right) \tag{3.6}$$

It is important to note that as long as z_0 is not a turning point the wave function and its derivatives are continuous. Inserting this expression into equation (3.4) I get the familiar Hamilton-Jacobi equation, for $S(p_x, p_y, z)$

$$\frac{1}{2}\left(\frac{\partial S(p_x, p_y, z)}{\partial z}\right)^2 - Fz = E' \tag{3.7}$$

The Hamilton-Jacobi equation is immediately integrable, with the solution

$$S(p_x, p_y, z) - S(p_x, p_y, z_0) = \frac{1}{3F}(2E' + 2Fz)^{3/2} - \frac{1}{3F}(2E' + 2Fz_0)^{3/2} \tag{3.8}$$

The next standard step is the expansion of the expression on the right-hand side in powers of z_0 up to the first order. This expansion is not a mere convenience – it is the critical step of the asymptotic theory since the original works of Perelomov, Popov and Terent'ev. The key importance of this step and its physical meaning are illustrated in Fig. 3.1.

The WKB solution above includes electric field fully, while the bound wave function at $z < z_0$ is field-free. Correspondingly, the behavior of the field-free bound wave-function in the classically forbidden region is different, and its exponential decay towards z_0 is faster than should have been for the proper *in-field* solution. The expansion of the *in-field* WKB solution at $z > z_0$ in powers of z_0 up to the first order cures this difficulty, as shown in Fig 3.1. This plot shows (i) the electric field-free potential that an electron in the bound state moves in and (ii) the potential the electron sees in the field. The shaded region is where the two differ for $z < z_0$; exponential error is related to the action in this region and is proportional to z_0^2. This is why dropping the terms $O(z_0^2)$ allows one to match the two wave functions smoothly and remove the dependence of the result on the selection of the matching point z_0 (referred to as fortunate cancellation of two opposing terms in [49]). This cancellation will be seen explicitly when I specify the wave function.

An alternative solution is to include polarization of the bound state at $z < z_0$, but ideally it has to be done to all orders in the electric field. Including such polarization numerically, in a static field, is possible using standard quantum chemistry electronic structure software packages.

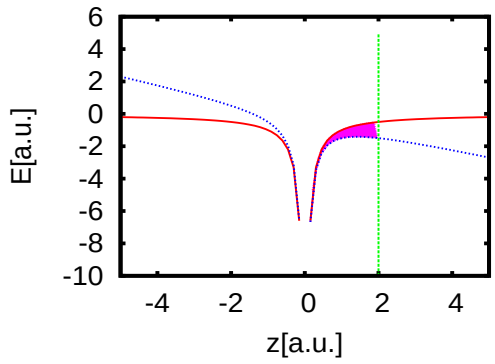

Figure 3.1: The Coulomb potential without a field(solid), with a constant electric field(dotted) and z_0(dashed). The shaded area is the difference between the potential with and without a constant field. The shaded area is proportional to z_0^2. In the asymptotic approximation terms of $O(z_0)$ are ignored and the effect of the constant field is removed allowing the wavefunctions to be matched.

After the expansion, expression for the action at the exit point from the barrier $z_e = I_p/F$ becomes

$$S(p_x, p_y, z_e) - S(p_x, p_y, z_0) = i\frac{\kappa^3}{3F} + i\frac{\kappa p_\perp^2}{2F} - i\kappa z_0 \tag{3.9}$$

We introduce $p_\perp^2 = p_x^2 + p_y^2$ here to simplify notation and highlight the importance of the perpendicular momentum in tunneling; $\kappa = \sqrt{2I_p}$ is the characteristic momentum of the bound state. Inserting this expression into equation (3.5), I obtain the tunnel ionization amplitude for a short range potential in a DC field:

$$a_{\mathrm{T}}(F, p_\perp) = \sqrt{\frac{p_z(z_0)}{p_z(z)}} e^{iS(p_x,p_y,z) - iS(p_x,p_y,z_0)} = \sqrt{\frac{\kappa}{p_z(z)}} \exp\left(-\frac{\kappa^3}{3F} - \frac{\kappa p_\perp^2}{2F} + \kappa z_0\right) \tag{3.10}$$

When going from the first term to the second term in equation 3.10 the asymptotic form of the action is used in the exponent. Also, the momentum $p_z(z_0)$ is replaced with κ, since $z_0 \ll z_e$.

The next step is to extend these results to long-range potentials. This is done using perturbation theory in action, following the original prescription of the PPT theory [20, 21, 22]. The action for the short-range potential is used as the zero-order approximation in the Hamilton-Jacobi equation, and corrections to the action is found in the first order in the core potential $V(z)$ (for details of the strong-field eikonal approximation see Ref.[34]).

The resulting correction to the action is

$$\Delta S = \int_{z_0}^{z} dz' \frac{V(z')}{p_z(z')} \tag{3.11}$$

where the momentum is $p_z(z) = \sqrt{\kappa^2 - 2Fz}$, i.e. calculated without the binding potential $V(z)$ of the core. Since $dz/p_z = d\tau$, I see that the integral is performed along the electron trajectory in the presence of the electric field only. Importantly, I take into account exponential suppression of tunneling with nonzero perpendicular momenta $p_\perp$. Indeed, Eq.(3.10) shows that characteristic perpendicular momentum is $p_\perp \sim \sqrt{F/\kappa} \ll \kappa$ (as long as $F \ll 1$). Hence, tunneling proceeds along the z-axis, with $x, y \ll z$ in the asymptotic region $z > z_0$. This allows one to set x, y to zero in the above equation. The integral in equation (3.11) is straightforward when the Coulomb potential is used $V(z) = Q/z$.

$$\Delta S = \frac{Q}{\kappa} \ln \left(\frac{1 + \sqrt{1 - 2Fz_0/\kappa^2}}{1 - \sqrt{1 - 2Fz_0/\kappa^2}} \right) \tag{3.12}$$

We now perform the same asymptotic expansion on Eqn. (3.12), dropping the terms of order z_0^2 and higher. Such expansion is just as important for the Coulomb correction as for the zero-order contribution (i.e. corresponding to the short-range potential). The Coulomb correction simplifies to

$$\Delta S = \frac{Q}{\kappa} \ln \frac{2\kappa^2}{Fz_0} \tag{3.13}$$

The above term is now included in a_T to get the final expression for the tunnel ionization amplitude of a Hydrogen atom in a static field,

$$a_\mathrm{T}(F, p_\perp) = \sqrt{\frac{\kappa}{p_z(z)}} \left(\frac{2\kappa^2}{Fz_0} \right)^{Q/\kappa} \exp\left(-\frac{\kappa^3}{3F} - \frac{\kappa p_\perp^2}{2F} + \kappa z_0 \right) \tag{3.14}$$

This concludes the calculation of the tunneling amplitude. Given the tunneling amplitude, the only missing component is the bound wave function in the mixed coordinate-momentum representation.

3.2 Mixed representation for a bound wave function

For a numerical wave function on the grid, mixed representation is obtained by simple application of the numerical Fourier transform with respect to the two dimensions orthogonal to the direction of tunneling. Here, however, I want to demonstrate the applicability

of the method analytically, and hence I need an analytical expression for the bound wave function in mixed representation. We will find that now for an atom in a state with angular momentum l and magnetic quantum number m.

The atomic wave function with quantum numbers l, m has a form

$$\Psi(x, y, z) = \frac{1}{\sqrt{2\pi}} e^{im\phi} \Psi_m(\rho, z) \tag{3.15}$$

where ϕ, ρ and z are the usual cylindrical coordinates. Note that this expression does not include the polarization of the field-free bound state. The wave function is 'unaware' of the modified potential barrier – an effect that depends on z_0^2, as discussed above. I now take the partial Fourier transform of equation (3.15):

$$\Phi(p_x, p_y, z_0) = \frac{1}{(2\pi)^{3/2}} \int dx dy e^{-ip_x x - ip_y y + im\phi} \Psi_m(\rho, z) \tag{3.16}$$

The double integral above can be transformed into polar coordinates.

$$\Phi(p_x, p_y, z_0) = \frac{e^{im\phi_0}}{(2\pi)^{3/2}} \int_0^\infty \rho d\rho \Psi_m(\rho, z_0) \int_0^{2\pi} d\phi e^{-ip_\perp \rho \cos\phi + im\phi} \tag{3.17}$$

Here $p_\perp$ is the perpendicular momentum $\sqrt{p_x^2 + p_y^2}$ and ϕ_0 is the angle the perpendicular momentum makes with the z axis. Recalling the integral expression for the Bessel function,

$$J_m(x) = \frac{1}{2\pi} \int_0^{2\pi} \cos\left(m\phi - x \sin\phi\right) d\phi \tag{3.18}$$

we calculate the ϕ integral to obtain

$$\Phi(p_x, p_y, z_0) = \frac{e^{im\phi_0}}{(2\pi)^{3/2}} (-i)^m \int_0^\infty \rho d\rho \Psi_m(\rho, z_0) J_m(\rho p_\perp) \tag{3.19}$$

Exponential suppression of tunneling with non-zero $p_\perp$ allows us to replace the Bessel function with its limit for small arguments:

$$\Phi(p_x, p_y, z_0) = \frac{e^{im\phi_0}}{(2\pi)^{3/2}} \frac{(-i)^m}{m!} \int_0^\infty \rho d\rho \Psi_m(\rho, z_0) \left(\frac{\rho p_\perp}{2}\right)^m \tag{3.20}$$

Indeed, given the characteristic values of the perpendicular momentum and the exponential dependence of the bound wave function on $r = \sqrt{z^2 + \rho^2}$ (proportional to $\exp(-\kappa r)$), it is straightforward to check that the product $\rho p_\perp$ is much less than unity. This fact enables us to replace the Bessel function with its asymptotic expression for small arguments. The Bessel functions with $m \neq 0$ will always be small, becoming smaller for larger m. This

fact reflects the properties of the Fourier transform. Non-zero m implies a node the bound state wave function along the direction of tunneling. It also means zero contribution from zero $p_\perp = 0$ into $\Phi(p_x, p_y, z_0)$ and hence higher characteristic perpendicular momentum. Thus, higher m correspond to higher characteristic $p_\perp$ and therefore a suppression of tunnel ionization. Thus, partial Fourier transform in combination with the Gaussian filter for perpendicular momenta in Eq.(3.10) gives both transparent and quantitative physical picture, connecting the nodal structure of the bound state to tunneling rates.

Using the asymptotic form of the Bessel function, I can now perform the remaining integral over ρ for the Hydrogen wave function. Its asymptotic form is

$$\Psi_{asymp}(x, y, z) = \frac{\kappa^{3/2} e^{im\phi}}{\sqrt{2\pi}} C_{\kappa l} N_{lm} (\kappa r)^{Q/\kappa - 1} e^{-\kappa r} P_l^m(\cos\theta) \tag{3.21}$$

Where,

$$C_{\kappa l} = \frac{(-1)^{n-l-1} 2^n}{\sqrt{n(n+l)!(n-l-1)!}} \tag{3.22}$$

$$N_{lm} = \sqrt{\frac{(2l+1)(l+m)!}{2(l-m)!}} \frac{1}{2^m m!} \tag{3.23}$$

and $\kappa = \sqrt{2I_p}$ where I_p is the ionization potential. The Legendre polynomial can be replaced with the limit for small angles, $P_l^m(\cos\theta) \propto \sin^m\theta$. Equation (3.21) can be simplified by taking into account that $\rho \ll z$ in the asymptotic region $z > z_0$ and hence $\sin\theta \approx \rho/z_0$ and $r \approx z + \rho^2/2z$. Inserting equation (3.21) into equation (3.20) and calculating the integral I obtain:

$$\Phi(p_x, p_y, z_0) = \frac{(-i)^m e^{im\phi_0}}{(2\pi)^{1/2}} C_{\kappa l} N_{lm} e^{-\kappa z_0} \left(\frac{p_\perp}{\kappa}\right)^m \kappa^{Q/\kappa - 1/2} z_0^{Q/\kappa} \tag{3.24}$$

Now using the above equation for $\Phi(p_x, p_y, z_0)$ and the equation for the tunneling amplitude from z_0 to z (see above), I can find the mixed representation wave function at any z with a simple multiplication. In particular, using Eq.(3.14), I find the wave function just before the exit point from the tunnel:

$$\begin{aligned} &\Phi(p_x, p_y, z \to z_e) = \Phi(p_x, p_y, z_0) * a_{ion}(F, p_\perp) = \\ &= \frac{1}{\sqrt{2\pi p_z(z)}} (-i)^m e^{im\phi_0} C_{\kappa l} N_{lm} \left(\frac{2\kappa^3}{F}\right)^{Q/\kappa} \left(\frac{p_\perp}{\kappa}\right)^m e^{-\kappa^3/3F - \kappa p_\perp^2/2F} \end{aligned} \tag{3.25}$$

Strictly speaking, this expression is not applicable right at the exit point where $p_z(z)$ is equal to zero and the WKB approximation diverges. Finally, the rate can be calculated by

going anywhere beyond the exit point, including just beyond it (the divergent term $1/\sqrt{p_z}$ cancels, providing continuity of current):

$$\Gamma_{lm} = \int dp_x dp_y p_z(z) |\Phi(p_x, p_y, z)|^2 = \frac{\kappa^2}{2} |C_{\kappa l}|^2 \frac{2l+1}{2^m m!} \frac{(l+m)!}{(l-m)!} \left(\frac{2\kappa^3}{F}\right)^{2Q/\kappa - m - 1} e^{-2\kappa^3/3F} \quad (3.26)$$

Equation (3.26) is identical to the static tunneling rate quoted by PPT[20].

3.3 Results & Discussion

There are important limitations to the application of asymptotic theory which uses field-free bound wave functions. As I have shown, the tunnelling amplitude must be expanded in powers of z_0 until the first order, dropping the terms proportional to z_0^2 and higher. This is the key to canceling error introduced by using the field-free bound wave function in the barrier region. Cancellation of large errors is smooth when calculations are analytic and benefit from using analytical expression for the tunnelling amplitude that includes the Coulomb field of the core. However, in the case of numerical implementation the correct result, which requires cancellation of large errors, is prone to numerical artifacts.

In complex multi-electron systems corrections to the single-center purely Coulomb potential are important. The exit point z_e is often sufficiently close to make dipole and higher-order multipole terms in the core potential significant. In practice, the potential is given numerically on a grid, making the possibility of analytical expansions in powers of z_0 questionable. The best solution is to calculate the polarized bound wave function in a finite basis set, making sure that the effect of the electric field at $z < z_0$ is included.

Important aspect of the analytical calculation is also the use of the asymptotic expansion of the wave function, which retains only the first-order corrections to action in powers of the binding potential. This approximation to the wave function at $z < z_0$ is important since the exact same approximation is used at $z > z_0$ for the tunnelling amplitude.

If the wave function is to be changed from its asymptotic field-free expansion to a numerical field-dressed solution on the grid, its behavior at $z = z_0$ will include corrections beyond the eikonal asymptote. Then, one can and should also improve ionization amplitudes beyond the eikonal approximation, calculating stationary action numerically. The calculation may still rely on the approximation of small tunneling angles and small perpendicular momenta relative to the direction of the electric field. Such calculation would naturally take into account the exact molecular potential.

By correcting the bound wave function to include the electric field and relaxing the eikonal approximation for the tunneling amplitude, it is possible to approximately obtain tunnel ionization rates for arbitrary molecules with two 2D Fourier transforms and a simple multiplication.

3.4 Conclusion

The method presented above has been shown to work for the simple case of an atom in a static field. The classic results of PPT and others were re-derived. Clear routes to more complicated systems have also been discussed. Both analytical and numerical schemes can be pursued. In future work I will be elaborating on this method to obtain analytical and computational ionization rates for several different molecules. I will also generalize our approach to oscillating electric fields and to multielectron systems.

Chapter 4

Strong Field Ionization of Molecules

4.1 Introduction

Ionization of an atom or a molecule is at the core of nearly every process in strong laser fields, from high harmonic generation (HHG) to laser induced electron diffraction(LIED), generation of high-energy electrons, correlated multiple ionization, etc. (see e.g. [41]). The ionization of atoms in strong low-frequency laser fields has been studied theoretically and experimentally over several decades, and now appears well understood. Among the most important theoretical advancements are semi-analytical models providing adequate quantitative description of the spectra of the so-called direct electrons, including the effects of the ionic core during and after ionization [34, 35] and the sub-cycle dynamics of non-adiabatic tunneling [20, 22, 21, 23, 24, 35] for moderate $\gamma \sim 1$ Keldysh parameters [26].

General understanding of atomic ionization has been extrapolated to molecules[56, 55]. However, it has now become clear that straightforward extrapolation is insufficient, stimulating theoretical efforts [61, 62, 64, 65, 63, 49, 66]. There are many important reasons for the renewed interest, including the advent of high harmonic generation spectroscopy of multi-electron dynamics in molecules [67, 68, 69]. This spectroscopy requires one to accurately calculate relative contributions of several molecular orbitals (electronic states of the molecular ion) participating in the high harmonic generation process[70, 71].

We propose simple and physically transparent upgrade of the existing theories. In atoms, our approach gives results identical to the classic results of Perelomov, Popov and co-workers [20, 22, 21] (see [72] for details), later popularized by Ammosov, Delone and Krainov [37] and now commonly referred to as the ADK theory. In molecules, the well-known molecular ADK theory (MO-ADK) [55] can be obtained as a limiting case of our approach, within clearly defined approximations . However, our general approach does not require spherical symmetry of the binding potential.

In contrast to the standard tunnelling approach of Perelomov, Popov and co-workers [20, 22, 21] and later work (ADK, MO-ADK) [37, 55], I explicitly keep track of the angle between the direction of the electric field and the characteristic direction of electron tunnelling. The degree to which the tunnelling electron can deviate from the direction of the electric field depends on the field strength, and is chiefly responsible for intensity-dependent features in the angle-resolved ionization rates for aligned molecules.

Simple analytical formulas can be derived using the additional assumption of a purely Coulombic asymptote of the core potential far from the nucleus. With this assumption, I am able to approximate the ionization rate as a product of two factors. The first is the tunneling factor, associated with the transmission amplitude during the electron motion in the classically forbidden region. The second is the geometrical factor, which reflects the geometry of the molecular orbital and the interference of tunnelling currents originating from different lobes of the ionizing orbital.

We give a detailed derivation of the ionization rate for a general wave function and look at the special cases of a multi-center linear combination of atomic orbitals(LCAO) wave function, of a single center expansion used in MO-ADK, and finally the fitted asymptotic wave function The important approximations used in each are examined in detail and justified when neccessary. Many examples are given including multi-center H_2, N_2, and O_2 and CO_2 and several polar molecules using the fitted asymptotic wave function.

The important parameter z_0 is discussed at length and a clear method for chosing this value is given. This choice is justified through a numerical implementation of the theory on simple molecular systems.

4.2 General Theory

Let z be the direction of the electric field that induces tunnel ionization. The ionization rate is given by the total current through the plane orthogonal to z:

$$\Gamma = \frac{1}{2} \int \mathrm{d}x \; \mathrm{d}y \; \Psi^*(x, y, z) \hat{p}_z(z) \Psi(x, y, z) + c.c. \tag{4.1}$$

where atomic units $e = m_e = \hbar = 1$ are used, $\hat{p}_z$ is the electron momentum operator orthogonal to the x-y plane, Ψ and Ψ^* are the wave function of the tunneling electron and its complex conjugate. The continuity equation ensures that the total current is z-independent after the tunneling electron exits the potential barrier.

To calculate the rate, I use our approach described in the previous chapter and in the following paper[72], where it has been verified for atomic systems. At some point z_0 in the classically forbidden region, sufficiently far from both the entrance z_{in} and the exit z_{ex} from

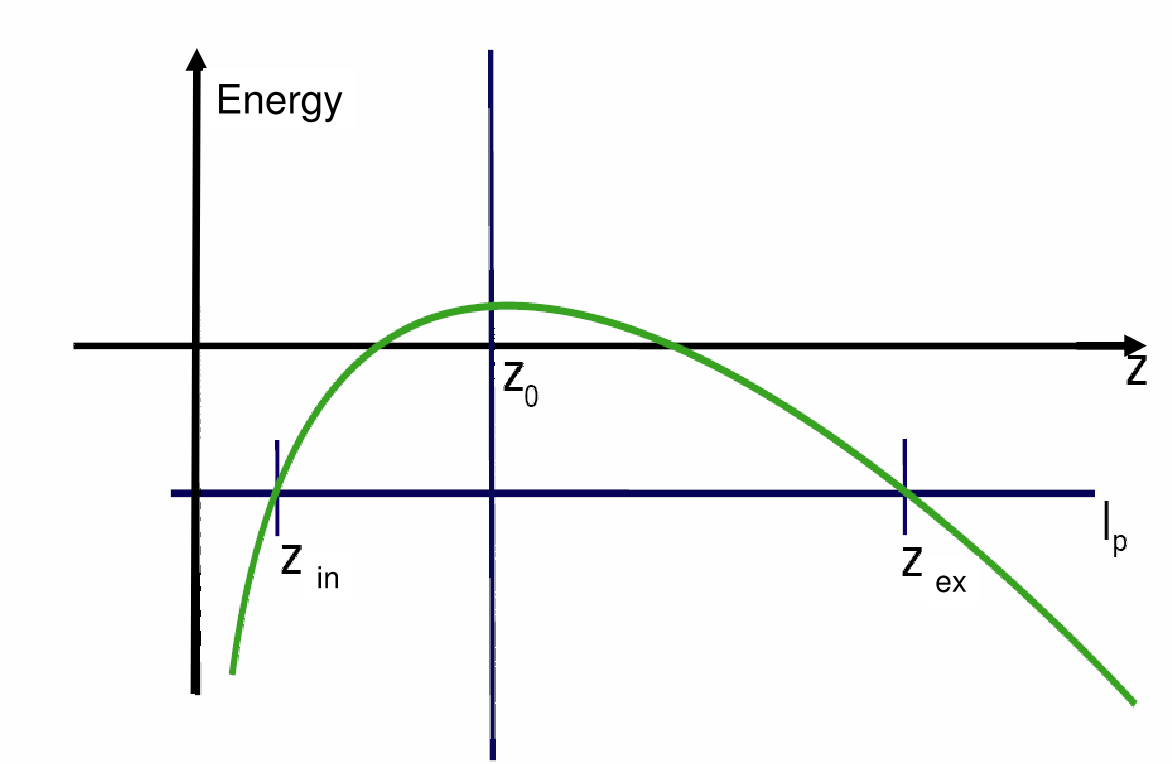

Figure 4.1: Schematic of tunneling, with z_{in} and z_{ex} the entrance and the exit point from the barrier; z_0 is the matching point.

the tunneling barrier (see Fig.4.2), I re-write the wave function of the tunneling electron $\Psi(x, y, z_0)$ in the mixed coordinate-momentum representation

$$\Psi(x, y, z_0) = \frac{1}{2\pi} \int dp_x \int dp_y e^{-ixp_x - iyp_y} \Phi(p_x, p_y, z_0) \tag{4.2}$$

where,

$$\Phi(p_x, p_y, z_0) = \frac{1}{2\pi} \int dx \int dy e^{ixp_x + iyp_y} \Psi(x, y, z_0) \tag{4.3}$$

The mixed representation wave function $\Phi(p_x, p_y, z_0)$ can be effectively propagated under the barrier using the semi-classical (WKB) method. A key approximation, previously used in the classic papers by Popov and coworkers [20, 22, 21], is that of small deviations between the tunneling trajectories and the z axis. Then, the wave function at a point z is approximated as [72]:

$$\begin{aligned} &\Phi(p_x, p_y, z) = \Phi(p_x, p_y, z_0) a_{\mathrm{T}}(z_0, z) \\ &a_{\mathrm{T}}(z_0, z) = \sqrt{\frac{|p_z(z_0)|}{|p_z(z)|}} \exp\left[- \int_{z_0}^{z} p_z(z') dz' - \frac{(p_x^2 + p_y^2)\tau_T}{2} \right] \end{aligned} \tag{4.4}$$

The tunnelling amplitude, which has been derived previously[20, 22, 21, 72] is the WKB solution describing the motion of a particle under a 3D barrier, with the core (ionic) potential treated perturbatively compared to the electric field. This approximation explains the 1D-like form of the expression for $a_{\mathrm{T}}(z_0, z)$, with the 3D nature of the motion appearing only through the momenta p_x, p_y.

It is in principle possible to perform this derivation using a general ionization potential taking into account the full 3D motion in the full core potential. I consider this an extension of the current theory and will return to it later when I discuss the numerical implementation.

In the classically forbidden region the electron momentum is imaginary, which is why the absolute value is used for p_z. The matching point z_0 is supposed to be chosen well before the exit of the barrier, and hence I approximate $|p_z(z_0)| \simeq \kappa = \sqrt{2I_p}$, where I_p is the ionization potential. Finally, τ_T is the tunneling time between z_0 and z,

$$\tau_T = \int_{z_0}^{z} \frac{dz'}{p_z(z')} \tag{4.5}$$

Given that $z_0 \ll z_{\mathrm{ex}}$, the tunneling time is approximately independent of z_0 and for $z = z_{\mathrm{ex}}$ one finds $\tau_T \simeq 2z_{\mathrm{ex}}/\kappa \simeq \kappa/F$. With the approximate expression for $\Phi(p_x, p_y, z)$ now at hand, the wave function in the coordinate space becomes

$$\Psi(x, y, z) \simeq \sqrt{\frac{\kappa}{|p_z(z)|}} e^{-\int_{z_0}^{z} p_z(z') dz'} \frac{1}{2\pi} \int dp_x dp_y \; e^{-ixp_x - iyp_y} \Phi(p_x, p_y, z_0) e^{-\frac{1}{2} p_\perp^2 \tau_T} \tag{4.6}$$

with $p_\perp^2 \equiv p_x^2 + p_y^2$. Thus, 3D tunnel ionization is the combination of what looks like 1D tunneling along the electric field with Gaussian filtering in the momentum space orthogonal to the direction of tunneling. This tunneling filter is $G(p_\perp) = \exp[-p_\perp^2 \tau_T/2]$. Using the convolution theorem, I can write the wave function as

$$\Psi(x,y,z) \simeq \frac{\sqrt{\kappa}}{\sqrt{|p_z(z)|}\tau} e^{-\int_{z_0}^{z} p_z(z')dz'} \left[\Psi(x,y,z_0) * e^{-\frac{1}{2\tau_T}\rho^2}\right] \tag{4.7}$$

where $\rho^2 = x^2 + y^2$ and I took into account that the inverse Fourier transform of the Gaussian filter $G(p_\perp)$ is $g(\rho) = (1/\tau)\exp[-\rho^2/2\tau_T]$. The convolution is defined as:

$$(f * g)(t) = \int_\infty^\infty f(\tau) g(t-\tau) d\tau \tag{4.8}$$

As always with asymptotic tunneling theories, one has to carefully deal with matching the bound wave function $\Psi(x,y,z_0)$ at the point z_0 to the in-field semi-classical tunneling amplitude from z_0 to z. The potential problems hidden in this approach have recently been highlighted in [49, 66], and ways to correct for the potential errors outlined in Ref.[49, 66] have been discussed in [72].

For atomic ionization, one has to match spherically symmetric bound state with the cylindrically symmetric behaviour at large distances from the origin, imposed by the electric field. The molecular case is less straightforward, as it lacks the spherical symmetry of the bound wave function. The procedure I use generalizes the approach developed by Popov and co-workers for the atomic case [20, 22, 21], and introduces additional corrections that turn out to be important in the molecular case. These corrections are absent in the direct generalization of the atomic theory for molecules, known as MO-ADK [55]. Their essence is to incorporate the angular width of the tunnelling wavefunction in the direction perpendicular to the direction of tunnelling z. If θ is the angle with the electric field (i.e. with the laboratory z-axis), then standard approximation of the tunnelling theories is to replace $\sin\theta \approx \theta$, $\cos\theta \approx 1$ and $1 - \cos\theta \approx 0$, while I attempt to keep all terms proportional to θ^2 and hence do not neglect $1 - \cos\theta$. More detailed discussion follows below.

Eq.(4.7) can now be substituted into the general expression for the tunneling rate Eq.(4.1).

$$\Gamma = \frac{\kappa}{\tau^2} e^{-2|\int_{z_0}^{z} p_z(z')dz'|} \int dxdy |\Psi(x,y,z_0) * e^{-\frac{\rho^2}{2\tau_T}}|^2 \tag{4.9}$$

From this equation I am able to derive a series of results, all of which are dependent on the choice of the wave function $\Psi(x,y,z_0)$. I will examine four different choices: first is expanding $\Psi(x,y,z_0)$ as a series of spherical harmonics, second a multi-center expansion using a linear combination of atomic orbitals, third using an approximate analytic expression for the wave function and finally a numerical scheme which uses the output of quantum chemistry codes to calculate the ionization rate on a grid.

4.2.1 Multi-center expansions and MO-ADK

The general form in equation 4.9 can be used in multiple ways. The key is choosing the wave function $\Psi(x,y,z)$ properly. I will proceed with a generic asymptotic form then specialize later.

$$\Psi(x,y,z) = \sqrt{\frac{\kappa}{2\pi}}(-1)^{\frac{|m|-m}{2}} C_{nl} N_{lm}(\kappa r)^{Q/\kappa-1} e^{im\phi} e^{-\kappa r} u_{nl}(r) \sin^{|m|}\theta \tag{4.10}$$

This equation is similar to the wavefunction used to calculate the atomic ionization rate in the previous chapter, equation 3.21. The Legendre polynomial has already been expanded for small θ. The factor N_{lm} was given in equation (3.23). Finally, $u_{nl}(r)$ is the radial part of the wave function that differs from the hydrogenic wave function. This term encapsulates everything in the Dyson orbital that does not appear in the atomic form in equation (3.21). The Dyson orbital is defined as the overlap between the neutral(N-dimensional) and ionic(N-1 dimensional) wavefunctions. It is the one-electron wave function which represents the outgoing electron.

We proceed with the calculation in the same way as in the previous chapter, by Fourier transforming the wave function and propagating it to the exit with the WKB wave function. The WKB term is identical to that given in equation (3.14) except for a correction for the non-coulombic short range part of the molecular potential.

$$a_{\mathrm{T}}(F,p_\perp) \;=\; \sqrt{\frac{\kappa}{p_z(z)}}\left(\frac{2\kappa^2}{Fz_0}\right)^{Q/\kappa} \exp\left(-\frac{\kappa^3}{3F} - \frac{\kappa p_\perp^2}{2F} + \kappa z_0\right) e^{-\int_{z_0}^{z_e}\frac{V_{Mol}(z')}{p_z(z')}dz'} \tag{4.11}$$

The correction is the last term in the expression above, where $V_{Mol}(z)$ is the short range component of the molecular potential. The Fourier transform and propagation is straight forward and the integrals have been performed in the previous chapter. I will show the wave function in equation 4.10 at the exit of the barrier, prior to taking the rate.

$$\sqrt{p_z(z_e)}\Phi_{nlm}(p_\perp,\phi_0,z) = C_{nl}N_{l|m|}(-1)^{|m|}e^{im\pi/2}\frac{e^{im\phi_0}}{2\pi}\left(\frac{2\kappa^3}{F}\right)^{Q/\kappa} e^{-\kappa^3/3F - p_\perp^2\tau/2}\left(\frac{p_\perp}{\kappa}\right)^{|m|} R(\theta,\phi) \tag{4.12}$$

The result is similar to the wave function calculated in the previous chapter, the main difference is the term $R(\theta,\phi)$; this is the combination of the two non-coulombic terms in the wave function and the ionization rate: $R(\theta,\phi) = u(z_0)e^{-\int_{z_0}^{z_e}\frac{V_{Mol}(z')}{p_z(z')}dz'}$. This term is, in principle, dependent on the orientation of the molecule in the ionizing field and the direction of tunneling. Since $R(\theta,\phi)$ is dependent on ϕ it complicates the calculation of the ionization rate. For now I will assume that $R(\theta,\phi)$ is just a number, which it is in a

purely coulombic potential, and can be taken out of the rate integral, I will come back to this approximation later to discuss its validity.

We calculate the rate for a multi-center wave function; I take a sum of the wave function above each at different centers and different n, l, m. The sum is weighted by the relative amplitudes of the Slater orbitals in a Linear Combination of Atomic Orbitals(LCAO) expansion of the molecular wave function. The wave function is defined as,

$$\Phi(p_\perp, \phi_0, z) = \sum_{nlm} g_n \Phi_{nlm} e^{-ip_\perp \rho_n} \tag{4.13}$$

Where the ρ_n are the distance in the x-y plane to the atomic center in question. Here the sum is over all centers and quantum numbers. The exponential is a result of the shift from the origin of the centers. The coefficient g_n contains amplitudes from each term in the LCAO and θ_L dependent factors from rotating the system to the lab frame. To calculate the rate I must square the wave function above and integrate out the perpendicular momenta:

$$\Gamma = \int\int p_z(z_e) p_\perp dp_\perp d\phi_0 |\Phi|^2 \tag{4.14}$$

The actual integrals are straightforward and again were done in the previous chapter, the difficult part is taking the norm of the multicenter wave function. The resulting rate can be expressed as follows.

$$\Gamma = R^2 \sum_n \left(|g_n|^2 \Gamma_n + \sum_{k>n} |g_k||g_n| \sqrt{\Gamma_n \Gamma_k} 2 \cos\left[(m_n - m_k)\phi_{nk} + \alpha_{nk}\right] A_{n,k}(\theta) \right) \tag{4.15}$$

$$A_{n,k}(\theta) = \frac{(-1)^{|m_n|+|m_k|+|m_n-m_k|/2-(m_n-m_k)/2}}{\sqrt{|m_n|!|m_k|!}} \int_0^\infty 2x dx e^{-x^2} x^{|m_n|+|m_k|} J_{|m_n-m_k|}(\frac{x\rho_{nk}\sqrt{F}}{\sqrt{\kappa}}) \tag{4.16}$$

Where ϕ_{nk} is the polar angle of $\rho_{nk} = \rho_n - \rho_k$ and $\alpha_{nk} = \arg(g_n g_k^*)$. The expression above gives several interesting results. First, I am able to derive closed form expressions for ionization rates in molecules with an arbitrary number of LCAO elements on any number of sites. The result is just a sum of single center ionization rates with a 'cross-term' which is an interference between single center ionization rates. I will see later that there is a better way to compute these rates without the large sums.

The form above can be taken for a single center; it then reduces exactly to the MO-ADK theory[55]. I can then see why the MO-ADK theory does not have any interference between states of different 'm'. The integral in $A_{n,k}(\theta)$ is zero unless $m_n = m_k$.

The lack of interference terms is solely the result of assuming the Coulomb correction is independent of angle, i.e. $R(\theta, \phi)$ is a constant. This assumption is what directly leads to the form of $A_{n,k}$. Had I not made that assumption then there would be cross terms from the expansion of $R(\theta, \phi)$ and states of different 'm' would then interfere. The validity of this assumption will be tested in the next section.

Equation (4.15) shows the most general result for the molecular ionization rate, it also can be reduced to MO-ADK. These are two important results. The form above is not particularly easy to use though; in the next section I will rederive the rate with a carefully chosen wave function that will allow for simple and intuitive rates to be calculated.

4.2.2 Analytic solution

We now derive simple, closed form analytical expressions for tunnel ionization of different orbitals in a linear molecule, with the electric field aligned at an angle θ_L relative to the molecular axis.

Let ionization create the molecular cation in some final electronic state. I shall denote $\Psi(x, y, z)$ the corresponding Dyson orbital, i.e. the overlap between the initial N-electron wave function of the neutral and the final $N-1$ electron wave function of the electronic state of the ion. In the asymptotic region $z_0 \gg z_{\text{in}}$ I write $\Psi(x, y, z_0)$ as:

$$\Psi(x, y, z_0) \simeq C_\kappa \kappa^{3/2} \frac{e^{-\kappa r_0}}{\kappa r_0} (\kappa r_0)^{Q/\kappa} f_M(\theta_M, \phi_M) \tag{4.17}$$

Here spherical angles θ_M and ϕ_M refer to the molecular frame, i.e. they are measured relative to the molecular axis Z_M; $z_0 \equiv r_0 \cos\theta_M$. The function $f_M(\theta_M, \phi_M)$, also given in the molecular frame, incorporates the geometry of the orbital that, in turn, also reflects the shape of the binding potential. Deviations from the single-center Coulomb potential, which are obviously very significant near the core, are responsible for how $f_M(\theta_M, \phi_M)$ looks like in the asymptotic region. Apart from $f_M(\theta_M, \phi_M)$, the radial asymptotic behavior corresponds to a purely Coulombic tail of the potential $-Q/r$, with Q the effective charge. This asymptotic form is quite adequate for a large range of molecules and orbitals, including H_2, N_2, O_2, CO_2, HCl, HF, etc [73]. For molecules lacking the inversion centre, the cation's dipole moment will no longer vanish, and the asymptotic form may emerge further away from the nuclei than for the symmetric molecules.

The angle between the molecular axis and electric field is denoted as θ_L. The plane $\phi_M = 0$ (i.e. the X-Z plane) is set to coincide with the plane defined by the molecular and laboratory axes Z_M and Z_L, see Fig.2. In what follows, angles θ and ϕ refer to the lab frame, while θ_M, ϕ_M refer to the molecular frame.

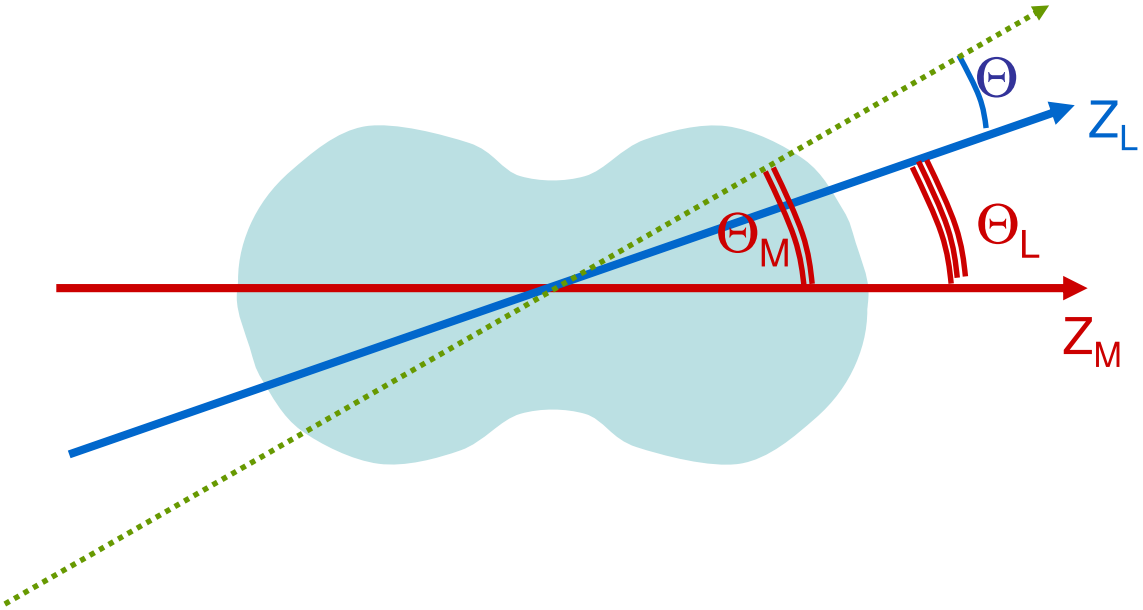

Figure 4.2: Schematic representation of a molecular orbital (shaded blue) and the two Z-axes, molecular Z_M and laboratory Z_L, which define the plane of tunnelling (X-Z). The tunnelling angle θ is relative to the lab axis.

The steps of the calculation are (i) transformation of $f_M(\theta_M, \phi_M)$ into the lab frame, which yields $f_L(\theta, \phi)$ after rotation by θ_L in the X-Z plane, (ii) calculation of the convolution between the transformed function and the tunneling 'filter' $g(\rho)$, and (iii) calculation of the tunneling current.

Substituting Eq.(4.17) into Eqs.(4.7,4.1), and calculating the tunneling integral between z_0 and z for the potential $-Q/r$ following [20, 22, 21] (i.e. using the eikonal approximation to match the asymptotic form of the radial wave function), I obtain the following expression for the tunneling rate

$$\Gamma = \Gamma_{A,s} R(\theta_L) \tag{4.18}$$

Here the first term

$$\Gamma_{A,s} = \frac{\pi}{\tau_T} C_\kappa^2 e^{-\frac{2\kappa^3}{3F}} \left[\frac{2\kappa^3}{F}\right]^{2Q/\kappa} \tag{4.19}$$

is the standard tunneling rate for an atomic s-orbital with spherically symmetric angular structure. The second term incorporates all aspects of the orbital geometry, including the

interference of the tunneling currents coming from the different lobes of the orbital. It is expressed as

$$R(\theta_L) = \frac{1}{R^{(0)}} \int_0^\infty \rho \, \mathrm{d}\rho \; e^{-\rho^2/\tau_T} \int_0^{2\pi} \mathrm{d}\phi |\tilde{f}_L(\rho, \phi; f)|^2 \tag{4.20}$$

where $\rho = r_0 \sin\theta$ and $\tilde{f}_L$ is the result of tunnel-filtering the original $f_L(\theta, \phi)$ in the momentum space, which is expressed via the convolution integral:

$$\tilde{f}_L = \int_0^\infty \rho' \, \mathrm{d}\rho' \; e^{-\rho^2/2\tau_T} e^{-\kappa\rho'^2/2z_0} \frac{1}{2\pi} \int_0^{2\pi} \mathrm{d}\phi' e^{\rho\rho' \cos(\phi-\phi')/\tau_T} f_L(\theta', \phi') \tag{4.21}$$

Finally, the normalization factor $R^{(0)}$ is obtained by performing the same calculation with $f_L(\theta, \phi) = 1$, i.e. for an atomic s-orbital.

In what follows, I focus on orbitals with Σ and Π symmetry. For the latter, ionization is dominated by the Π_x-orbitals. Orthogonal to it Π_y orbital has a nodal plane in the $x-z$ plane and hence its ionization in that plane is suppressed.

For Σ and Π_x orbitals, the angular dependence $f_M(\theta_M, \phi_M)$ has the following form

$$f_M(\theta_M, \phi_M) = F(\cos\theta_M, \sin\theta_M \cos\phi_M) \tag{4.22}$$

(while for the Π_y orbital $\sin\theta_M \cos\phi_M$ would be replaced with $\sin\theta_M \sin\phi_M$). For convenience, I will use the notation $F(u, v)$, where $u = \cos\theta_M$ and $v = \sin\theta_M \cos\phi_M$.

The transformation between the molecular and the lab frame is

$$\begin{aligned} \cos\theta_M &\to \cos\theta_L \cos\theta - \sin\theta_L \sin\theta \cos\phi \\ \sin\theta_M \cos\phi_M &\to \cos\theta_L \sin\theta \cos\phi + \sin\theta_L \cos\theta \end{aligned} \tag{4.23}$$

with θ and ϕ the angles in the lab frame, and θ_L the angle between the molecular axis and the electric field. Substituting these expressions into $F(u, v)$, I can calculate all the integrals using the fact that the angle θ between the tunneling electron and the field is small, and expanding $F(u, v)$ in Taylor series up to the second order with respect to θ.

For the moment, in contrast to the standard approximation $\cos\theta = 1$ [20, 22, 21], we shall keep the small parameter $1 - \cos\theta \approx \theta^2/2$. Small tunnelling angles also imply that $\rho\rho'/\tau_T < 1$, allowing one to use it as a small parameter while calculating the convolution integral over ϕ' in Eq.(4.21). The final result is

$$R(\theta_L, z_0) \simeq \left[F_0 - (1 - \cos\theta_T(z_0)) F_2 + \frac{1}{4} \sin^2\theta_T(z_0) F_3 \right]^2 + \frac{1}{2\tau_T} \frac{1}{(\kappa + z_0/\tau_T)^2} F_1^2 \tag{4.24}$$

where

$$\theta_T(z_0) = \sqrt{\frac{2}{(\kappa + z_0/\tau_T)z_0}} \tag{4.25}$$

is the characteristic angular width of the tunnelling wave function at the matching point z_0. The coefficients F_k are related to the function $F(u, v)$ and its derivatives taken with respect to u, v and calculated at $u = \cos\theta_L$ and $v = \sin\theta_L$:

$$\begin{aligned} F_0 &= F(\cos\theta_L, \sin\theta_L) \\ F_1 &= F_v \cos\theta_L - F_u \sin\theta_L \\ F_2 &= F_u \cos\theta_L + F_v \sin\theta_L \\ F_3 &= F_{vv} \cos^2\theta_L + F_{uu} \sin^2\theta_L - F_{uv} \sin 2\theta_L \end{aligned} \tag{4.26}$$

So far, our result for the geometrical factor maintains its dependence on the matching point z_0. However, I can simplify Eq.(4.24) further and remove this dependence using one of several methods. The traditional way is to use the assumption that $z_0 \ll z_{\rm ex}$ which is valid only for weak fields. Taking into account that $\kappa\tau_T = 2z_{\rm ex}$, I see that, formally, $z_0/\tau_T \ll \kappa$. Then, the dependence of the coefficient in front of F_1 (the last term in the expression Eq.(4.24) on the matching point z_0 disappears. Now, let us look at the terms $1 - \cos\theta_T(z_0)$ and $\sin^2\theta_T(z_0)$. Since I expect $z_0/\tau_T \ll \kappa$, we see that $1 - \cos\theta_T \sim \sin^2\theta_T \sim \theta_T^2 \sim 1/\kappa z_0$. Given that the matching point is supposed to be sufficiently far, $\kappa z_0 \gg 1$, the terms proportional to F_2 and F_3 have a small parameter $1/\kappa z_0 \ll 1$ compared to F_0. This leads to simplified expression

$$R(\theta_L, z_0) \to R(\theta_L) \simeq F_0^2 + \frac{1}{2\tau_T\kappa^2} F_1^2 \tag{4.27}$$

where the dependence of $R(\theta_L, z_0)$ on the matching point is removed, as common in the asymptotic tunnelling theories. Applying the result Eq.(4.27) to the atomic s- and p-orbitals leads to the results identical with standard expressions [20, 22, 21, 37, 49].

While Eq.(4.27) and the overall result for the molecular tunnelling ionization rate use the same approximations as the standard tunnelling theories, our expressions are simpler than the standard expressions of MO-ADK[55]. Instead of expanding the wavefunction into the spherical harmonics, as done in the MO-ADK, all one needs in Eq.(4.27) is the first derivative in the direction perpendicular to the electric field, which yields F_1.

In relatively weak fields, where the requirement $1 \ll z_0 \ll z_{\rm ex}$ holds well, the term proportional to F_1 becomes important only near the zeroes (nodal planes) of F_0. However, in most practical situations I am interested in tunnel ionization for relatively strong fields of a few Volts per Angstrom, with ionization lifetimes about 10 fsec, i.e. with substantial

ionization probabilities during the few cycles of the laser pulse. Under such conditions the rather strong requirement $1 \ll z_0 \ll z_{\rm ex}$ can no longer be met. The F_1-term becomes important in a broader range of angles, not only where $F_0 = 0$. The terms proportional to F_2 and F_3 are also no longer negligible. One can easily check by expanding $1-\cos\theta_T(z_0) \approx \theta_T(z_0)^2/2$ and $\sin^2\theta_T(z_0) \approx \theta_T(z_0)^2$ that the terms proportional to F_2 and F_3 are of the same order as that proportional to F_1. The associated corrections are also of the same order as long as $F_0 \neq 0$.

To calculate ionization rates in this case, I can no longer use the traditional method of ignoring the terms proportional to $\theta_T^2(z_0)$, which means that the z_0-dependence in Eq.(4.24) should be handled differently. To deal with this problem, I keep all the terms proportional to $\theta_T^2(z_0)$ and calculate the characteristic tunnelling angle $\theta_T(z_0)$ at the exit point $z_{\rm ex}$:

$$\theta_T(z_{\rm ex}) = \sqrt{\frac{2}{(\kappa + z_{\rm ex}/\tau_T)z_{\rm ex}}} \tag{4.28}$$

with $z_{\rm ex} \approx I_p/F$. The tunnelling angle approaches 20-30^o as the field strength reaches Volts per Å(intensity approaching 10^{14}W/cm^2).

Thus, setting $z_0 \to z_{\rm ex}$ in Eq.4.24, I obtain the final expression for the molecular orbital geometry-dependent term, better suited for strong electric fields and high ionization rates

$$R(\theta_L) = R(\theta_L, z_{\rm ex}) \simeq \left[F_0 - \frac{\theta_T^2(z_{\rm ex})}{2}F_2 + \frac{\theta_T^2(z_{\rm ex})}{4}F_3\right]^2 + \frac{1}{2\tau_T}\frac{1}{(\kappa + z_{\rm ex}/\tau_T)^2}F_1^2 \tag{4.29}$$

Our result shows to what extent the alignment-dependent tunnelling rate $\Gamma(\theta_L)$ directly maps the ionizing orbital. The leading term in $R(\theta_L)$ Eq.(4.29) is F_0^2, and it is indeed given by the wave function in the direction of tunnelling. Corrections to this simple picture are determined by F_1, F_2, F_3. These terms are particularly important in the vicinity of nodal planes, where $F_0 \approx 0$.

The effects of the higher order terms are particularly evident in the ionization rates of carbon dioxide. It has recently been argued [74, 75, 65, 66, 76] that alignment dependent molecular ionization rates map the geometry of the ionizing orbital, at least for relatively simple orbitals. Intuitively, the rate of tunnel ionization in the strong infrared fields is expected to (i) minimize when the ionizing laser field is aligned with the nodal plane of the molecular orbital and (ii) maximize when the laser field is aligned along the most spatially extended component of the orbital.

However in some cases experimental observations [59] strongly disagree with this intuitive picture. For the CO_2 molecule, one expects that tunnel ionization from the highest occupied molecular orbital (HOMO) should peak when the laser field is aligned at about 30° relative to the molecular axis, i.e. along the most spatially extended component of the

HOMO. The same result is predicted by the standard tunnelling theory MO-ADK [55]. However, the experiment [59] observes sharply peaked ionization at about 45° .

We have performed numerical simulations using the technique described in Ref.[63] which show agreement with experimental trends[59]. The calculation was done at a wavelength of 1600nm for varying intensities and includes only a single channel, ionized from the HOMO. Both the Π_x and Π_y components were included. Figure 4.3(a) clearly shows the same peak location as the experimental results. The distribution is peaked in the 40-45° range. The other trend in the numerical results is the peak position moving with field strength. The general trend is for the peak to move closer to 45° as the intensity increases.

We use the function $F(\cos\theta_M, \sin\theta_M \cos\phi_M)$ suggested in Ref.[73]):

$$F(\cos\theta_M, \sin\theta_M \cos\phi_M) = \cosh(\lambda \cos\theta_M)(1 + c^2 \cos^2\theta)(\cos\theta_M)^n (\sin\theta_M \cos\phi_M)^m \quad (4.30)$$

where for Σ orbitals $m = 0$ and for Π_x orbitals $m = 1$. For distances $r_0 = 6 - 8$ a.u. from the origin the parameters in Eq.(4.30) are $\lambda = 2.5$, $n = 1$, $m = 1$, $c = 0$, $C_\kappa = 0.66$, for the Dyson orbital corresponding to the ionization from the CO_2 ground state to the CO_2^+ ground state. The Dyson orbital was evaluated from the complete active space self-consistent field (CASSCF) wavefunctions [77] using the GAMESS code with the modified aug-cc-pV5Z basis [78, 79], where the L=5 functions were removed and 2 sets each of uncontracted even-tempered S, P, and D functions with orbital exponents scales by factors 0.4 and 0.16, relative to the most diffuse functions of the same symmetry in the original basis set were added. The CASSCF calculations use 16 (neutral) or 15 (cation) active electrons in 11 orbitals. The (3x) 1s atomic orbitals were not included in the active space.

The resulting angle-dependent factor $R(\theta_L)$, calculated using Eq.(4.29) (for a static field), is compared in Fig.4.3(b) with the results of ab-initio calculations for various field strengths . They are consistent with recent numerical results of [64].

The general shape of the analytical result is in agreement with numerics, as well as the fact that the peak is intensity dependent, but the details of the intensity-dependence of the peak differs. The appearance of a local feature near $\theta_L = 0$ for stronger intensities is also present in both calculations and the experiment. This agreement confirms our analysis, showing rotation of the maxima in the ionization rates with the field, though the exact dependence of the peak on field strength is an ongoing question.

The rotation is dictated by maxima in the momentum-space representation of the orbital, which are located around 50-60° . As described above, the momentum space features become progressively more important with increasing field strength. The interplay of coordinate and momentum-space features manifests itself via the contribution of the terms proportional to F_2 and F_3, which *interfere* with F_0. The $F_{1,2}$ terms arise from derivatives in directions orthogonal to z and maximize near sharp coordinate-space features. Naturally, such sharp features correspond to higher momentum components.

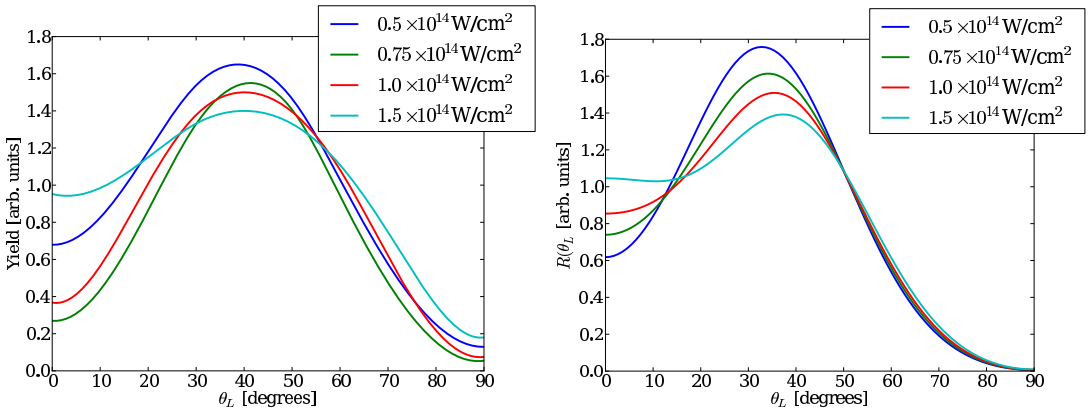

Figure 4.3: Ionization of a CO_2 molecule into the ground electronic state of the cation at the equilibrium geometry of the neutral. Contributions from both Π_x and Π_y channels are included. (a) Total ionization yield from numerical simulations including single ionization channel. The yields for different intensities has been scaled to clearly show the change of the peak vs intensity. (b) Angle-dependent factor $R(\theta_L)$ from the analytical analysis.

While our current analysis leaves out such intriguing effects as the interplay of different orbitals (channels) in molecular ionization [67, 68, 69, 80], which may become important in determining total strong-field ionization rates [64, 80], the first steps towards extension to multi-channel case have already been done [80].

4.2.3 Numerical solution

The above process attempts several analytic and semi-analytic treatments of the general equation (4.9). The analytic methods are quite successful and are designed specifically to avoid performing computationally intensive simulations, though there are several approximations made to allow for an analytical treatment. The benefit of a numerical approach is to verify these approximations and to find limits to the region in which the analytical methods are valid.

The numerical approach is done by solving equation (4.9) exactly after making use of the convolution theorem. Any approximation made in the analytical treatment is then not made and I get a solution that is closer to exact. The equation which is solved numerically is:

$$\Gamma = \frac{\kappa}{2\pi 2\pi\tau^2} e^{-2|\int_{z_0}^{z} p_z(z')dz'|} \int dp_x dp_y |\Phi(p_x, p_y, z_0) e^{-p_\perp \tau/2}|^2 \tag{4.31}$$

The algorithm is straight forward, all that is needed is the Dyson orbital on a grid. The

Dyson orbital is Fourier transformed then integrated with proper weights for the ionization probability. The Dyson orbital is obtained in the same method as the previous section; GAMESS is used to compute the complete active space self-consistent field (CASSCF) wave functions with a modified aug-cc-pV5Z basis[78, 79, 77]. There is however an important difference. The GAMESS orbitals here are polarized; they are calculated with a static electric field. The reason this is done is to produce polarized Dyson orbitals, which are slightly stretched in the direction of the field and are more suitable for matching the WKB solution in the tunnel.

The method described above requires the GAMESS orbital at every laser polarization, and since I am typically interested in angular ionization rates there can be many. For a full angular distribution the GAMESS calculations end up taking on the order of the length of time of an *ab-initio* numerical simulation. This means there is little or no benefit to using this algorithm. However two important assumptions can be tested. First, the WKB wave function is corrected for a coulombic potential and since the GAMESS orbitals can be used to calculate self-consistent potentials I can quantitatively measure how different the Coulomb potential is to the molecular potential inside the barrier. Second, the parameter z_0 is still present in the numerical calculation and must be chosen. The parameter formally dropped out of the analytical calculation. The ionization rate can now be calculated as a function of z_0 and the way it changes studies. By proving that the ionization rate changes slowly with the matching parameter I can justify the approximation used to remove z_0 from the analytic solution.

The electron density can be found directly from the output of a GAMESS calculation. This electron density is then used to solve Poission's equation for the one-electron potential associated with the Dyson orbital. Figure 4.4 shows the Coulomb potential and the potential calculated by GAMESS for H_2 aligned and anti-aligned to the laser field. The figure clearly shows that there is very little difference between the Coulomb potential and either orientation of the H_2 molecule. Indeed by 5 atomic units the difference between the real potential and the Coulomb potential is almost insignificant. This justifies our choice to approximate the true potential as coulombic.

The molecular potential can be approximated as a Coulomb potential only to a point. For a larger molecule or even a diatomic with a large internuclear separation this approximation will fail. It can be assumed that the approximation holds well enough to give physically relevant results but it must be treated carefully for larger systems.

The other key approximation is how the parameter z_0 is dealt with. In the theories above I have simply set z_0 to z_{ex} by analytically extending it to the exit of the barrier. In other theories, such as PPT, approximations are made in such a way as to cause the quantity z_0 to formally drop out of the final equations. This process neglects some important corrections which are kept in our more general derivation. However, it must be shown that the method that we use to remove z_0 dependence is valid.

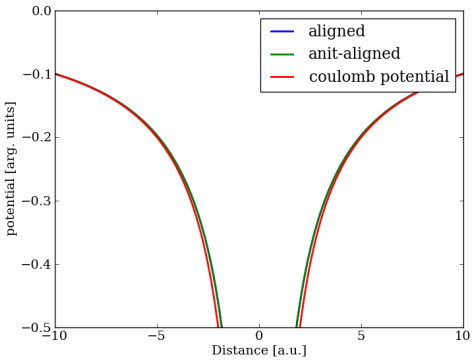

Figure 4.4: Comparison between the potential associated with the Dyson orbital of a Hydrogen molecule and the Coulomb potential. The two potentials differ very little in the under the barrier region.

We show that in the case of the Hydrogen and Nitrogen molecules the value of z_0 indeed doesn't matter, from this I can infer that there is little dependence in the general case as well.

First I compute the ionization rate numerically as described above. I perform this calculation at several alignment angles and several intensities. The value of z_0 is varied for each angle and intensity and I can see how the rate changes as a function of z_0.

Figure 4.5 shows the results of the numerical simulation for two alignment angles of H_2, aligned and anti-aligned. Each line represents a single intensity and the dotted line is what is calculated using the analytical formula. It is immediately clear that for the range of intensities that are of interest the rate is nearly flat across most of the tunneling region. The only deviations are near the exits and entrance of the tunnel; this is totally expected as the whole theory breaks down in these regions. The deviations also become more strong with intensity, again this is expected as the theory is invalid for higher intensities. I can conclude that the choice of z_0 is arbitrary and any value sufficiently inside the barrier yields the same result. This validates our choice of z_0 in the analytical derivation.

The numerical version of our general theory has proven to be useful in verifying assumptions made in the analytic derivation, though it is not very efficient on its own. I have shown that the choice of z_0 is not important and that the use of a Coulomb potential is a good approximation in the case of small molecules.

To close this chapter I will briefly discuss the limitations of this theory. The theory is limited in applicability in the same way as other quasi-static tunneling theories. The field can't be to strong or to high frequency. This translates to a Keldysh parameter of $\gamma < 1$. The tunneling regime must still hold with no over the barrier or multi-photon ionization.

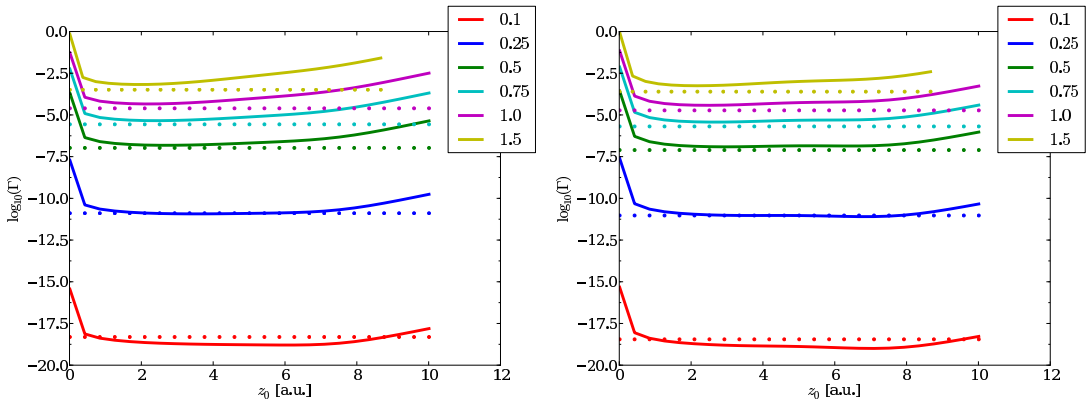

(a) aligned Hydrogen molecule.

(b) anti-aligned Hydrogen molecule

Figure 4.5: Ionization of a H_2 molecule computed using the numerical algorithm. The rate is nearly unchanged for most of the tunneling region. Lines are different intensities, given by the values in the legend multiplied by 10^{14}. The rate is plotted on a log scale and the dotted lines represent the rate calculated using the analytical formulas of the previous section.

Other key issues are related to complications relating to molecular systems. The theory will not work if there are many low-lying levels out of which electrons can tunnel. The multielectron nature of the process would override the simple tunneling picture used here. Finally the system can not be to large spatially and the ionizing orbital should be well localized.

Chapter 5

Applications of Tunnel Ionization: Laser Induced Electron Diffraction

The richness and complexity of tunneling in strong laser fields has been shown in the previous two chapters. While interesting in its own right tunnel ionization's real utility is in its applications to other phenomenon in strong field physics. Tunnel ionization forms the first step of the celebrated three step model[38, 40], this model which gives a fundamental explanation to most strong field phenomenon is well known throughout the field. This chapter will introduce the three step model and its applications in strong field physics. The model itself and most applications will be briefly commented on while laser induced electron diffraction will undergo a more thorough treatment.

5.1 Three - Step Model and selected applications

The three step model is a simple model which predicts the effect of an intense laser field on an atom. It was first proposed by Corkum[38] and Lewenstein[40] nearly 20 years ago and has its origins in work by Kuchiev[81]. The model uses a simple classical picture of the ionized electron to describe the dynamics in the strong field. The first step is ionization; this is tunnel ionization under the barrier created by the oscillating electric field of the laser. The second step is propagation, where the classical electron is pushed away from the ion then turned around by the field and accelerated back into the parent ion. The final step is the recollision step where the electron collides with the parent ion and does one of several things: recombines, leading to high harmonic generation(HHG), elastically scatters, leading to diffraction or inelastically scatters which leads to non-sequential double ionization. Figure 5.1 schematically shows the semi-classical three step model. The simple

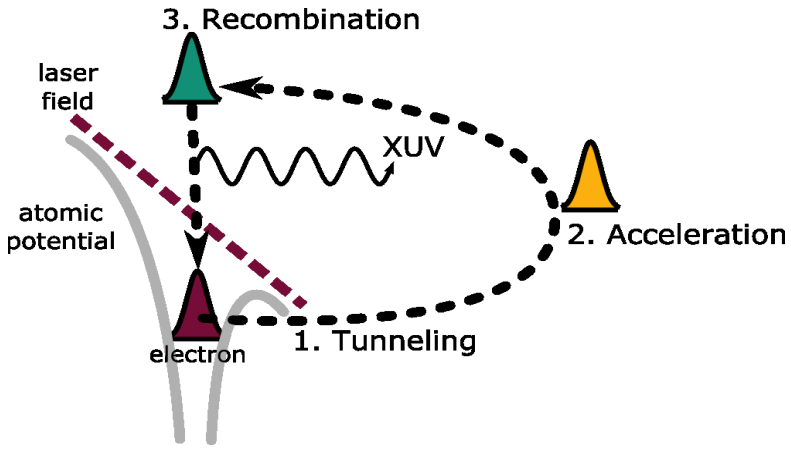

Figure 5.1: Schematic of the three step model. Showing 1. Tunneling, 2. Acceleration in the field, and 3. Recombination. Taken from [82].

three step model is remarkably accurate and has enjoyed much success in the past two decades.

We will now proceed with a derivation of the three-step model in the form of the Strong field approximation(SFA) applied to High Harmonic Generation(HHG) then discuss important discoveries and applications of the three-step model.

5.1.1 Derivation of SFA for HHG

The typical approach to laser matter interaction is to assume that the field is weak, this allows for the standard perturbation theory approximations to be used[9, 83]. The perturbation theory clearly breaks down when in the strong field regime. The reasonable thing to do would be to use perturbation theory but with a different perturbation. This is the essence of the Keldysh type theories; use the potential of the field free system as the perturbation and treat the laser field exactly. In this system I are able to derive an expression for HHG and illustrate the three-step model. I start with the time-dependent Schrödinger equation:

$$i|\dot{\Psi}\rangle = [\hat{H}_0 + \hat{V}(t)]|\Psi\rangle = \hat{H}_0|\Psi\rangle + |F(t)\rangle \tag{5.1}$$

Here $V(t)$ describes the interaction with the laser field and H_0 is the field-free Hamiltonian. I introduce the notation $|F(t)\rangle = \hat{V}(t)|\Psi\rangle$ for a reason, I will treat equation 5.1 as an inhomogeneous differential equation where $F(t)$ is the inhomogeneous part and the homogeneous part is the field-free equation.

$$i|\dot{\Psi}\rangle = \hat{H}_0|\Psi\rangle \tag{5.2}$$

The solution to equation 5.2 is trivial,

$$|\Psi^{(0)}\rangle = e^{-i\hat{H}_0 t}|\Psi(t=0)\rangle \tag{5.3}$$

where $|\Psi(t=0)\rangle$ is the initial wave function of the system and the superscript (0) designates this as a solution to the field free case. The inhomogeneous equation 5.1 can be solved using a standard approach. We look for $\Psi(t)$ with the following form:

$$|\Psi(t)\rangle = e^{-i\hat{H}_0 t}|C(t)\rangle \tag{5.4}$$

where $C(t)$ is a trial function found by plugging equation 5.4 into equation 5.1. Solving for $C(t)$ I find:

$$|C(t)\rangle = -i\int^t dt' e^{i\hat{H}_0 t'}|F(t')\rangle + |\Psi(t=0)\rangle \tag{5.5}$$

This can be used to find the formal solution of the Schrödinger equation.

$$|\Psi(t)\rangle = -i\int^t dt' e^{i\hat{H}_0(t-t')}\hat{V}(t')e^{-i\int^{t'}\hat{H}(t'')dt''}|\Psi(t=0)\rangle + e^{-i\hat{H}_0 t}|\Psi(t=0)\rangle \tag{5.6}$$

Where I used the full propagator of equation 5.1:

$$|F(t)\rangle = \hat{V}(t)|\Psi(t)\rangle = \hat{V}(t)e^{-i\int^t \hat{H}(t')dt'}|\Psi(t=0)\rangle \tag{5.7}$$

This solution is exact, without any approximations being made. The first term is the field induced piece and the second term is the field free term. Though complicated and opaque this equation is the starting point for some interesting approximations. First I will project this state onto the final state of the system, called $|\Psi_f\rangle$. I will assume that this state was not originally populated so that the field free term is zero. The transition amplitude is then:

$$a_{fi}(t,t_i) = -i\int_{t_i}^t dt'\langle\Psi_f|e^{i\hat{H}_0(t-t')}\hat{V}(t')e^{-i\int^{t'}\hat{H}(t'')dt''}|\Psi(t=0)\rangle \tag{5.8}$$

The term above is called the direct S-matrix amplitude. It connects the initial state $|\Psi(t=0)\rangle$ to the final state $|\Psi_f\rangle$. The physical interpretation of the direct S-matrix term is as follows; from time t_i to some instant t' the system evolves under the influence of both the field free potential and the laser field. At t' it is instantaneously kicked by the field for the last time, then it evolves under the field free Hamiltonian until it is measured in the final state at t. This means that from the moment t' the system sits in the final state accumulating phase and does not make any more transitions.

Another more illuminating way to view equation 5.8 is to use the property of the Schrödinger equation that makes it symmetric under time reversal. By performing this time reversal I arrive at the time-reverse direct S-matrix amplitude:

$$a_{fi}(t,t_i) = -i\int_{t_i}^{t} dt' \langle \Psi_f | e^{-i\int^{t'}\hat{H}(t'')dt''}\hat{V}(t')e^{i\hat{H}_0 t'}|\Psi(t=0)\rangle \tag{5.9}$$

It is from this equation that I can make the Strong Field Approximation(SFA) and derive the three-step model. I must first look at the physical meaning of equation 5.9. It is similar in concept but completely different in physical terms to the time-direct version. From the initial time t_i until some instant t' the electron sits in the ground state acquiring phase, then at t' it is instantaneously kicked by the laser field into the continuum where it evolves under the full Hamiltonian until the final time t. In this picture it is important to realize that the ground state is the only bound state to take part in the evolution and all other states are ignored. While the electron is in the continuum it is dominated by the effect of the laser field. It is then plausible to replace the full propagator in equation 5.9 with an approximate propagator that only accounts for the effect of the laser field, ignoring the atomic potential. This is the Strong Field Approximation (SFA).

The reason this is useful is that the propagator for an electron in an oscillating field is known analytically. It is called the Volkov propagator. The use of the Volkov propagator significantly simplifies the S-matrix amplitude as we will see below; first I will sketch the derivation of the Volkov propagator.

The free electron in the laser field follows a simple motion: it only oscillates in the electric field of the laser. If at time t' it has a kinetic momentum $\mathbf{p}(t')$, then I know its kinetic momentum at any later time t by the following equation

$$\mathbf{p}(t) = \mathbf{p}(t') - \mathbf{A}(t') + \mathbf{A}(t) \tag{5.10}$$

where $A(t)$ is the vector potential of the electric field defined as

$$\mathbf{E}(t) = -\frac{\partial \mathbf{A}(t)}{\partial t} \tag{5.11}$$

The instantaneous energy during these oscillations is

$$E(t) = \frac{1}{2}[\mathbf{p}(t') - \mathbf{A}(t') + \mathbf{A}(t)]^2 \tag{5.12}$$

and the Volkov propagator is

$$e^{-i\int_{t'}^{t}\hat{H}(t'')dt''}|\mathbf{p}(t')\rangle = e^{-i\int_{t'}^{t}E(t'')dt''}|\mathbf{p}(t)\rangle \tag{5.13}$$

This propagator can then be used in equation 5.9 to simplify the amplitude of finding an electron in state $|\mathbf{p}\rangle$ at time t.

$$a_{\mathbf{p}}(t) = -i \int_{t_i}^{t} dt' e^{-i\int_{t'}^{t} E(t'')dt'' + iI_p(t'-t_0)} \langle \mathbf{p} + \mathbf{A}(t') - \mathbf{A}(t) | \hat{V}(t') | g \rangle \tag{5.14}$$

The physical interpretation given above is even more clear in this form and we can now look at high harmonic generation. First I should point out several major flaws with the SFA and their consequences.

1. the ionization amplitude is incorrect as it doesn't consider the core. This can be mitigated by using well known tunneling theories (see Chapters 2 and 4).

2. propagation is also wrong as it does not include scattering off the core or the Coulomb effects in the continuum.

3. the SFA is the first term in a perturbative expansion in terms of the atomic potential, this series does not converge in general.

4. the SFA is not gauge invariant, this is a major drawback. The above derivation was performed in the length gauge ($V = d\mathcal{E}$), the other approach is to use the velocity gauge ($V = \hat{p}A$). Where $\hat{p}$ is the canonical momentum. The gauge problem manifests itself in the pre-factor so the theory is good to exponential accuracy and most of the physics is preserved even when dropping the pre-factor.

5. The SFA uses Volkov waves (plane waves) which is complete and not orthogonal to the initial state of the system so I end up with an overcomplete basis set. This again only affects the pre-factor and I can maintain the important physics and ignore the prefactor

Despite these problems the SFA works surprisingly well and it has broad applicability, I will now apply it to HHG as an illustration of the three-step model.

High harmonics are generated when an electron is recaptured by its parent ion. The electron releases all of the energy gained in the field as one big photon which will be a harmonic of the incident field. The laser induced polarization can be defined as follows

$$\mathbf{P}(t) = N\mathbf{d}(t) = N\langle \Psi(x,t) | \mathbf{d} | \Psi(x,t) \rangle \tag{5.15}$$

Where N is the number density. All that is needed is $\langle \Psi(x,t) | \mathbf{d} | \Psi(x,t) \rangle$ and the wave function is already known from the SFA:

$$\Psi(t) = a_g(t)|g\rangle + \int d\mathbf{p} |\mathbf{p}\rangle a_{\mathbf{p}} \tag{5.16}$$

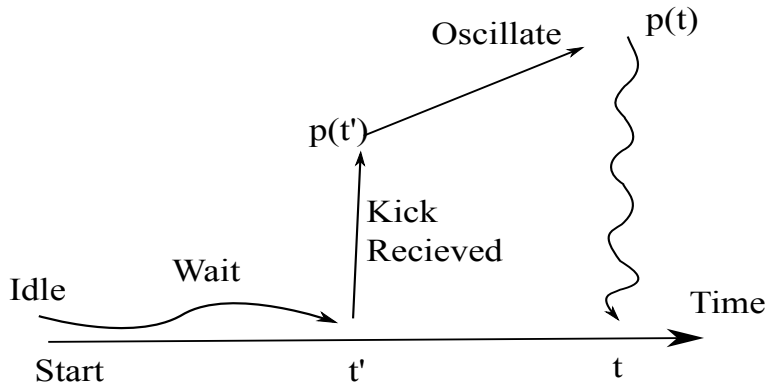

Figure 5.2: Graphical explanation of the harmonic component of the dipole $d(\Omega)$. The electron is kicked into the continuum at time t' with momentum $p(t')$, oscillates between t' and t finally reaching the state with momentum $p(t)$ from which it emits a photon of energy Ω.

Now, calculating the dipole moment I get

$$\mathbf{d}(t) = -i \int_{t_i}^{t} dt' \int d\mathbf{p} e^{-i\int_{t'}^{t} E(t'')dt'' + iI_p(t'-t_0)} \langle \mathbf{p} + \mathbf{A}(t') - \mathbf{A}(t) | \hat{V}(t') | g \rangle \langle g | \mathbf{d} | \mathbf{p} \rangle \quad (5.17)$$

We have assumed that the ionization is not too strong so that I can ignore the first term in equation 5.16. Since the SFA is accurate only in the exponent they are incorrect and are not needed, to simplify this equation I will drop all prefactor terms. I will also Fourier transform the dipole as we are interested in the Fourier components of the dipole.

$$\mathbf{d}(\Omega) \approx -i \int dt \int_{t_i}^{t} dt' \int d\mathbf{p} e^{-i\int_{t'}^{t} E(t'')dt'' - iI_p(t'-t_0) + i\Omega t} \mathcal{E} \cos \omega t' \quad (5.18)$$

The physical interpretation of the above equation is demonstrated graphically in Fig 5.2. The electron can be born at any time t' - thus the integral over t'. It can emit a harmonic at any moment t - thus the integral over t and the electron can be in any $|\mathbf{p}\rangle$ state at the moment of emission hence the integral over $\mathbf{p}$. The phase term Ωt corresponds to the emission of a photon with energy Ω and the rest of the phase is from the propagation away from and back to the parent ion. The I_p term is due to the energy being measured from the ground state.

We will use the stationary phase method to perform the integrals in equation 5.18. This is valid when the ponderomotive energy, the average energy of a free electron oscillating in a laser field, is much larger than the frequency of the field.

$$U_p = \mathcal{E}^2/4\omega^2 \gg \omega \quad (5.19)$$

For typical experimental parameters this inequality holds and the stationary phase method is valid. To perform the integrals I must find the stationary phase points for all three integrals in equation 5.18, below we define the phase and the three stationary phase points.

$$\Phi(t,t',p) = \int_{t'}^{t} E(t'')dt'' + I_p(t-t') - \Omega t \tag{5.20}$$

$$\int_{t'}^{t} dt''[\mathbf{p} + \mathbf{A}(t'') - \mathbf{A}(t)] = 0 \tag{5.21}$$

$$\frac{1}{2}[\mathbf{p} + \mathbf{A}(t') - \mathbf{A}(t)]^2 + I_p = 0 \tag{5.22}$$

$$\frac{1}{2}\mathbf{p}^2 + I_p = \Omega \tag{5.23}$$

The three stationary phase equations can be rewritten in a transparent way:

$$\mathbf{x}(t) = \mathbf{x}(t') \tag{5.24}$$

$$\frac{1}{2}\mathbf{p}^2(t') + I_p = 0 \tag{5.25}$$

$$\frac{1}{2}\mathbf{p}^2(t) + I_p = \Omega \tag{5.26}$$

The first equation specifies that the electron must return to where it was born in order to emit a photon. This means that the electron has to return to its parent ion in order to recombine. The second condition cannot be satisfied classically as the electron must have negative energy. This can only happen in tunneling so that the time is complex. Finally the third condition is a simple statement of energy conservation.

These three equations are the essence of the three step model. Step one the electron must tunnel, step two the electron oscillates in the field and returns to its parent ion and step three the electron recombines and emits a photon.

We will briefly present the result of the stationary phase integration and some of the main features of the resulting spectrum. The integral above reduces to the following amplitude which can be separated into three terms representing each step of the three step model.

$$d(\Omega) = \sum_t a_{ion}(t_b)a_{prop}(t_b,t)a_{rec}(t,\Omega)e^{-i\int_{t_b}^{t}\frac{1}{2}[A(t'')-A(t_b)]^2dt''-iI_p(t-t_b)+i\Omega t} \tag{5.27}$$

$$a_{prop} \propto \frac{1}{(t-t_b)^{3/2}} \tag{5.28}$$

$$a_{resc} \propto \mathcal{E}\cos\omega t_b d_g(\Omega) \tag{5.29}$$

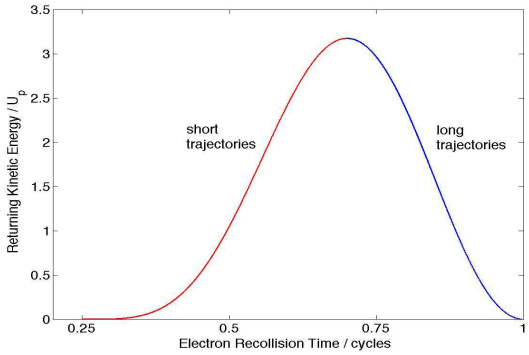

Figure 5.3: Kinetic energy of the electron at the moment of first return to the nucleus, as a function of the moment of return. Provided by David Hoffman.

The sum counts all the stationary phase trajectories that lead to the same energy, in general there are many. In equation 5.28 the whole harmonic component of the HHG spectrum is given by two of the three factors, the third factor is the ionization component and is identical to the ADK/PPT formulas discussed in Chapter 2 for ions and Chapter 4 for molecules. The propagation factor a_{prop} describes the spreading of the wave packet with time and the recollision term describes the overlap between the returning electron and the ground state — the probability of a specific frequency being emitted at a specific time.

Figure 5.3 shows one of the most important results of this analysis of HHG: the energy of return is limited from above. Figure 5.3 shows the return energy in units of the ponderomotive potential as a function of recollision time in cycles. The maximum return energy is $3.17U_p$ which occurs at nearly 0.75 cycles, which corresponds to a phase of 17 degrees at time of birth.

This upper limit means that the HHG spectrum cannot extend past $I_p + 3.17U_p$. The procedure to find this cut-off is to solve the stationary phase equations 5.24,5.25,5.26 for all possible times of birth. This gives a unique connection to time of recollision and the final momentum of the electron.

From figure 5.3 it is clear that for every possible energy there are two possible return times. These are known as short and long trajectories and there is much interesting physics surrounding them. Another important feature of this phenomenon is that the HHG pulse is chirped, this also has major experimental implications which I will not discuss here.

Finally as a reference I have included a typical HHG spectrum obtained using the above analysis. The cut-off can clearly be seen as well as the plateau region.

In this section I have introduced the three step model and derived it for the process

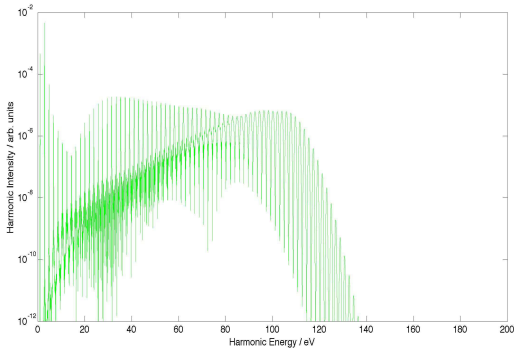

Figure 5.4: A typical HHG spectrum for 800nm light and 10^{14}W/cm^2 intensity. The cut-off and plateau region are clearly visible. Courtesy of David Hoffman.

of high harmonic generation. Next section will be devoted to illustrating recent results in HHG and non-sequential double ionization(NSDI) followed by an in depth look at laser induced electron diffraction(LIED).

5.1.2 Current status of HHG and NSDI

First I refer the reader to a recent review of strong field physics, this reviews the current status of most strong field phenomena[41]. We will highlight some of the important results contained in this review and explore the cutting edge of the field that is not contained in the above review. The two topics I will pay particular attention to are attosecond streaking and high harmonic spectroscopy.

Attosecond streaking

Attosecond streaking refers to the process of measuring an IR pulse using an attosecond XUV pulse in a pump probe configuration. The idea is to generate an XUV pulse through HHG then use that pulse to probe another process. First discussed here: [84, 85, 86], this method accurately measures the electric field of the IR probe[87, 88, 2]. Recently there have been several other applications of this concept to measure 'tunneling time'[89], and phase delays between states in solids[90] and gases[91] as well as valence electron motion in gases[92].

The concept behind the attosecond streak camera is straight-forward. An attosecond XUV pulse is used to single-photon ionize a gas which launches a wave packet directly into the continuum. This is done in the presence of an IR field; the delay between the IR field

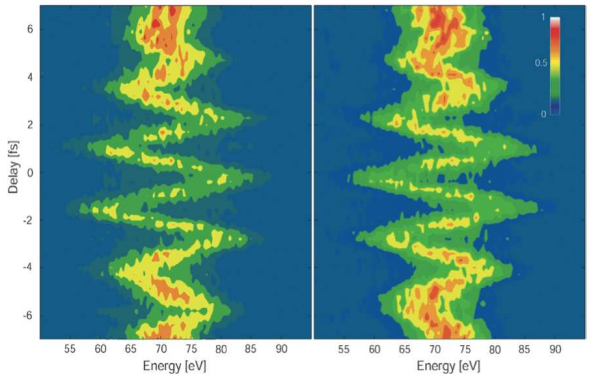

Figure 5.5: Light wave oscillations of a phase stabilized few-cycle laser pulse recorded over a delay interval of ± 7fs around the envelope maximum of the laser field for two different phase settings of its CEP that differ by π. Taken from [87]

and the XUV field can be controlled. Once again we make use of the simple analysis of an electron in the continuum presented above:

$$\mathbf{p}(t) = \mathbf{p}(t_b) - \mathbf{A}(t_b) + \mathbf{A}(t) \tag{5.30}$$

This states that the momentum at some time t can be related to the momentum at some other time t_b by the vector potential. The final momentum is recorded in the experiment and the initial momentum is known as the initial state is known. The vector potential at the detector is zero so therefore the vector potential at the time of birth can be found. By scanning the delay between the two fields the vector potential at any time can be found and the vector potential of the IR pulse can be retrieved (both strength and phase). In principle streaking is that simple, though in practice things are much harder. See for example[84] for a complete description of the algorithms used to retrieve the vector potential using this streaking method. Figure 5.5 shows the vector potential of a short pulse recorded using the attosecond streak camera. The figure shows the resulting vector potential for two separate CE phases.

Tomography and High harmonic spectroscopy

The original paper on tomography from the NRC group[93] has set off a huge wave of research and caused a great stir in the community with over 500 citations in six years. The principle behind this paper is to image the molecular orbitals, particularly the highest occupied molecular orbital(HOMO) of a target molecular gas. This technique would enable the coveted molecular movie to finally be produced.

The idea of tomography comes from the structural minimum discovered by Lein et al.[94, 95, 96]. They found that HHG from molecules is angle dependent and exhibits a minimum at the photon energy which corresponds to a destructive interference from the emission from different atoms in a molecule.

The idea that high harmonic spectra contains information on the target and the ability to align molecular samples to a high degree is what led to the first tomography experiment[93]. In the experiment HHG spectra were taken from aligned molecular samples with many different polarizations. These 'slices' then contained information on the molecule at a variety of angles. Standard tomographic reconstruction algorithms can then be used to reconstruct the orbital from which the electron ionized.

Figure 5.6 shows the results obtained for N_2. The agreement between the reconstruction in the top frame and the *ab-initio* results in the bottom frame is remarkable. The beating along the edges of the reconstruction arise from not sampling the high energy part of the orbital (the cut-off of the HHG spectrum is too low). The shocking results obtained for N_2 has lead to a huge body of work to extend this to other molecules and to theoretically confirm or refute the results shown in [93].

Theoretical studies led by Smirnova et al.[77, 97, 98, 99] have recently concluded that the tomographic reconstruction of N_2 was an outlier and that any other molecules would not allow for such clean reconstructions. This theoretical evidence is based on several realizations: first, the plane wave reconstruction used experimentally is not accurate (this points to a breakdown in the SFA) and, second, multi-electron effects cannot be ignored, specifically multiple ionization channels are present and therefore multiple molecular orbitals coherently interfere.

Despite the realization that molecular orbital tomography is not as straight forward as once thought there is still much advancement in the field. The discovery of multiple ionization channels has lead to the so called 'dynamic minimum' which competes with the structural minimum of Lein has lead to several useful results and much research into hole motion in molecular ions and new types of spectroscopy[100, 101, 102, 103, 104, 105]. There has also been attempts to adapt tomographic reconstructions to work for more than just N_2 for example see:[71, 70].

While the original tomographic reconstruction was not the molecular movie that it was originally designed to be it has ignited a huge amount of research and many more exciting methods are being developed which will hopefully lead to the elusive molecular movie.

Non-sequential double ionization

Non-sequential double ionization (NSDI) is the third process that can occur in strong laser fields. It was discovered by Suran and Zapesochnyi[106, 107] and subsequently

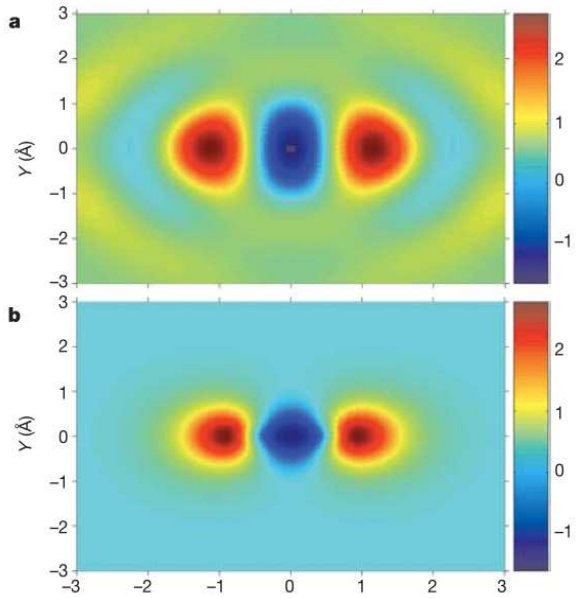

Figure 5.6: Molecular orbital wavefunction of N_2. a) Reconstructed wavefunction of the HOMO of N_2. The reconstruction is from a tomographic inversion of the high harmonic spectra taken at 19 projection angles. Both positive and negative values are present, so this is a wavefunction, not the square of the wavefunction, up to an arbitrary phase. b) The shape of the N_2 $2p\sigma_g$ orbital from an *ab-initio* calculation. The colour scales are the same for both images. Taken from [93]

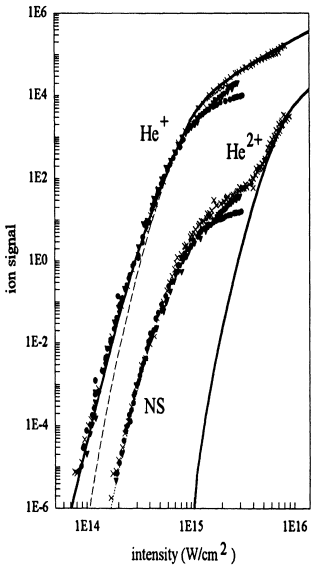

Figure 5.7: Measured He ion yields for linear polarized, 100 fsec, 780nm light. Calculations are shown as solid (SAE) and dashed (ac-tunneling) lines. The measured intensities are multiplied by 1.15. The solid curve on the right is the calcuated sequential He^{2+} yield. Taken from [108]

rediscovered[108] for strong IR fields. A resurgence of interest has followed new experimental techniques which enable better detection and analysis of the electrons in coincidence. The key lies in the COLd-Target Recoil Ion Momentum Spectroscopy (COLTRIMS) technique[109] also known as the reaction microscope. This allows for the detection of the ion fragments and any electrons in coincidence. The momentum of all the fragments are recorded to give a clear picture of the non-sequential process.

NSDI can occur when the recolliding electron inelastically scatters off its parent ion, in contrast to when it recombines(HHG) or elastically scatters(LIED). The recolliding electron gives some of its energy to its parent ion leading to a second correlated ionization. This process is among the simplest examples of electron-electron dynamics in strong fields.

The signature of the NSDI process is the so called 'knee'[107] in the ionization yield as a function of intensity, see figure 5.7. The knee occurs when the transition from sequential double ionization to non-sequential double ionization occurs. The sequential process is when a second electron is tunnel ionized in seperate events later in the laser pulse. The transition to NSDI occurs when the field becomes strong enough that the recolliding electron has enough energy to cause a second ionization.

The most recent results on NSDI relate to the understanding of the correlated momentum spectra obtained by the COLTRIMS aparatus including the so called 'fingers' and of below-threshold NSDI. Below-threshold NSDI occurs when the electron recollision does not give sufficient energy to the parent ion to cause a second ionization. The energy is enough to excite an electron to a high enough state that it is immediately field ionized. For a full discussion see for example: [110].

5.2 Laser Induced Electron Diffraction (LIED)

Electron diffraction is one of key tools in studying structures. Modern electron diffraction setups use an electron gun to image a target. The spatial and temporal resolution of the setup are determined by the de Broglie wavelength of the electron and the duration of the electron pulse. The combination of sub-Angstrom spatial and few hundred femtoseconds temporal resolution are possible today [111, 112]. Given that electrons repel each other, shortening of the electron pulse to 100 femtoseconds and below to improve the temporal resolution requires significant reduction in the electron density. Maintaining strong signals favours high densities, i.e. solid-state targets (see e.g. [111]).

It has recently been proposed that laser-induced electron re-scattering could be an alternative to traditional electron diffraction [113]. In this approach the number of electrons in the diffracting pulse is reduced to one (per molecule): the electron used for diffraction is taken from the molecule itself. Hence, there are no space-charge effects to lengthen the electron pulse, making sub-femtosecond temporal resolution possible. Since the electron does not have to be transported from afar, the scattering probability is orders of magnitude higher. The electron is detached from the parent molecule by an infrared laser field. Oscillating in the laser field, it re-scatters on its parent ion [38], picking up diffractive information. In principle, it should be possible to obtain sub-Angstrom spatial and sub-femtosecond temporal resolutions[95, 94, 114, 115, 116, 117, 118, 119, 120].

There have been several studies exploring the feasibility of laser-induced electron diffraction (LIED). Two and three-dimensional calculations have been carried out which show signatures of diffraction [95, 94]. Analytical calculations [114] and numerical two-dimensional [114] and three-dimensional [115, 116] simulations clearly show diffraction in H_2^+ and give recipes to measure and read diffraction patterns [121].

Recent advances in experimental technology have led to the first experimental studies of LIED [74]. Angle and energy-resolved electron spectra appear to contain diffraction patterns, when measured in coincidence with singly charged molecular ions. Coincidence measurements allow one to effectively separate the elastic scattering channel from inelastic channels. Indeed, in the presence of a strong laser field, excitation of the molecular ion by the re-colliding electron almost inevitably leads to further ionization, i.e. production of

doubly charged ions. The appearance of singly charged ion effectively rules out inelastic channels.

So far, theoretical and experimental studies of LIED have concentrated on linearly polarized laser fields. This restriction confines the motion of the recolliding electron along the laser polarization axis, leading to extra complications in the diffraction pattern. Indeed, each half cycle, an electron wavepacket is ejected from the molecular ion. In a linearly polarized field, a train of several wavepackets recollides within one pulse. Overlap of multiple diffraction events, each yielding different energy spectra due to changing laser intensity, makes the already complicated task of analyzing diffraction pattern even more difficult. In longer pulses, it is also possible for an electron wavepacket to make multiple returns to its parent ion [122, 123], with different energies. The diffraction information it retains from the first recollision is convoluted by several recollision and diffraction events.

The primary goal of LIED is to obtain structural information from the target molecule. The retrieval of this information turns out to be extremely complicated; some of the problems are:

1. non-monochromatic electron pulse. The returning electron wave packet contains energies ranging from 0ev $\rightarrow$ 100eV, the superposition of all these energies convolutes the energy resolved spectrum in the presence of the laser field.

2. the presence of the laser field. The laser field distorts the spectrum and adds an extra dependence on recollision time and the spectrum ends up being 'stretched' by the field

3. multiple recollisions of the same wave packet. After a wave packet recollides it does not go straight to the detector, instead it continues to oscillate in the field and in principle is able to return to the core and elastically scatter several more times. This is shown in Figure 5.8(b). This shows the current density seen by the parent ion from a single electron wave packet. There are many recollisions from the same wave packet with at least 2 of significance.

4. multiple ionization events from the same pulse. For nearly every pulse currently available in a lab there are at least two ionization events that contribute to the LIED spectrum, in most cases there are many more. This is illustrated in 5.8(a) where the ionization events for a short pulse are circled in green.

It turns out that all of these problems can be overcome. Items 1 and 2 listed above can be solved using the monochromatic cuts of [114] and items 3 and 4 can be minimized by the use of orthogonal two color(OTC) fields as discussed below and in [124, 72].

Before beginning the discussion of OTC fields I will first outline the process of using the monochromatic cuts. To understand the effect of the field on the spectrum I invoke the

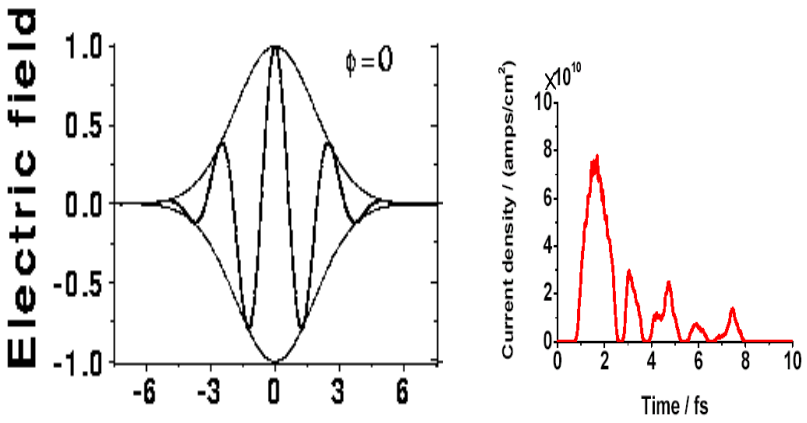

Figure 5.8: Illustrations of complications in determining structure from LIED. (a) Typical short pulse used in LIED calculations, the two contributing ionization events are circled in green. (b) Current density seen by parent ion for single electron wave packet. Showing several recollision events from the same electron

semi-classical analysis of the previous section. It is clear that the velocity of a scattered electron without the laser field is $v_x^2 + v_y^2 = v^2$ where v is the incoming velocity and v_x, v_y are the parallel and perpendicular components of the velocity after scattering. The effect of the laser induced oscillation changes the elastic scattering condition to the following:

$$(v_x - v_0 \sin \omega t)^2 + v_y^2 = v^2(t), v_0 = E/\omega \tag{5.31}$$

Here v_x, v_y are the *final* components of the velocity and $v(t)$ is the incoming velocity, which is now a function of the time of recollision. This shows that the diffraction image taken at a specific energy will lie on a circle of radius $v(t)$ and will be shifted along the x-axis by $v_0 \sin \omega t$ (the vector potential at the time of recollision). The technique to recovering the diffraction image is to take a cut along the circle described by equation 5.31. This is then guaranteed to be a circle of constant energy of recollision and a meaningful diffraction spectrum can be recovered from this monochromatic cut.

Figure 5.9 shows the results of an *ab-initio* calculation performed by Spanner et al. [114]. These spectra highlight the important aspects of LIED spectra and serves as a test case for reading diffraction images using the monochromatic cuts. The figures show the electron momentum spectrum from diffraction from a Hydrogen molecular ion (H_2^+) at an internuclear distance of 4 atomic units. This diatomic should exhibit Young's double slit type diffraction peaks and minima. First let us describe the basic features of figure 5.9. The strong signal in the center of the momentum spectra are the direct electrons, these extend to $2U_p$ and wash out the forward scattering part of the diffraction image. The back

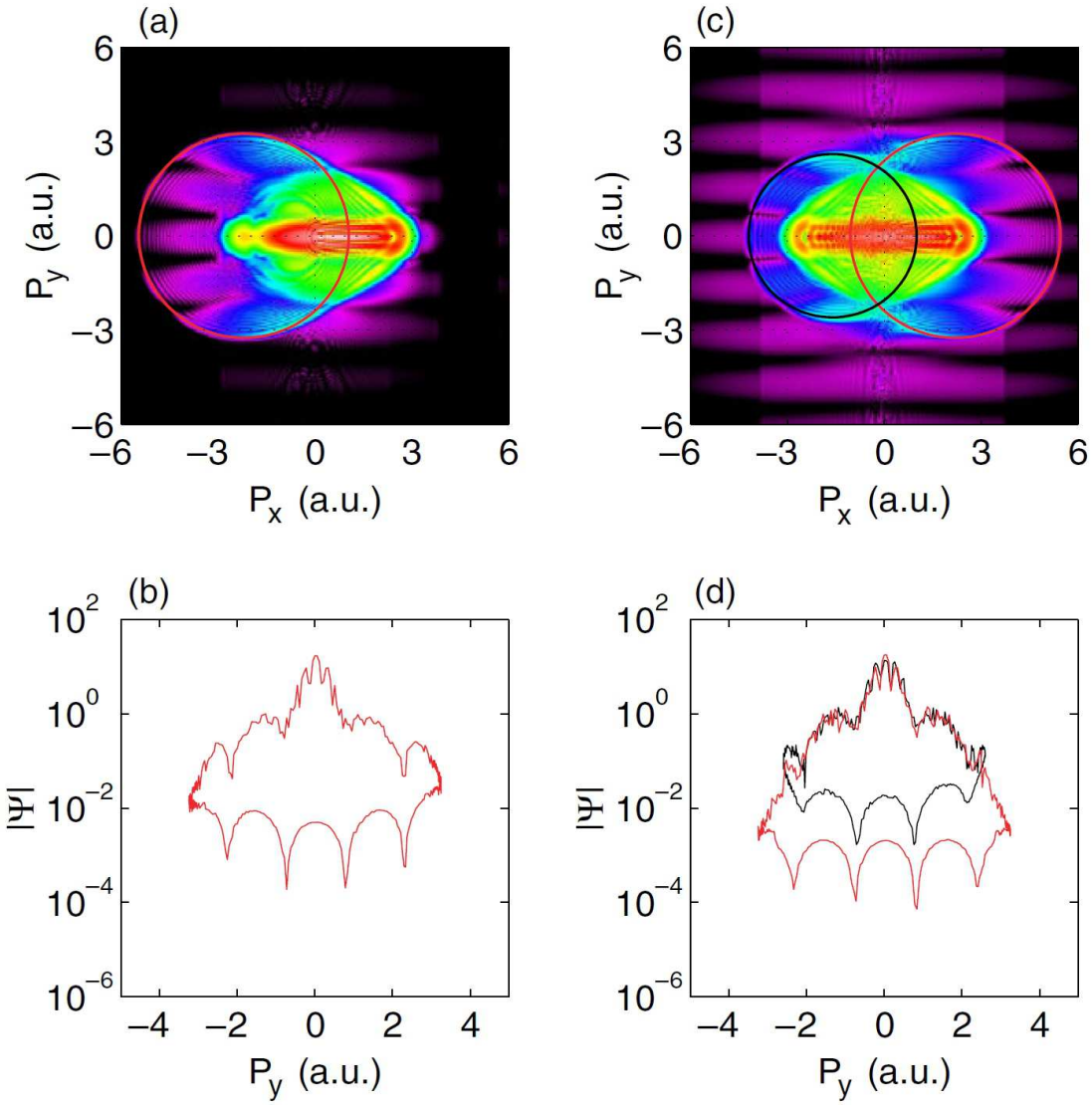

Figure 5.9: (a) Electron spectrum $|\Psi(v_x, v_y)|$ for a 1.25 cycle pulse with a constant amplitude, E=0.14 a.u. (I$\approx 6.9 \times 10^{14}$ W cm^{-2}) and $\lambda = 800nm$, each new color represents the order of magnitude; (b) spectral cut for a fixed moment of recollision ($\omega t \approx 4.4$);(c),(d) same as (a), (b) but for a 5 fs pulse $f(t) = \cos^2(\pi t/2T)$, T=5fs. Taken from [114]

scattering region extends to the higher energy part of the spectrum the peaks and valleys are clearly caused by diffraction. The circular fringes are interference fringes between long and short trajectories in the same ionization rate. The key elements for reading these images is to have strong signal in the backscattering region (requires a lot of statistics experimentally) and high contrast between peaks and minima. The cuts in figure 5.9(d) show the monochromatic cuts for two ionization events. The red line corresponds to the first circle in figure 5.9 and the black to the second circle. The peaks and minima can be fitted to the expression for double slit diffraction and the fitting factor will correspond to the internuclear separation.

For very short pulses the linear field works quite well. For longer pulses the effects discussed above start to blur the clear diffraction image and another method has to be used. Below I discuss the use of OTC fields to control rescattering and allow for the use of longer pulses. Using OTC fields one can steer trajectories and prevent wave packets from recolliding.

5.3 Orthogonal Two Color Fields

We analyze the use of orthogonally polarized two-colour (OTC) fields to eliminate the problems associated with LIED. Two orthogonal polarizations drive the electron motion in two dimensions. Classically, proper tuning of the frequencies, strenghts and the relative phase of the two fields allows one to guide and shape the electron trajectories [125, 126, 127] . These classical trajectories form the skeleton for the quantum propagation of the electron wavepackets. Shaping the trajectories, one gains control not only over the recollision times, angles, number and energy of the recollision events, but also over the sub-cycle ionization rates which control populations of different continuum trajectories. Recent studies have shown that controlling ionization rates and times by using laser fields with time-dependent polarization one can control key aspects of attosecond pulse trains [128, 129, 130], which result when the returning electron recombines to its original bound state. It has been suggested that by controlling recollision angles and times one can select the polarization of attosecond pulses and produce single-shot tomographic maps [125, 127].

Our goal is to control electron trajectories to limit the number of returning wavepackets. The ultimate result is only a single recollision event by a shaped electron wavepacket. Not only this makes the LIED pattern easier to read, but it also dramatically improves the temporal resolution, which is determined by the duration of this single recollision event.

As mentioned above, I use two orthogonally polarized laser pulses to achieve control of the re-collision event. The x axis is defined as the polarization of the primary field. The primary field is the stronger of the two and is a few cycle pulse fixed at a central wavelength of 800nm. The orthogonal field, defining the y axis, is a weaker field with

a variable wavelength. For computational convenience the secondary field has the same pulse length and envelope as the primary field. This restriction is for simplicity only as in principle the envelopes could be completely arbitrary. For example, the orthogonal field could be much longer than the primary field and the result would be similar to those shown below as long as the orthogonal field is too weak to ionize on its own. I shall start with the qualitative analysis, and then move to numerical simulations. For the qualitative analysis, I explicitly assume that ionization occurs in the direction of the primary field, while the weaker second color is responsible for steering the electronic wave packet. We do not make such assumption in the full numerical simulations. The field strength of the secondary field is fixed to one half the primary field, this ensures the validity of the above assumption. There are three remaining tunable parameters: the frequency of the secondary field and the carrier envelope phase of each field. Tuning of these parameters gives control over the LIED spectra. Equations (5.32,5.33) give the general expression for the vector potentials.

$$A_x(t) = \frac{E_{x0}}{\omega_x} f(t) \sin(\omega_x t + \phi_x) \tag{5.32}$$

$$A_y(t) = \frac{\eta E_{x0}}{\kappa\omega_x} f(t) \sin(\kappa\omega_x t + \phi_y) \tag{5.33}$$

The associated electric field is defined as $\mathbf{E}(t) = -\frac{d\mathbf{A}(t)}{dt}$. In Eqns (5.32,5.33) E_{0x} is the electric field strength of the primary field and η is the ratio of the strength of the two fields, here fixed to 0.5. The frequency of the primary field is ω_x and κ is the ratio of the frequencies. I fix the frequency of the primary field and tune κ. The envelope function is, $f(t) = \cos^2(\pi t/2T)$, T is the full-width half max of the pulse. The ϕ_i are the carrier envelope phases of each pulse. In a previous paper[124] only the relative phase of the two colors was investigated. The relative phase is $\Delta\phi = \phi_y - \kappa\phi_x$; In the few-cycle regime, the relative phase between the two colors is no longer sufficient to describe the two-color control, the carrier-envelope phases of both colors have to be explicitly specified. This statement is illustrated in Fig. 5.10. The top frame of Fig. 5.10(a) shows an OTC given by equations (5.32,5.33) with CEP phases $\phi_x = \pi/3$,$\phi_y = \pi/2$ and the top frame of Fig. 5.10(b) is the same fields with CEP phases $\phi_x = \phi_y = 0$. Both frames have the same $\Delta\phi = 0$. The major differences between the figures is the height and location of the peaks. This affects the ionization rate and the amount of energy an electron can gain while in the continuum. The displacement of the electron in the orthogonal direction is also affected, thereby changing the character of the re-collision.

We focus our study on two values of κ and vary the values of ϕ_x and ϕ_y. The two values of κ illustrate two different types of control: short-wavelength and long-wavelength. The types of control refer to the wavelength of the control field relative to the primary field, which is fixed at 800nm. For the short-wavelength control field I set $\kappa = 3/2$, which corresponds to the control field wavelength of 533 nm. For the long-wavelength control

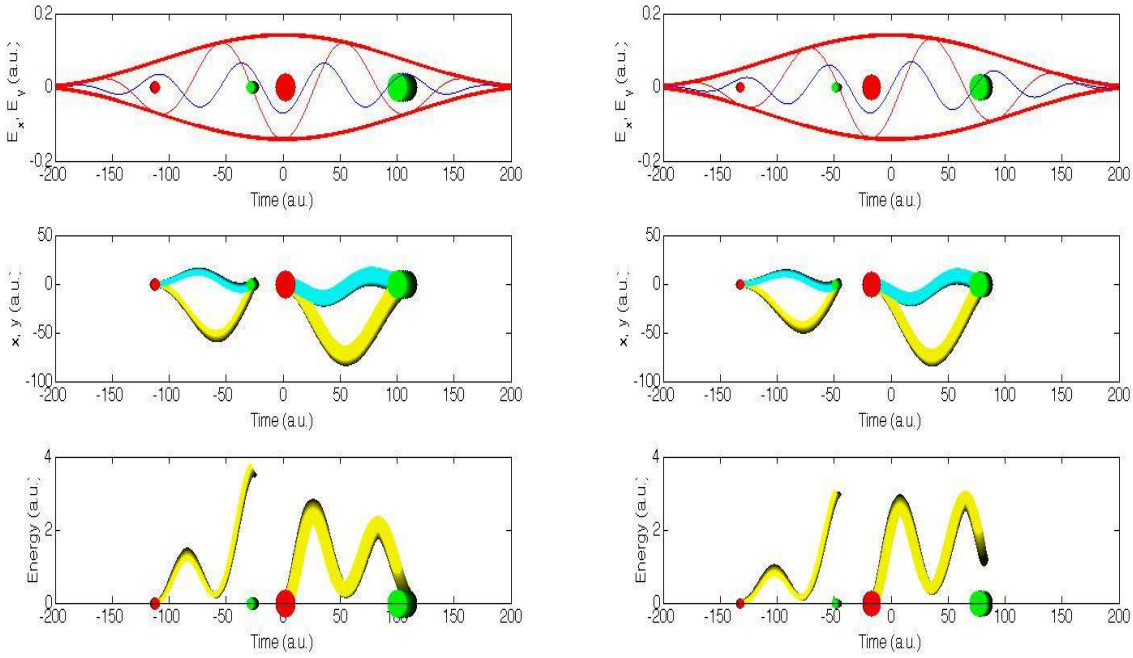

(a) $\phi_x = \phi_y = 0$ (b) $\phi_x = \pi/3$ and $\phi_y = \pi/2$

Figure 5.10: Classical simulations for two different configurations of CEPs. The ratio of the frequencies is set to $\kappa = 1.5$ and the ratio of the field strengths is $\eta = 0.5$. Top frame illustrates ionization(red) and re-collision(green) windows in the field. Middle frame shows electron displacement in direction parallel to field(yellow) and perpendicular to the field(blue). Bottom frame shows return energies for each ionization event.

field, I set $\kappa = 2/3$, which gives the control field wavelength of 1200 nm. Non-integer values of κ are used to break the spatial symmetry between consecutive ionization events, which allows us to enhance a specific ionization/re-collision event compared to its neighbors, separated by 1/2 of the laser cycle of the primary field. The 533nm field also allows for sub-cycle control: the control field changes faster than the ionizing field, causing long and short trajectories to see different strengths of the control field. Long and short trajectories are affected differently, and with the right values of ϕ_x and ϕ_y one or the other will not re-collide. The long-wavelength control has the opposite effect, the field changes little over a single ionization event so it is less likely that suppression of either long or short trajectories occurs. However, in this case, for short pulses the strength of the longer-wavelength control field changes significantly over different ionization events, allowing for the effective elimination of all but one ionization event as well as the interference between multiple overlapping re-collision events.

Classical calculations are helpful to better understand the mechanism behind OTC control described above. By using classical calculations it is simple to show why both CE phases are important over just the relative phase. In the top panel of Fig 5.10, I show the electric fields in both directions. Red dots represent the ionization window and green dots the re-collision window. By fixing the relative phase $\Delta\phi$ while changing the value of both CEPs, the windows change position but not width. The same occurs with the shape of the trajectories returning to the core, this can be observed in the middle panel of Fig 5.10 where the electron displacement in x and y as a function of time is shown for both ionization events.

In contrast, the ionization yield and the energy of the re-collision does depend on the position of the ionization window within the envelope of the field . In the case of $(\phi_1 = 0, \phi_2 = 0)$ shown in the left panel, the first ionization event re-collides with more energy than the second event. This is due to the fact that the field envelope is growing in the first event, while it decreases for the second ionization event; this means that the electric field accelerating the electrons in the return to the core is weaker in the second event.

The third panel shows a comparison of the energy of the returning electrons as function of time for the two cases. In the case of $(\phi_1 = \pi/3, \phi_2 = \pi/2)$ the main ionization window is no longer in the middle of the pulse, but a bit earlier which allows the electrons to be accelerated by a stronger field resulting in a higher re-collision energy as shown in the panel. Therefore, both CEPs are important in the case of two colors in short pulses as shown here. The right choice of CEPs will provide a better diffraction spectra by avoiding interferences with the direct electrons signal.

A clean diffraction scenario is one that minimizes effects that degrade or complicate the image. These effects, detailed before in Refs.[114, 124], include multiple ionization events in a single laser pulse and multiple returns of the same liberated electron. The

combination of ultrashort laser pulses and orthogonal fields allows one to effectively address these problems. Under ideal conditions a single re-collision event occurs during the laser pulse; the resulting diffraction pattern will be free of complicated interference patterns and easier to interpret using prescriptions put forth by Refs.[115, 114]. Our calculations also demonstrate that the application of OTC fields allow one to exert control over long versus short trajectories from the same ionization event. For certain sets of field parameters it is possible to suppress either long or short trajectories and remove complicated interferences between the two sets of trajectories. This is particularly important for targets that are weakly aligned.

There are several additional criteria for judging the fitness of a LIED spectra. Most important is high population in the high energy part of the spectrum[114, 124, 121, 131], which is best suited for extracting the molecular structure. Another important parameter is the contrast between the fringes. This work analyzes how the control over the carrier-envelope phases of the two orthogonally polarized laser fields can be used to improve the quality of the LIED spectra, and I present the best optimized conditions for the production of good spectra.

The control appears in two ways. First, the wavepacket is steered away from the core by the second color. By optimizing the pulse, an electron wavepacket can be steered to only partially collide with the ion or miss the ion completely. Second, the total electric field which controls ionization is lowered during some ionization events and raised during others by choosing κ,η, and ϕ_i.

We can see in Fig. 5.11(a) that the second color increases the total field strength for the central ionization (near the peak at 5 femtoseconds in Fig. 5.11(a)) event but contributes nothing to the event a half cycle earlier. These are the only two ionization events that contribute to diffraction. The ionization rate, calculated using the Yudin-Ivanov formula[23], is plotted in Fig. 5.11(b). The central ionization event is significantly stronger than the event before. The presence of the second color contributes to this relationship.

The main control comes from steering the electron in two dimensions. A wavepacket will hit or miss the core depending on the perpendicular drift velocity given to it by the field. For weaker y-component of the field, this drift is controlled by the the vector potential of the second color at the moment of ionization, $v_\perp \sim A_y(t_b)$. Fig. 5.11(a) shows how the chosen frequency ω_y minimizes the y-drift for the central ionization event while maximizing it for the ionization event before it. Indeed, for the central ionization event the y-field has its maximum, and its vector-potential goes through zero. The ionization event before it has the $y-$field equal to zero, and hence the $A_y(t)$ passes through the maximum.

Fig. 5.12 shows examples of typical classical trajectories originating near the peaks of the two ionization events. These trajectories are given zero initial velocities and thus represent the center of the corresponding electronic wavepackets. The return for the central

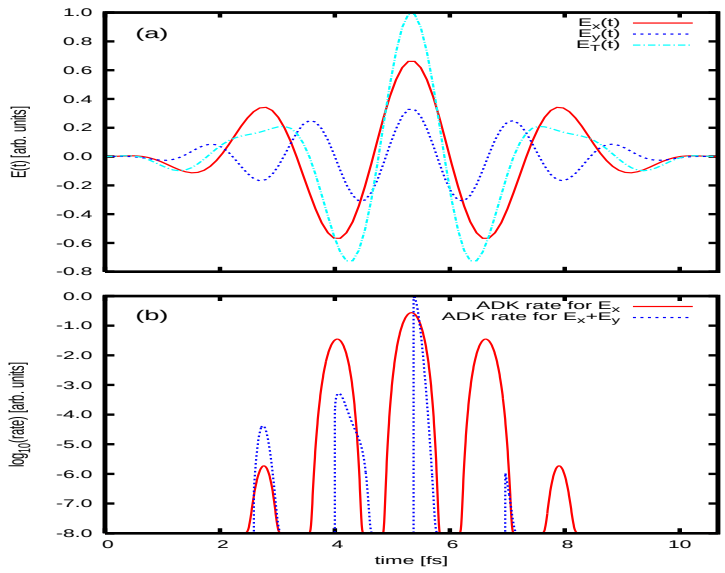

Figure 5.11: (a) Electric field of the field in the x direction (solid red), y direction(dashed blue) and the total field (dotted blue). (b) ADK ionization rates for the linear x direction field(solid red) and the two-color field(dotted blue).

ionization event (dashed blue curve (a)) and the miss for the previous event (purple dotted curve (d)) are evident.

Since the quantum wavepacket is spreading, it is possible that a part of it will re-collide with the parent ion even if the center of the wavepacket misses the target. Classically, this is possible for the trajectory with initial $v_{\perp 0}$ large enough to counter the perpendicular drift $v_\perp$ given by the field. Fig 5.12 shows the classical trajectories with the values of $v_{\perp 0}$ that make them return. For the ionization event near 4 femtoseconds the trajectory needs a large (0.8au) initial velocity in order to return. Creating an electron with such velocity by tunneling is unlikely: it corresponds to an increase in the effective ionization potential $I_{p,eff} = I_p + v_{\perp 0}^2/2$ [132]. Quantum-mechanically, this means that the recollision occurs with the very edge of the wavepacket.

For the main ionization event, the trajectory that returns to the origin is nearly identical to the trajectory starting with zero initial velocity. Hence, for this ionization event the recollision is almost head on, with the center of the wavepacket.

The tunnel ionization rate recalculated with the effective ionization potential $I_{p,eff} = I_p + v_{\perp 0}^2/2$ is plotted in 5.11(b). The new ionization rate for the ionization event I are trying to suppress is four orders of magnitude lower than the ionization rate at the peak. The huge difference in ionization rates essentially reduces the pulse that leads to diffraction to

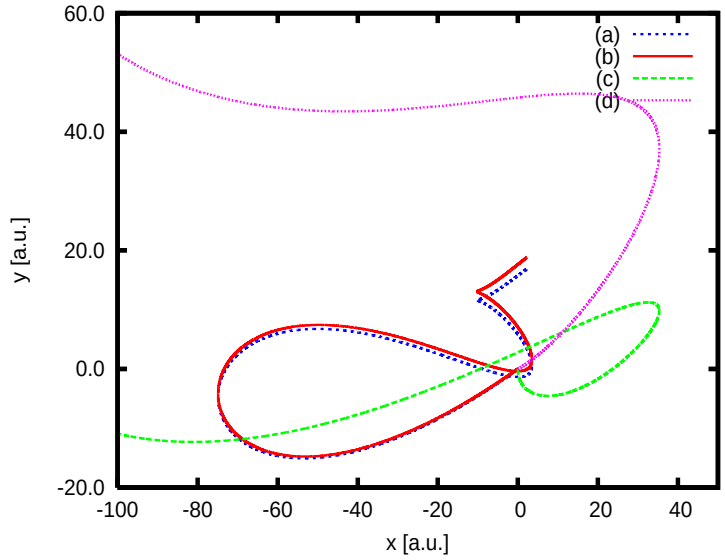

Figure 5.12: Classical trajectories in a two color field. Red solid line shows trajectory for the central ionization event, starting with zero v_y. Blue dashed line is the trajectory that starts with slightly non-zero v_y that ensures return to the origin. Purple dashed line shows the trajectory for the ionization event a half-cycle before the central event, starting with zero v_y. Green dashed line is the trajectory with a large v_y that ensures return to the origin.

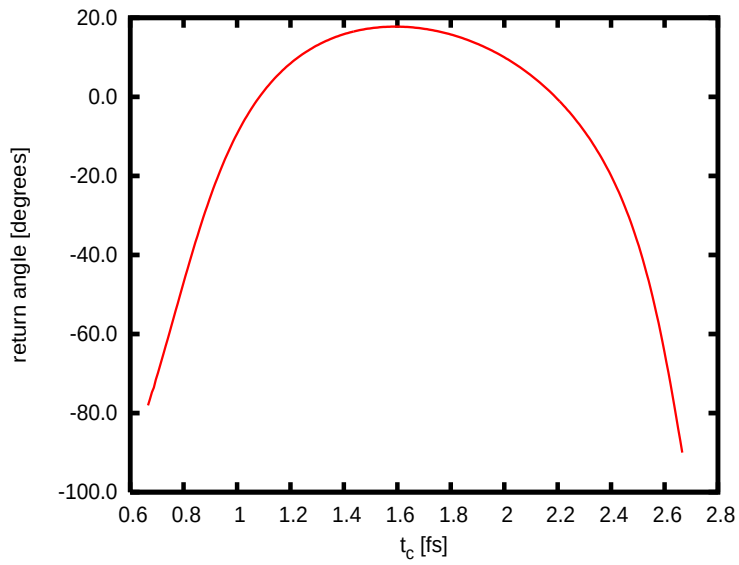

Figure 5.13: Angle of return versus time of return for a recolliding electron wavepacket. Return time is measured from the maximum of the field

a single cycle or less, with associated increase in the time resolution. We can see from Fig. 5.12 that the wavepacket no longer recollides at a uniform angle. The angular dependence of the diffraction image now becomes important. Fig 5.13 shows the angle of return as a function of return time. The return angles range anywhere between zero and ninety degrees. Importantly, the bulk of the wavepacket produced by the main ionization event returns at nearly the same angle, ensuring simplicity of the diffraction pattern.

5.4 Control of LIED using OTC: Results

We will now discuss the results of using OTC to image molecules using LIED. The results shown below are taken from [124, 72]. Two methods have been employed to calculate the electron momentum spectra. First is a qualitative method based on an analytical analysis of the S-Matrix, second is a much more quantitative *ab-initio* method. Both methods are discussed below followed by key results.

5.4.1 S-Matrix Method

Consider a diatomic molecule in an intense two-color infrared (IR) laser field. The system starts in its initial state $|\Psi_0\rangle$ with an energy $E_g = -I_p$, where I_p is the ionization potential.

The Hamiltonian is $\hat{H} = \hat{H}_0 + \hat{V}_L$ where $\hat{H}_0$ is the field free Hamiltonian and $\hat{V}_L$ is the electron-laser interaction. We work in the length gauge, resulting in $\hat{V}_L = \mathbf{E}(t) \cdot \mathbf{x}$.

Using the strong-field S-matrix formalism[45], I can write the probability amplitudes to find the system in the state with final momentum k_f as (atomic units are used throughout):

$$\begin{aligned} a_{\mathbf{k}}(\mathbf{k}_f, t) &= \langle \mathbf{k}_f | \Psi(t) \rangle = a_{\mathrm{resc}}(\mathbf{k}_f) + a_{\mathrm{dir}}(\mathbf{k}_f) = \\ &- \int_{t_0}^{t_c} dt' \int_{t_0}^{t} dt_c \int d\mathbf{k} \langle \mathbf{k}_f | e^{-i\int_{t_c}^{t} \hat{H}(\tau) d\tau} \hat{V}_c(t_c) | \mathbf{k} \rangle \\ &\quad \langle \mathbf{k} | e^{-i\int_{t'}^{t_c} \hat{H}_V(\tau) d\tau} \hat{V}_L(t') e^{-i\int_{t_0}^{t'} \hat{H}_0(\tau) d\tau} | \Psi_0 \rangle \\ &- i \int_{t_0}^{t} dt' \langle \mathbf{k}_f | e^{-i\int_{t'}^{t} \hat{H}_V(\tau) d\tau} \hat{V}_L(t') e^{-i\int_{t_0}^{t'} \hat{H}_0(\tau) d\tau} | \Psi_0 \rangle \end{aligned} \tag{5.34}$$

Here $\hat{V}_c$ is the potential of the molecular core, time-ordering operator for the exponential operators is implied.

This *exact* expression is known as the time-reversed S-matrix amplitude. Its particular form allows one to attribute different physical processes to the various terms in this expression. The second term describes ionization and is usually associated with the so-called 'direct' electrons that do not recollide with the parent ion. The moment t' is associated with the moment of ionization. The first term describes the recolliding electron, which interacts elastically with the ionic core at the moment t_c after ionization at the moment t'. Since this is the only term responsible for laser-induced diffraction, for the moment I drop the 'direct' term from the further analysis.

Equation 5.34 can be derived from the S-Matrix equations described above. Equation 5.6 is the first term in a perturbative expansion of the atomic/molecular core. I can derive the second term(equation 5.34) using the following identity:

$$|\Psi(t)\rangle = e^{i\int_{t_0}^{t} \hat{H}(t'')dt''} |\Psi(t=0)\rangle \tag{5.35}$$

$$e^{i\int_{t_0}^{t} \hat{H}(t'')dt''} = -i \int^{t} dt' e^{i\hat{H}_0 t'} \hat{V}(t') e^{-i\int^{t'} \hat{H}(t'')dt''} + e^{-i\hat{H}_0 t} \tag{5.36}$$

Using this identity and changing the partitioning scheme to $\hat{H} = \hat{H}_V + \hat{V}_c$, where $\hat{H}_V$ is the Volkov propagator and $\hat{V}_c$ is the core potential, and inserting equation 5.36 into 5.6 one arrives at equation 5.34.

For Eq.5.34 to be useful, something must be done to the final propagator from t_c to t, which uses the full Hamiltonian. The zero-order approximation is to ignore the ionic potential after t_c completely. This is commonly known as the strong field approximation (SFA) corrected for single recollision. Already this approximation correctly captures key qualitative features of the strong-field scattering. Since I are interested in the qualitative

analysis of how control over the electron trajectories affects the global diffraction patterns, this approximation is reasonable. Further improvement is possible using the Strong-Field Eikonal-Volkov Approximation (SF-EVA), see [97, 34], and I hope to consider it elsewhere.

Once the ionic potential in the final propagator is dropped, the propagator from t_c to t becomes the Volkov propagator, yielding

$$\langle \mathbf{k}_f | e^{-i\int_{t_c}^{t} \hat{H}_V(\tau)d\tau} = e^{-\frac{i}{2}\int_{t_c}^{t}[\mathbf{k}_f+\mathbf{A}(\tau)]^2 d\tau} \langle \mathbf{k}_f + \mathbf{A}(t_c)| \tag{5.37}$$

Here $\hat{H}_V = \hat{H} - \hat{V}_c$ is the Hamiltonian for the free electron in the laser field. Correspondingly, the continuum state characterized by the *kinetic* momentum $\mathbf{k}_f$, $|\mathbf{k}_f\rangle$ is a plane wave. I have taken into account that after the end of the laser pulse $\mathbf{A}(t) = 0$.

Now the rescattered amplitude in Eq.(5.34) becomes:

$$\begin{aligned} a_{\rm resc}(\mathbf{k}_f) &= -\int_{t_0}^{t_c} dt' \int_{t_0}^{t} dt_c \int d\mathbf{k}\; e^{-\frac{i}{2}\int_{t_c}^{t}[\mathbf{k}_f+\mathbf{A}(\tau)]^2 d\tau - \frac{i}{2}\int_{t'}^{t_c}[\mathbf{k}+\mathbf{A}(\tau)-\mathbf{A}(t_c)]^2 d\tau + I_p(t'-t_0)} \times \\ &\times \langle \mathbf{k}_f + \mathbf{A}(t_c)|\hat{V}_c|\mathbf{k}\rangle \langle \mathbf{k} - \mathbf{A}(t_c) + \mathbf{A}(t')|\hat{V}_L(t_b)|\Psi_0\rangle \end{aligned} \tag{5.38}$$

For the two colors polarized orthogonally to each other, the vector-potential has two components. The main component of the electric field, with the carrier frequency $\omega_1 = \omega$, is polarized along the x axis. The weaker component of the laser field, with the frequency $\omega_2 = 1.5\omega$, is polarized along the y-axis. I shall also assume that the laser-molecule interaction is in the tunneling regime for the main x-component of the laser field. That is, I assume that the corresponding Keldysh parameter is small, $\gamma_x^2 = I_p/2U_{p,x} < 1$. Here $U_{p,x} = E_x^2/4\omega^2$ is the ponderomotive potential associated with the x-component of the laser field.

The following steps are rather standard. First, I calculate the momentum integral analytically in a standard way, using the stationary phase method (see e.g. [133]). The stationary phase point with respect to the kinetic momentum $\mathbf{k}$ is

$$\mathbf{k}_c(t', t_c) = \mathbf{A}(t_c) - \frac{1}{(t_c - t')}\int_{t'}^{t_c} \mathbf{A}(\tau)d\tau \tag{5.39}$$

In terms of the initial momentum at t', $\mathbf{k}_b(t', t_c) = \mathbf{k}_c(t', t_c) - \mathbf{A}(t_c) + \mathbf{A}(t')$, this equation reads

$$\int_{t'}^{t_c} [\mathbf{k}_b(t', t_c) - \mathbf{A}(t') + \mathbf{A}(\tau)]d\tau = 0 \tag{5.40}$$

As usual, it ensures that the electron born at t' returns to its initial position at t_c. For each pair of t' and t_c, it yields the x and y components of the initial kinetic momenta $\mathbf{k}_b = \mathbf{k}_c - \mathbf{A}(t_c) + \mathbf{A}(t')$. The integral is performed by expanding the phase of the integral

in powers of $(\mathbf{k}-\mathbf{k_c})$ to the second order and assuming that the dipole transition matrix elements are slow functions of momentum.

$$a_{\rm resc}(\mathbf{k}_f) \approx -\int_{t_0}^{t_c} dt' \int_{t_0}^{t} dt_c e^{-\frac{i}{2}\int_{t_c}^{t}[\mathbf{k}_f+\mathbf{A}(\tau)]^2 d\tau - \frac{i}{2}\int_{t'}^{t_c}[\mathbf{k}_c+\mathbf{A}(\tau)-\mathbf{A}(t_c)]^2 d\tau + I_p(t'-t_0)} \left(\frac{2\pi}{t_c-t'-i\tau}\right)^{3/2} \langle \mathbf{k}_f+\mathbf{A}(t_c)|\hat{V}_c|\mathbf{k}_c\rangle \langle \mathbf{k}_c-\mathbf{A}(t_c)+\mathbf{A}(t')|\hat{V}_L(t_b)|\Psi_0\rangle \tag{5.41}$$

Moving to the integral over t', I use the limit $\gamma^2 < 1$ to simplify the derivation compared to the more standard, straightforward saddle-point analysis, often referred to as the method of 'quantum trajectories' [134]. The standard saddle point equation with respect to t' reads:

$$[\mathbf{k}_c(t',t_c)+\mathbf{A}(t')-\mathbf{A}(t_c)]^2 + 2I_p = 0 \tag{5.42}$$

Instead of looking for complex-valued solutions of Eq.(5.42) in the two-color field, I are taking a slightly different route. First, I note that the ionization is dominated by the x-component of the driving laser field, and hence tunneling occurs primarily in that direction. Second, I note that the small value of the Keldysh parameter $\gamma^2 = I_p/2U_p < 1$ means that the saddle points for t'-integral are close to the real time axis.

Therefore, instead of expanding the phase of the integrand around the saddle point Eq.(5.42), I can begin by looking for the real-valued solutions $t' = t_b$ of the simpler equation

$$k_{c,x}(t_b,t_c) + A_x(t_b) - A_x(t_c) = 0 \tag{5.43}$$

This equation means that the x-component of the kinetic momentum of the electron at the moment of birth $t' = t_b$ is equal to zero, $k_{b,x}(t_b,t_c) = 0$. Together with the condition of return Eq.(5.39) for the motion along the x-axis

$$k_{c,x}(t',t_c) = A_x(t_c) - \frac{1}{(t_c-t_b)}\int_{t_b}^{t_c} A_x(\tau)d\tau \quad , \tag{5.44}$$

it connects the moment of birth t' and the moment of return t_c in the exact same way as for the usual classical trajectories in the one-color problem.

The main idea of this approach is to expand the t'-dependent phase in the integrand in Eq. (5.38) in Taylor series around the point t_b given by Eqs.(5.44,5.43) and not around the exact saddle point given by Eqs.(5.39,5.42). As a price for this simplification, the Taylor expansion has to be done up to the third order for the x-component of the phase in the integral Eq. (5.38). Indeed, Eq.(5.43) ensures that the second derivative of the Volkov

phase for the x-component of the motion is equal to zero. The resulting integral can be expressed in terms of the Airy functions, and then the asymptotic limit of the Airy function for large arguments can be used to simplify the expression. For weaker y field, the result is

$$a_{\rm resc}(\mathbf{k}_f) \propto \sum_{t_b} \int_{t_0}^{t} dt_c e^{-\frac{i}{2}\int_{t_c}^{t}[\mathbf{k}_f+\mathbf{A}(\tau)]^2 d\tau - \frac{i}{2}\int_{t_b}^{t_c}[\mathbf{k}_b(t_c,t_b)+\mathbf{A}(\tau)-\mathbf{A}(t_b)]^2 d\tau + I_p(t'-t_0)} \left(\frac{2\pi}{t_c - t' - i\tau}\right)^{3/2} \langle \mathbf{k}_f + \mathbf{A}(t_c)|\hat{V}_c|\mathbf{k}_c\rangle a_{\rm ion}(t_b, k_{b,y}(t_b,t_c)) \tag{5.45}$$

Where the ionization amplitude is

$$a_{\rm ion}(t_b, k_{b,y}(t_b,t_c)) \propto \exp\left(-\frac{2^{3/2}}{3}\frac{I_{\rm p,eff}^{2/3}}{|\mathbf{E}(t_b')|}\right) \tag{5.46}$$

and the effective ionization potential is

$$I_{\rm p,eff}(t_b,t_c) = I_p + \frac{1}{2}[k_{b,y}(t_b,t_c)]^2 \tag{5.47}$$

$I_{p,eff}$ takes into account that the electron has to leave the tunnel with non-zero initial momentum in order to return to the origin. The dipole matrix element between the ground state and the $\mathbf{k}_b$ state has been absorbed into Eq (5.46) along with the prefactor resulting from the t' integration. The moment of birth t_b is defined by Eq. (5.44) and the nonzero y-component of the initial kinetic momentum, $k_{b,y}(t_b,t_c)$ is defined by the condition that at the moment t_c the electron returns to its initial position not only for x- but also for the y-motion, after starting at the moment t_b:

$$k_{b,y}(t_b,t_c) = A_y(t_b) - \frac{1}{t_c - t_b}\int_{t_b}^{t_c} A_y(\tau)d\tau \tag{5.48}$$

The sum in 5.45 is over all trajectories that can return to the core at the given moment t_c. In our pulse, multiple returns are suppressed and hence there is only one essential term in the sum.

As discussed in the previous section, the presence of the y-field enters via the effective ionization potential, which is higher if the electron has to start with non-zero velocity in the y-direction. This velocity is high for the first ionization event at 4 femtoseconds and is negligible for the main ionization event.

Finally, the last integral is calculated using the stationary phase method. For a given final momentum $\mathbf{k_f}$, the corresponding stationary phase equation for the moment of collision t_c is

$$\frac{1}{2}[[\mathbf{k}_f + \mathbf{A}(t_c)]^2 = \frac{1}{2}\mathbf{k}_c(t_b',t_c)^2 - I_p\frac{\partial t_b'}{\partial t_c}|_{t_c} \tag{5.49}$$

We note that for each ionization event (i.e. each half-cycle of the laser field), there are two solutions to Equation (5.49).

The result of the integration is

$$a_{\rm resc} \quad \propto \quad \sum_{t_c,t_b} -e^{i\phi(\mathbf{k}_0,t_b,t_c)} a_{\rm coll}(t_b,t_c) a_{\rm ion}(I_p,t_b) \frac{2\pi}{(t_c - t_b - i\tau)^{3/2}} \tag{5.50}$$

where the summation is over all collision moments t_c that yield the same final momentum $\mathbf{k_f}$ (two for each half-cycle), and over all ionization moments t_b that could yield collision at the same instant t_c. In our pulse, where multiple returns are suppressed, there is only one important t_b for each t_c.

The collision amplitude in the equation Eq. (5.50) is

$$a_{\rm coll}(t_b,t_c) \sim \sqrt{\frac{2\pi}{\mathbf{E}(t_c)[\mathbf{k}_f + \mathbf{A}(t_b) - \mathbf{A}(t)]}} \langle \mathbf{k}_f - \mathbf{A}(t) + \mathbf{A}(t_c) | \hat{V}_c(t_c) | \mathbf{k}_0 \rangle \tag{5.51}$$

The phase in the equation Eq. (5.50) is given by the classical action of the stationary phase trajectory:

$$\phi(\mathbf{k}_b,t_b,t_c) = -\frac{1}{2}\int_{t_c}^{t} [\mathbf{k}_f + \mathbf{A}(\tau) - \mathbf{A}(t)]^2 d\tau - \frac{1}{2}\int_{t_b}^{t_c} [\mathbf{k}_0 + \mathbf{A}(\tau) - \mathbf{A}(t_c)]^2 d\tau + I_p(t_b - t_0) \tag{5.52}$$

Since for each ionization event (i.e. each half-cycle of the laser field), there are two solutions to Equation (5.49) (the long and short trajectories) this phase does not disappear when I calculate the probabilities $|a_{\rm resc}|^2$. It produces an interference between the (in our case two) essential trajectories leading to the same final momentum of the electron. This interference results in the ring structures in the electron spectrum.

To generate spectra from Eq. (5.50) I have to first solve the stationary phase equations Eq's. (5.43,5.44,5.49). For each $\mathbf{k}_f$ there are two sets of $(\mathbf{k}_b, t_b, t_c)$ which correspond to the long and short trajectories discussed in the previous paragraph. The resulting amplitudes for each set of stationary phase points are summed coherently to give a total recollision amplitude for all possible $\mathbf{k}_f$. This way the entire angle and energy resolved spectrum can be calculated. The calculations were done by solving the stationary phase equations numerically, then using these solutions to calculate the total spectrum from Eq. (5.50). The results are given below.

5.4.2 *ab-initio* Method

The second method makes use of the integration of the Time Dependent Schrödinger Equation (TDSE) in 2D, in the polarization plane of the two fields. The TDSE includes

the effects from the core exactly, all bound states, and the entire momentum spectrum, however it lacks the physical insight to the process that the SFA-based method gives. I integrate the TDSE numerically using the split operator technique implemented in the qFishbowl[135] code. The Hamiltonian in 2D is.

$$H = \frac{p_x^2}{2} + \frac{p_x^2}{2} - \sum_{\pm} \frac{Z_{eff}}{\sqrt{a^2 + (x \pm R_0\cos(\theta)/2)^2 + (y \pm R_0\sin(\theta)/2)^2}} + p_x A_x(t) + p_y A_y(t) \tag{5.53}$$

Soft core parameter $a^2 = 0.5$ and $R_0 = 4.0$ a.u. is the internuclear distance. The angle θ defines the alignment of the molecule with respect to the x axis, $Z_{eff} = -1$. The energy for the ground state in this configuration is $E_0 = -0.96$ a.u.

The momentum distribution is obtained by projecting out the bound states and then making a Fourier transform for the free electrons. The final momentum distribution is taken at the end of the pulse and therefore, electrons colliding later than this time are not considered.

5.4.3 533 nm

We now show results of SFA-based and *ab-initio* quantum calculations on the model H_2^+ molecule described above. The primary field is centered at 800 nm and the control field is centered at 533 nm. The intensities are 7×10^{14} W cm^{-2} for the primary field and 1.75×10^{14} W cm^{-2} for the control field. The pulses are 5 femtoseconds in duration. Figure 5.14 shows four angle and energy resolved momentum spectra calculated with the SFA-based formalism. Each frame corresponds to different combinations of CE phases. Here, the molecule is aligned parallel to the primary laser pulse ($\theta = 0$). The top two frames of fig. 5.14 have the same relative phase $\Delta\phi = 0$. While the location and strength of the diffraction peaks are the same in both frames there is substantially more signal in the high energy backscattering region of fig 5.14(b). The difference is nearly one atomic unit in momentum. This is clear evidence that the CEP of both fields is important in short pulses. The effect of changing the CEP phases while holding the relative phase constant is to change the energy of the returning electron. The variations in the return energy seen in the figures are not due to the presence of the control field; they are determined by the CEP phase of the primary field. At the same time it is the relative orientation of the two colors that is responsible for the quality and location of the diffraction peaks.

The four panes in fig 5.14 highlight the power of using OTC fields for LIED. Each exhibits an important feature of OTC fields and each one has a single good re-collision. Figures 5.14(a) and 5.14(b) both have a relative phase of zero, fig 5.14(a) is for the same parameters as shown in [124] while fig 5.14(b) is the same relative phase but optimized for

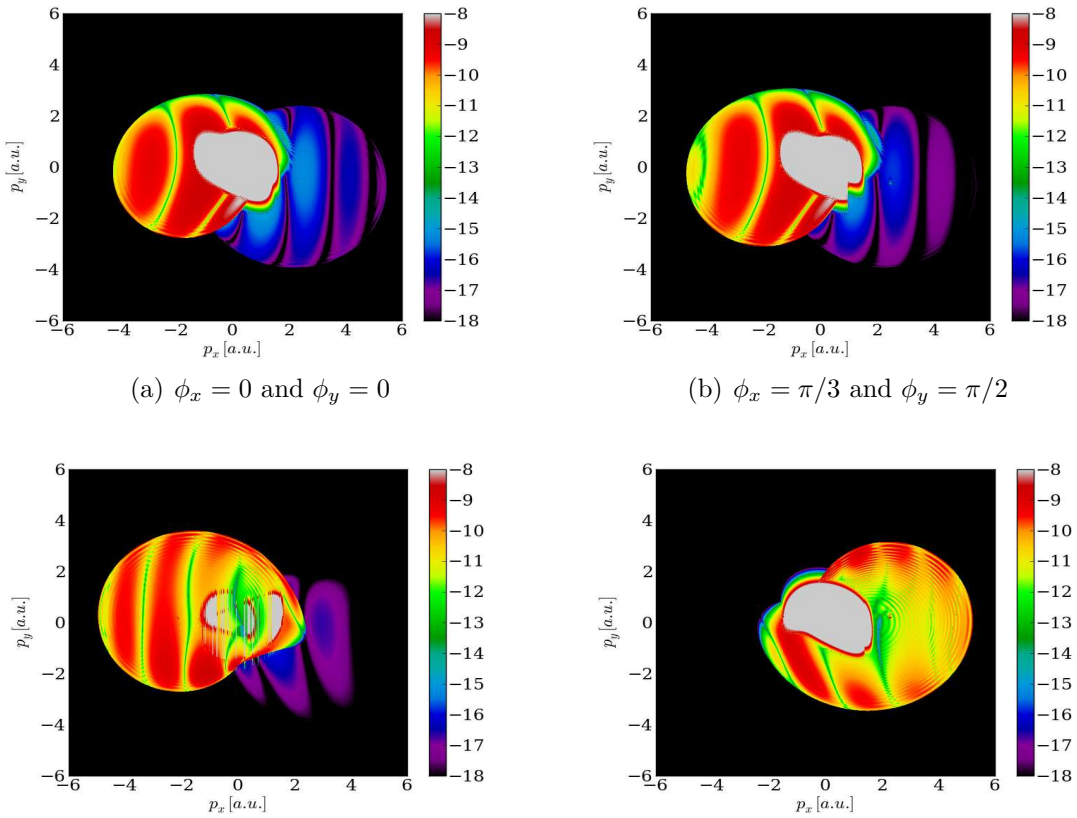

(a) $\phi_x = 0$ and $\phi_y = 0$

(b) $\phi_x = \pi/3$ and $\phi_y = \pi/2$

(c) $\phi_x = \pi/2$ and $\phi_y = \pi/2$

(d) $\phi_x = -\pi/4$ and $\phi_y = 0$

Figure 5.14: Angle and energy resolved momentum spectra of LIED in OTC fields with $\kappa = 1.5$ and $T = 5$fs. Frame (a) and frame (b) have the same relative phase $\Delta\phi = 0$. The color scale is logarithmic; the numbers on the scale are orders of magnitude. The momentum is measured in atomic units.

a higher return energy. Both demonstrate a single strong re-collision and good signal in the backscattering region. The returning electron wave packet responsible for this spectrum is a fraction of a femtosecond in length and only includes short trajectories. Indeed, the absence of interference fringes along the peaks indicates that the long trajectories are not present. The isolation of short or long trajectories is very important for weakly aligned samples, as the diffraction fringes are different for long and short trajectories. The difference comes from the varying angle of re-collision across the wave packet and the varying time spent in the continuum leads to different phases for the long or short trajectories and therefore different diffraction criteria. The changing angle of re-collision adds to the complexity of the resulting photo-electron spectrum because the recollision

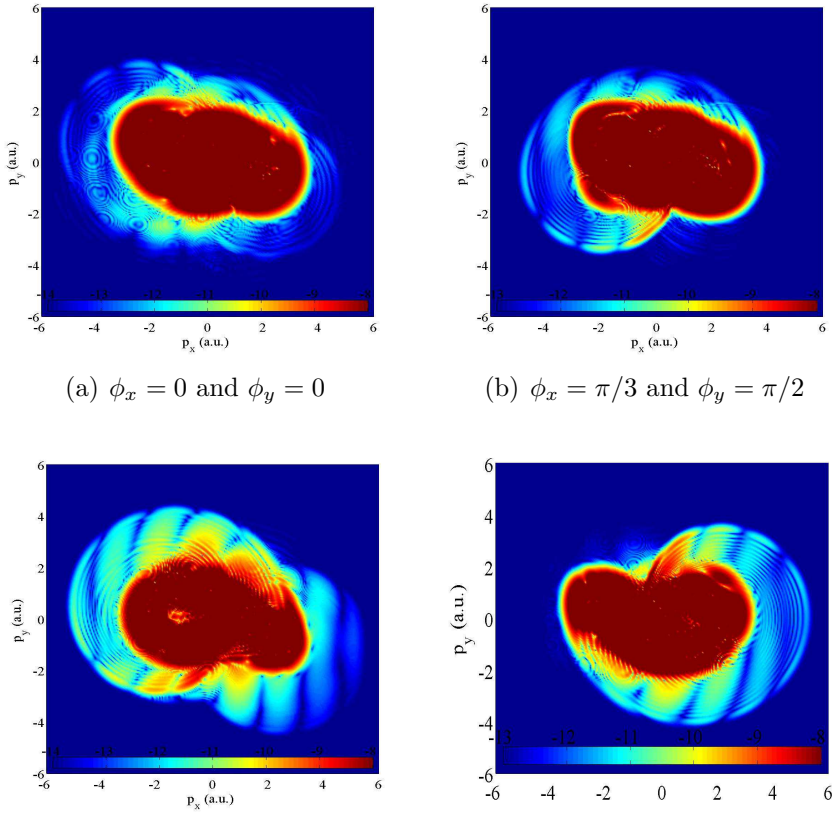

(a) $\phi_x = 0$ and $\phi_y = 0$

(b) $\phi_x = \pi/3$ and $\phi_y = \pi/2$

(c) $\phi_x = \pi/2$ and $\phi_y = \pi/2$

(d) $\phi_x = -\pi/4$ and $\phi_y = 0$

Figure 5.15: *ab-initio* angle and energy resolved LIED spectra with $\kappa = 1.5$ and $T = 5$fs. Frame (a) and frame (b) have the same relative phase $\Delta\phi = 0$. The color scale is logarithmic; the numbers on the scale are orders of magnitude. The momentum is measured in atomic units.

matrix element is dependent on recollision angle. For the type of fields considered here the angle of recollision is constant for the bulk of the recollision[124]. Figure 5.14(c) is another good example of strong backscattering signal and suppression of long trajectories. The significant feature in this plot is that a large portion of the overall signal is outside of the $2U_p$ region($U_p = E_{x0}^2/4\omega_x^2$ is the ponderomotive energy, the average energy of an electron in an oscillating field, in this case U_p=1.53a.u. or 41eV. The $2U_p$ region is then roughly 2.5 a.u. in momentum on the figures). Since the direct electrons are confined to the $2U_p$ region[136] it is important to look in the high energy region to avoid interference from the direct electrons. The high signal outside the direct electron region and the absence of long trajectories make this spectrum ideal for analyzing the LIED pattern. Figure 5.14(d)

carries the attempt to achieve high backscattering signal to the extreme. In this spectra only the signal above $2U_p$ was considered in optimization. Nearly all the population lies in areas which can be easily read at the expense of having the interference fringes from the presence of both long and short trajectories. The SFA-based calculation leads to a good qualitative understanding of what is possible with OTC fields but *ab-initio* calculations are needed for a complete understanding of LIED in OTC fields.

These results can be compared to the results of studies of the effect of ellipticity on high harmonic generation. Mairesse et al.[137] observed a modulation on the relative amplitudes of individual harmonics which depended on ellipticity. This ability to control which harmonics are created is identical to the results shown here, where high energy electrons are allowed to rescatter and low energy electrons are suppressed. In both cases the ellipticity is what provides the control over the returning electron wavepacket. The effect of ellipticity on LIED spectra will in general have an analogous effect on the XUV radiation emmited in high harmonic generation.

We now show the *ab-initio* calculations for the same field setup. Figure 5.15 shows the same field configurations as the SFA-based plots above. The qualitative similarities between the two methods validate the SFA-based approach as a tool for a quick analysis of the degree of control exerted by the selected configuration of the laser fields. The high population in the center of the plots is the contribution of the direct electrons, which is underestimated in the SFA based calculations as a result of the saddle point analysis. The main differences from Fig. 5.15 is the contribution of the direct electrons to the total spectrum, which covers a substantial part of the LIED pattern. Apart from the direct electron contributions the figures are in qualitative agreement, with the same energies and fringe patterns. The differences arise for several reasons, most important of which is the effects of the core on the continuum electron. The *ab-initio* calculations account for this exactly and the SFA calculations only perturbatively. The effect of the Coulomb core is in general to make the isolation of short or long trajectories less complete. The SFA calculations show strong suppression of the fringes caused by interference between long and short trajectories which are much less obvious in the *ab-initio* results. This is an indirect observation of Coulomb focusing[138] which is pulling more short and long trajectories back to the core to recollide.

5.4.4 1200 nm

We now turn to the second control scheme: long-wavelength control. The purpose of this scheme is to maximize the return energy and to maximally suppress all but one ionization event. The longer wavelength of the control field allows for both long and short trajectories to see the same field resulting in uniform behavior over an entire pulse. Each ionization event then experiences different parts of the control field leading to a suppression of all

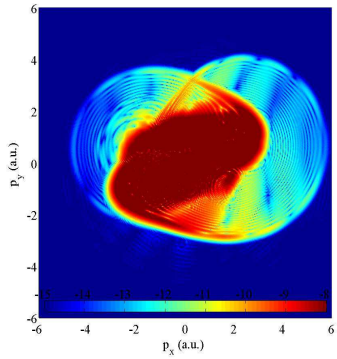

Figure 5.16: *ab-initio*: $\phi_x = \pi/6$ and $\phi_y = \pi/3$. Angle and energy resolved LIED spectra. The pulse is 5 fs FWHM at 7×10^{14}W/cm^2 for the primary field.

but one re-colliding electron wave packet. The higher re-collision energy due to the long wavelength control field is another important benefit of long-wavelength control. For these simulations I used the same field and molecule configuration as above. Figure 5.16 shows *ab-initio* calculations for two interesting CE phase combinations and is an example of a very high energy re-collision event. The backscattering region is at six atomic units of momentum (nearly 0.5keV in energy). The ring structure from the interference of long and short trajectories is particularly prominent in these plots, which means the entire electron wave packet is allowed to re-collide. The high signal in the backscattering region combined with good contrast and high energy make this set of CE phases particularly appealing.

5.4.5 Outlook

The results presented above show the flexibility of OTC fields. The three control parameters: κ, the ratio of frequencies and ϕ_x,ϕ_y the CE phases of the ionization and control fields combine to give a high degree of control over the LIED spectra. In principle the ratio of the fields can be used as another control parameter; the degree of control provided by this parameter is not as great as the ratio of frequencies and the carrier envelope phases and so it was not considered here. Configurations to maximize return energies, suppress all but a single returning ionization wave packet, suppress long or short trajectories in a single ionization event, or to maximize the signal in the backscattering region can all be prepared. The strong backscattering signal is important for reading the LIED spectra[114, 124, 121, 139]. The suppression of long or short trajectories is important when the molecule is not aligned perpendicular to the ionization field. Indeed, in this case the long and short trajectories produce different diffraction fringes that interfere and obscure the diffraction pattern.

There are many uses for OTC fields in LIED spectroscopy, some of which the authors hope to explore in the future. These include tailoring the OTC fields to produce more monochromatic returning electron wave packets, studying rotating or vibrating molecules to measure motion between re-colliding electron wave packets and manipulating the Volkov phase of the ejected electron to eliminate or reduce the chirp of the electron wave packet thereby removing the intrinsic chirp on HHG emission. The polarization gating of Corkum et al [140] could be combined with OTC fields to produce a single re-collision event with much longer pulses.

Chapter 6

Conclusion

Through the past three chapters we have examined the effects of intense laser fields on atoms and small molecules. We have discussed how atoms and molecules ionize in strong fields. The theories of atomic ionization have been in existence for several decades so a thorough and newer treatment of these theories was given in the context of modern applications. The theories of PPT and Landau were derived in the classical fashion and the exponential dependence of the field strength and ionization potential is emphasized. The importance of the prefactor in the expression was also briefly mentioned. Finally the derivation of PPT was redone using the modern Fourier transform approach developed by the author.

In the next chapter the Fourier transform based approach to tunnel ionization rates was applied to small molecules. First we apply our theory to the theory of molecular ADK. We are able to show that under specific assumptions our theory goes into MO-ADK as a limiting case. This key result shows that this new theory is inherently better than MO-ADK as it is exactly derivable from the general theory. Next we extend MO-ADK to multiple centers. This theoretical exercise showed the importance of the magnetic quantum number and how different magnetic quantum numbers mix. A much more intuitive method of calculating rates was then presented, which gives accurate and physically transparent rates for a variety of molecules. Finally, a numerical implementation of the molecular ionization theory was presented with discussions on the importance of the matching point, z_0, and the possibility of a time dependent theory.

In the final chapter we reviewed the state of the art in the strong field community. This includes recent results in high harmonic generation and laser induced electron diffraction. The current work being performed in this field mostly centers around imaging techniques and that is where the future work will lie. The most promising techniques are those related to high harmonic generation: tomographic reconstruction and imaging hole dynamics. While the possibility of tomographic reconstruction of molecular orbitals is controversial

it is an extremely promising tool for imaging dynamics in small molecules. The imaging of hole dynamics is much more exciting and it potentially can be used in a wide range of larger molecules, giving insight into the rearrangement processes and electronic motion in molecules.

There is also great momentum building in the high frequency laser field, the use of attosecond pulses from high harmonic generation along with the completion of X-ray free electron lasers gives a number of new tools with which the fundamentals of light matter interactions can be further understood. More important these new x-ray sources allow for unprecedented looks inside biomolecules and proteins. The brightness of these sources can in theory lead to atomic resolution, three dimensional x-ray diffraction images of large biomolecules and viruses. Indeed, with the technologies described above the molecular movie is a near possibility. The advance of our understanding of light matter interaction in the recent decade and the resulting technology is what will soon make it possible.

Bibliography

[1] T. H. Maiman. Stimulated Optical Radiation in Ruby. *Nature*, 187(4736):493–494, August 1960. ISSN 0028-0836. URL http://dx.doi.org/10.1038/187493a0.

[2] E Goulielmakis, M Schultze, M Hofstetter, V S Yakovlev, J Gagnon, M Uiberacker, A L Aquila, E M Gullikson, D T Attwood, R Kienberger, F Krausz, and U Kleineberg. Single-cycle nonlinear optics. *Science (New York, N.Y.)*, 320(5883): 1614–7, June 2008.

[3] Laser - Wikipedia, the free encyclopedia. URL http://en.wikipedia.org/wiki/Laser.

[4] R Neutze, R Wouts, D van der Spoel, E Weckert, and J Hajdu. Potential for biomolecular imaging with femtosecond X-ray pulses. *Nature*, 406(6797):752–7, August 2000. ISSN 0028-0836. URL http://dx.doi.org/10.1038/35021099.

[5] Albert Einstein. Über einen die Erzeugung und Verwandlung des Lichtes betreffenden heuristischen Gesichtspunkt. *Annalen der Physik*, 17:132 – 148, 1905. URL http://en.wikipedia.org/wiki/Annus_Mirabilis_papers\#cite_note-einsta-8.

[6] Joachim Ankerhold. *Quantum Tunneling in Complex Systems*, volume 224 of *Springer Tracts in Modern Physics*. Springer, Berlin ; New York, 2007.

[7] Mohsen Razavy. *Quantum theory of tunneling*. Singapore : World Scientific, 2003.

[8] David J Griffiths. *Introduction to Quantum Mechanics*. Prentice Hall, 2 edition, 2004. ISBN 0131118927.

[9] L D Landau and E M Lifshitz. *Quantum Mechanics Non-Relativistic Theory: Volume 3*. Butterworth-Heinemann, 1981.

[10] David Joshua Tannor. *Introduction to quantum mechanics: a time-dependent perspective*. University Science Books, Sausalito, Calif., 2007.

[11] B H Brandsen and C J Joachain. *Quantum Mechanics*. Prentice Hall, 2 edition, 2000.

[12] Rectangular Potential Barrier - Wikipedia, the free encyclopedia. URL `http://en.wikipedia.org/wiki/Rectangular_potential_barrier`.

[13] Joachim Ankerhold. *Quantum Tunneling in Complex Systems: The Semiclassical Approach (Springer Tracts in Modern Physics)*. Springer, 2007. ISBN 3540680748. 212 pp.

[14] V P Maslov and M V Fedoriuk. *Semi-Classical Approximation in Quantum Mechanics*. Number 7 in Mathematical Physics and Applied Mathematics. D. Reidel Publishing, Boston, 1981.

[15] J Liouville. Sur le development des fonctions ou parties des fonctions en s eries dont les divers termes sont se sujetti satisfaire a une meme equation differentielle du second ordre contenant un param etre variable (second m emoire). *J. Math. Pures et Appl*, 2:16–36, 1837.

[16] G Green. On the motion of waves in a variable canal of small depth and width. *Trans. Cambridge Philos. Soc*, 6:457–462, 1837.

[17] Gregor Wentzel. Eine Verallgemeinerung der Quantenbedingungen fr die Zwecke der Wellenmechanik. *Zeitschrift fr Physik*, 38(6-7):518–529, June 1926.

[18] H. A. Kramers. Wellenmechanik und halbzahlige Quantisierung. *Zeitschrift fr Physik*, 39(10-11):828–840, October 1926.

[19] Léon Brillouin. La mécanique ondulatoire de Schrödinger: une méthode générale de resolution par approximations successives. *Comptes Rendus de l'Academie des Sciences*, 183:24 – 26, 1926.

[20] A M Perelomov, V S Popov, and M V Terent'ev. Ionization of atoms in an alternating electrical field. *JETP*, 23(6):924, 1966.

[21] A M Perelomov and V S Popov. Ionization of atoms in an alternating electrical field. III. *JETP*, 25(2):336, 1967.

[22] A M Perelomov, V S Popov, and M V Terent'ev. Ionization of atoms in an alternating electrical field. II. *JETP*, 24(1):207, 67.

[23] Gennady L Yudin and Misha Yu. Ivanov. Adiabatic tunnel ionization: Looking inside a laser cycle. *Physical Review A (Atomic, Molecular, and Optical Physics)*, 64(1): 13409–13413, June 2001.

[24] Misha Yu. Ivanov, Michael Spanner, and Olga Smirnova. Anatomy of strong field ionization. *J. Mod. Op.*, 52(2-3):165–184, 2005.

[25] George B. Arfken and Hans J. Weber. *Mathematical Methods for Physicists, Sixth Edition: A Comprehensive Guide*. Academic Press, 2005. 1200 pp.

[26] L V Keldysh. Ionization in the field of a strong electromagnetic wave. *JETP*, 20(5): 1307–1314, 1965.

[27] V S Popov. Tunnel and multiphoton ionization of atoms and ions in a strong laser field (Keldysh theory). *Physics-Uspekhi*, 47(9):855–885, 2004.

[28] V S Popov, V P Kuzentsov, and A M Perelomov. Quasiclassical approximation for nonstationary problems. *JETP*, 26(1):222, 68.

[29] V S Popov. Imaginary-time method in quantum mechanics and field theory. *Physics of Atomic Nuclei*, 68(4):686–708, 2005.

[30] V S Popov. Imaginary Time Method and Its Application to Quantum Theory, 2005.

[31] V S Popov. "The Imaginary Time" in Quantum Physics, 2004.

[32] R. Kopold, W. Becker, and D. B. Milosevic. Quantum orbits: a space-time picture of intense-laser-induced processes in atoms. *Journal of Modern Optics*, 49(12):1987–1999, October 2002.

[33] P Salières, B Carré, L Le Déroff, F Grasbon, G G Paulus, H Walther, R Kopold, W Becker, D B Milosević, A Sanpera, and M Lewenstein. Feynman's path-integral approach for intense-laser-atom interactions. *Science (New York, N.Y.)*, 292(5518): 902–5, May 2001.

[34] Olga Smirnova, Michael Spanner, and Misha Yu. Ivanov. Analytical solutions for strong field-driven atomic and molecular one- and two-electron continua and applications to strong-field problems. *Physical Review A (Atomic, Molecular, and Optical Physics)*, 77(3):33407–33434, 2008.

[35] S V Popruzhenko, G G Paulus, and D Bauer. Coulomb-corrected quantum trajectories in strong-field ionization. *Physical Review A (Atomic, Molecular, and Optical Physics)*, 77(5):53409–53416, 2008.

[36] L D Landau and E M Lifshitz. *Mechanics*, volume 1 of *Course of Theoretical Physics*. Butterworth Heinemann, Oxford, 3 edition, 1960. ISBN 7506242559.

[37] M V Ammosov, N B Delone, and V P Krainov. Tunnel ionization of complex atoms and atomic ions in an alternating electromagnetic field. *JETP*, 91(6):2008–20013, December 1986.

[38] Paul B Corkum. Plasma Perspective on Strong-Field Multiphoton Ionization. *Physical Review Letters*, 71(13):1994–1997, September 1993.

[39] Jeffery L Krause, Kenneth J Schafer, and Kenneth C Kulander. High-Order Harmonic Generation from Atoms and Ions in the High Intensity Regime. *Physical Review Letters*, 68(24), 1992.

[40] M Lewenstein, P Balcou, Misha Yu. Ivanov, A L'Huillier, and Paul B Corkum. Theory of high-harmonic generation by low-frequency laser fields. *Physical Review A (Atomic, Molecular, and Optical Physics)*, 49(3):2117–2132, March 1994.

[41] Ferenc Krausz and Misha Ivanov. Attosecond physics. *Reviews of Modern Physics*, 81(1):163–234, February 2009.

[42] Denys I Bondar. Instantaneous multiphoton ionization rate and initial distribution of electron momentum. *Physical Review A (Atomic, Molecular, and Optical Physics)*, 78(1):15405, 2008.

[43] Farhad H M Faisal. Multiple absorption of laser photons by atoms. *Journal of Physics B: Atomic and Molecular Physics*, 6(4):L89—-L92, 1973.

[44] H R Reiss. Effect of an intense electromagnetic field on a weakly bound system. *Phys. Rev. A*, 22(5):1786–1813, November 1980.

[45] A Becker and Farhad H M Faisal. Intense-field many-body S-matrix theory. *J. Phys. B*, 38(3):R1—-R56, February 2005.

[46] C Smeenk, L Arissian, A Staudte, D M Villeneuve, and P B Corkum. Momentum space tomographic imaging of photoelectrons. *Journal of Physics B: Atomic, Molecular and Optical Physics*, 42(18):185402 (5p), 2009.

[47] A Rudenko, K Zrost, C D Schröter, V L B de Jesus, B Feuerstein, R Moshammer, and J Ullrich. Resonant structures in the low-energy electron continuum for single ionization of atoms in the tunnelling regime. *Journal of Physics B: Atomic, Molecular and Optical Physics*, 37(24):L407—-L413, 2004.

[48] A S Alnaser, C M Maharjan, P Wang, and I V Litvinyuk. Multi-photon resonant effects in strong-field ionization: origin of the dip in experimental longitudinal momentum distributions. *Journal of Physics B: Atomic, Molecular and Optical Physics*, 39(17):L323—-L328, 2006.

[49] Ilya I Fabrikant and Gordon A Gallup. Semiclassical propagation method for tunneling ionization. *Physical Review A (Atomic, Molecular, and Optical Physics)*, 79 (1):13406, 2009.

[50] E Wells, Merrick J DeWitt, and R R Jones. Comparison of intense-field ionization of diatomic molecules and rare-gas atoms. *Phys. Rev. A*, 66(1):13409, July 2002.

[51] Merrick J DeWitt, E Wells, and R R Jones. Ratiometric Comparison of Intense Field Ionization of Atoms and Diatomic Molecules. *Phys. Rev. Lett.*, 87(15):153001, September 2001.

[52] C Guo, M Li, J P Nibarger, and G N Gibson. Single and double ionization of diatomic molecules in strong laser fields. *Phys. Rev. A*, 58(6):R4271—-R4274, December 1998.

[53] A Talebpour, C-Y. Chien, and S L Chin. The effects of dissociative recombination in multiphoton ionization of. *Journal of Physics B: Atomic, Molecular and Optical Physics*, 29(18):L677—-L680, 1996.

[54] Vladimir I Usachenko, Pavel E Pyak, and Vyacheslav V Kim. Comparative study of strong-field ionization in laser-irradiated F and other diatomic molecules: Density-functional-theory-based molecular strong-field approximation. *Physical Review A (Atomic, Molecular, and Optical Physics)*, 79(2):23415, 2009.

[55] X M Tong, Z X Zhao, and C D Lin. Theory of molecular tunneling ionization. *Phys. Rev. A*, 66(3):33402, September 2002.

[56] J Muth-Böhm and A Becker. Suppressed Molecular Ionization for a Class of Diatomics in Intense Femtosecond Laser Fields. *Phys. Rev. Lett.*, 85(11):2280–2283, September 2000.

[57] Vinod Kumarappan, Lotte Holmegaard, Christian Martiny, Christian B Madsen, Thomas K Kjeldsen, Simon S Viftrup, Lars Bojer Madsen, and Henrik Stapelfeldt. Multiphoton Electron Angular Distributions from Laser-Aligned CS Molecules. *Physical Review Letters*, 100(9):93006, 2008.

[58] I V Litvinyuk, Kevin F Lee, P W Dooley, D M Rayner, D M Villeneuve, and Paul B Corkum. Alignment-Dependent Strong Field Ionization of Molecules. *Phys. Rev. Lett.*, 90(23):233003, June 2003.

[59] D Pavicic, Kevin F Lee, D M Rayner, Paul B Corkum, and D M Villeneuve. Direct Measurement of the Angular Dependence of Ionization for N, O, and CO in Intense Laser Fields. *Physical Review Letters*, 98(24):243001, 2007.

[60] Andre Staudte, S Patchkovskii, D Pavicic, H Akagi, Olga Smirnova, D Zeidler, M Meckel, D M Villeneuve, R Dörner, Yu M Ivanov, and Paul B Corkum. Angular Tunneling Ionization Probability of Fixed-in-Space H Molecules in Intense Laser Pulses. *Physical Review Letters*, 102(3):33004, 2009.

[61] Manohar Awasthi and Alejandro Saenz. Internuclear-distance dependence of ionization of H2 in strong laser fields. *Journal of Physics B: Atomic, Molecular and Optical Physics*, 39(13):S389—-S395, 2006.

[62] Yulian V Vanne and Alejandro Saenz. Ionisation of H2 in intense ultrashort laser pulses: parallel versus perpendicular orientation. *Journal of Modern Optics*, 55(16): 2665–2684, September 2008.

[63] Michael Spanner and Serguei Patchkovskii. One-electron ionization of multielectron systems in strong nonresonant laser fields. *Physical Review A*, 80(6):063411, December 2009.

[64] Simon Petretti, Yulian V. Vanne, Alejandro Saenz, and Piero Decleva. Alignment-dependent ionization of n2, o2, and co2 in intense laser fields. *Physical Review Letters*, 104(22), June 2010.

[65] M Abu-samha and L B Madsen. Theory of strong-field ionization of aligned CO. *Physical Review A (Atomic, Molecular, and Optical Physics)*, 80(2):23401, 2009.

[66] Gordon A. Gallup and Ilya I. Fabrikant. Semiclassical complex-time method for tunneling ionization: Molecular suppression and orientational dependence. *Physical Review A*, 81(3):033417, March 2010.

[67] Olga Smirnova, Yann Mairesse, Serguei Patchkovskii, Nirit Dudovich, David Villeneuve, Paul Corkum, and Misha Yu Ivanov. High harmonic interferometry of multi-electron dynamics in molecules. *Nature*, 460(7258):972–7, August 2009.

[68] Olga Smirnova, Serguei Patchkovskii, Yann Mairesse, Nirit Dudovich, and Misha Yu Ivanov. Strong-field control and spectroscopy of attosecond electron-hole dynamics in molecules. *Proceedings of the National Academy of Sciences of the United States of America*, 106(39):16556–61, September 2009.

[69] Y. Mairesse, J. Higuet, N. Dudovich, D. Shafir, B. Fabre, E. Mével, E. Constant, S. Patchkovskii, Z. Walters, M. Yu. Ivanov, and O. Smirnova. High Harmonic Spectroscopy of Multichannel Dynamics in Strong-Field Ionization. *Physical Review Letters*, 104(21), May 2010.

[70] Anh-Thu Le, R R Lucchese, and C D Lin. Uncovering multiple orbitals influence in high harmonic generation from aligned N2. *Journal of Physics B: Atomic, Molecular and Optical Physics*, 42(21):211001 (5p), 2009.

[71] S. Haessler, J. Caillat, W. Boutu, C. Giovanetti-Teixeira, T. Ruchon, T. Auguste, Z. Diveki, P. Breger, A. Maquet, B. Carré, R. Taïeb, and P. Salières. Attosecond imaging of molecular electronic wavepackets. *Nature Physics*, 6(3):200–206, January 2010.

[72] Ryan Murray, Wing-Ki Liu, and Misha Yu. Ivanov. Partial Fourier-transform approach to tunnel ionization: Atomic systems. *Physical Review A*, 81(2):023413, February 2010.

[73] A A Radzig and B M Smirnov. *Reference Data on Atoms, Molecules, and Ions*. Springer-Verlag: Berlin, Heidelberg, New York, Toronto, 1985.

[74] M Meckel, D Comtois, D Zeidler, Andre Staudte, D Pavicic, H C. Bandulet, H Pepin, J C Kieffer, Reinhard Dorner, D M Villeneuve, and Paul B Corkum. Laser-Induced Electron Tunneling and Diffraction. *Science*, 320(5882):1478–1482, 2008.

[75] F. Faisal. S-matrix theory of high harmonic generation and ionization of coherently ro-vibrating linear molecules by intense ultrashort laser pulses, 2010. ISSN 1432-881X. URL `http://www.springerlink.com/content/c43740937t086458/`.

[76] Simon Petretti, Yulian V. Vanne, Alejandro Saenz, and Piero Decleva. Alignment-dependent ionization of n2, o2, and co2 in intense laser fields. *Physical Review Letters*, 104(22), June 2010.

[77] Serguei Patchkovskii, Zengxiu Zhao, Thomas Brabec, and D M Villeneuve. High harmonic generation and molecular orbital tomography in multielectron systems. *The Journal of Chemical Physics*, 126(11):114306, 2007.

[78] Rick A. Kendall, Thom H. Dunning, and Robert J. Harrison. Electron affinities of the first-row atoms revisited. Systematic basis sets and wave functions. *The Journal of Chemical Physics*, 96(9):6796, 1992. ISSN 00219606. URL `http://link.aip.org/link/JCPSA6/v96/i9/p6796/s1/html`.

[79] Thom H. Dunning. Gaussian basis sets for use in correlated molecular calculations. I. The atoms boron through neon and hydrogen. *The Journal of Chemical Physics*, 90(2):1007, 1989. ISSN 00219606. URL `http://link.aip.org/link/JCPSA6/v90/i2/p1007/s1/html`.

[80] Zachary B Walters and Olga Smirnova. Attosecond correlation dynamics during electron tunnelling from molecules. *Journal of Physics B: Atomic, Molecular and Optical Physics*, 43(16):161002, August 2010. ISSN 0953-4075. URL `http://stacks.iop.org/0953-4075/43/i=16/a=161002`.

[81] M Y Kuchiev. Atomic Antenna. *JETP Letters*, 45(7):404–406, 1987.

[82] High Harmonic Generation - Wikipedia, the free encyclopedia. URL `http://en.wikipedia.org/wiki/High\_Harmonic\_Generation`.

[83] N B Delone and Vladimir P Krainov. *Atoms in Strong Light Fields*, volume 28 of *Springer series in chemical physics*. Springer, 1985. ISBN 0387124128.

[84] J Itatani, F Quere, Gennady L Yudin, Misha Yu. Ivanov, Ferenc Krausz, and Paul B Corkum. Attosecond Streak Camera. *Physical Review Letters*, 88(17):173903, April 2002.

[85] M Hentschel, R Kienberger, Ch. Spielmann, G A Reider, N Milosevic, T Brabec, P Corkum, U Heinzmann, M Drescher, and F Krausz. Attosecond metrology. *Nature*, 414(6863):509–513, November 2001.

[86] R Kienberger, E Goulielmakis, M Uiberacker, Andrius Baltuska, V S Yakovlev, F Bammer, Armin Scrinzi, Th Westerwalbesloh, U Kleineberg, U Heinzmann, M Drescher, and Ferenc Krausz. Atomic transient recorder. *Nature*, 427(26):817, February 2004.

[87] M Schultze, E Goulielmakis, M Uiberacker, M Hofstetter, J Kim, D Kim, F Krausz, and U Kleineberg. Powerful 170-attosecond XUV pulses generated with few-cycle laser pulses and broadband multilayer optics. *New Journal of Physics*, 9(7):243, 2007.

[88] Markus Drescher, Michael Hentschel, Reinhard Kienberger, Gabriel Tempea, Christian Spielmann, Georg A Reider, Paul B Corkum, and Ferenc Krausz. X-ray Pulses Approaching the Attosecond Frontier. *Science*, 291(5510):1923–1927, March 2001.

[89] Petrissa Eckle, Mathias Smolarski, Philip Schlup, Jens Biegert, Andre Staudte, M Schoffler, H G Muller, Reinhard Dorner, and Ursula Keller. Attosecond angular streaking. *Nat Phys*, 4(7):565–570, July 2008.

[90] M. Schultze, M. Fiess, N. Karpowicz, J. Gagnon, M. Korbman, M. Hofstetter, S. Neppl, A. L. Cavalieri, Y. Komninos, T. Mercouris, C. A. Nicolaides, R. Pazourek, S. Nagele, J. Feist, J. Burgdorfer, A. M. Azzeer, R. Ernstorfer, R. Kienberger, U. Kleineberg, E. Goulielmakis, F. Krausz, and V. S. Yakovlev. Delay in Photoemission. *Science*, 328(5986):1658–1662, June 2010.

[91] A L Cavalieri, N Müller, Th Uphues, V S Yakovlev, A Baltuska, B Horvath, B Schmidt, L Blümel, R Holzwarth, S Hendel, M Drescher, U Kleineberg, P M Echenique, R Kienberger, F Krausz, and U Heinzmann. Attosecond spectroscopy in condensed matter. *Nature*, 449(7165):1029–32, October 2007.

[92] Eleftherios Goulielmakis, Zhi-Heng Loh, Adrian Wirth, Robin Santra, Nina Rohringer, Vladislav S. Yakovlev, Sergey Zherebtsov, Thomas Pfeifer, Abdallah M. Azzeer, Matthias F. Kling, Stephen R. Leone, and Ferenc Krausz. Real-time observation of valence electron motion. *Nature*, 466(7307):739–743, August 2010.

[93] J Itatani, J Levesque, D Zeidler, Hiromichi Niikura, H Pepin, J C Kieffer, Paul B Corkum, and Villeneuve D M. Tomographic imaging of molecular orbitals. *Nature*, 432:867, 2004.

[94] Manfred Lein, P P Corso, Jon P Marangos, and P L Knight. Orientation dependence of high-order harmonic generation in molecules. *Physical Review A (Atomic, Molecular, and Optical Physics)*, 67(2):23819–23825, February 2003.

[95] Manfred Lein, N Hay, R Velotta, Jon P Marangos, and P L Knight. Role of the Intramolecular Phase in High-Harmonic Generation. *Physical Review Letters*, 88 (18):183903–183907, April 2002.

[96] N Hay, M Lein, R Velotta, R De Nalda, E Heesel, M Castillejo, P L Knight, and Jon P Marangos. Investigations of electron wave-packet dynamics and high-order harmonic generation in laser-aligned molecules. *Journal of Modern Optics*, 50(3-4): 561–577, January 2003.

[97] Olga Smirnova, A S Mouritzen, S Patchkovskii, and Misha Yu. Ivanov. Coulomb-laser coupling in strong-field assisted photoeffect and molecular tomography. *J. Phys. B*, 40:F197—-F206, June 2007.

[98] Olga Smirnova, Yann Mairesse, Serguei Patchkovskii, Nirit Dudovich, David Villeneuve, Paul Corkum, and Misha Yu Ivanov. High harmonic interferometry of multi-electron dynamics in molecules. *Nature*, 460(7258):972–7, August 2009.

[99] Olga Smirnova, Michael Spanner, and Misha Yu. Ivanov. Coulomb and polarization effects in sub-cycle dynamics of strong-field ionization. *Journal of Physics B: Atomic, Molecular and Optical Physics*, 39(13):S307—-S321, 2006.

[100] Olga Smirnova, Serguei Patchkovskii, Yann Mairesse, Nirit Dudovich, and Misha Yu Ivanov. Strong-field control and spectroscopy of attosecond electron-hole dynamics in molecules. *Proceedings of the National Academy of Sciences of the United States of America*, 106(39):16556–61, September 2009.

[101] Y. Mairesse, J. Higuet, N. Dudovich, D. Shafir, B. Fabre, E. Mével, E. Constant, S. Patchkovskii, Z. Walters, M. Yu. Ivanov, and Olga Smirnova. High Harmonic Spectroscopy of Multichannel Dynamics in Strong-Field Ionization. *Physical Review Letters*, 104(21), May 2010.

[102] C. Vozzi, F. Calegari, E. Benedetti, J.-P. Caumes, G. Sansone, S. Stagira, M. Nisoli, R. Torres, E. Heesel, N. Kajumba, J. Marangos, C. Altucci, and R. Velotta. Controlling Two-Center Interference in Molecular High Harmonic Generation. *Physical Review Letters*, 95(15), October 2005.

[103] Tsuneto Kanai, Shinichirou Minemoto, and Hirofumi Sakai. Quantum interference during high-order harmonic generation from aligned molecules. *Nature*, 435(7041): 470–4, May 2005.

[104] R. Torres, T. Siegel, L. Brugnera, I. Procino, Jonathan G. Underwood, C. Altucci, R. Velotta, E. Springate, C. Froud, I. C. E. Turcu, S. Patchkovskii, M. Yu. Ivanov, O. Smirnova, and J. P. Marangos. Revealing molecular structure and dynamics through high-order harmonic generation driven by mid-IR fields. *Physical Review A*, 81(5), May 2010.

[105] H. Wörner, J. Bertrand, P. Corkum, and D. Villeneuve. High-Harmonic Homodyne Detection of the Ultrafast Dissociation of Br2 Molecules. *Physical Review Letters*, 105(10), September 2010.

[106] V V Suran and I P Zapesochnyi. Observation of Sr2+ in multiple-photon ionization of strontium. *Sov. Tech. Phys. Lett.*, 1(11):420, 1975.

[107] A. L'Huillier, L. Lompre, G. Mainfray, and C. Manus. Multiply Charged Ions Formed by Multiphoton Absorption Processes in the Continuum. *Physical Review Letters*, 48(26):1814–1817, June 1982.

[108] B. Walker, B. Sheehy, L. DiMauro, P. Agostini, K. Schafer, and K. Kulander. Precision Measurement of Strong Field Double Ionization of Helium. *Physical Review Letters*, 73(9):1227–1230, August 1994.

[109] J Ullrich, R Moshammer, A Dorn, R D rner, L Ph H Schmidt, and H Schmidt-B cking. Recoil-ion and electron momentum spectroscopy: reaction-microscopes. *Reports on Progress in Physics*, 66(9):1463–1545, September 2003.

[110] Denys I Bondar, Wing-Ki Liu, and Misha Yu. Ivanov. Two-electron ionization in strong laser fields below intensity threshold: Signatures of attosecond timing in correlated spectra. *Physical Review A (Atomic, Molecular, and Optical Physics)*, 79(2): 23417, 2009.

[111] Jason R Dwyer, Robert E Jordan, Christoph T Hebeisen, Maher Harb, Ralph Ernstorfer, Thibault Dartigalongue, and R J Dwayne Miller. Femtosecond electron diffraction: an atomic perspective of condensed phase dynamics. *J. Mod. Op.*, 54(7): 905–922, May 2007.

[112] Hyotcherl Ihee, Vladimir A Lobastov, Udo M Gomez, Boyd M Goodson, Ramesh Srinivasan, Chong-Yu Ruan, and Ahmed H Zewail. Direct Imaging of Transient Molecular Structures with Ultrafast Diffraction. *Science*, 291(5503):458–462, 2001.

[113] Tony Zou, A D Bandrauk, and Paul B Corkum. Laser-induced ellectron diffraction: a new tool for probing ultrafast molecular dynamics. *Chemical Physics Letters*, 259: 313–320, September 1996.

[114] Michael Spanner, Olga Smirnova, Paul B Corkum, and Misha Yu. Ivanov. Reading diffraction images in strong field ionization of diatomic molecules. *J. Phys. B*, 37: L243—-L250, 2004.

[115] S N Yurchenko, S Patchkovskii, I V Litvinyuk, Paul B Corkum, and Gennady L Yudin. Laser-Induced Interference, Focusing, and Diffraction of Rescattering Molecular Photoelectrons. *Phys. Rev. Lett.*, 93(22):223003–223007, November 2004.

[116] S X Hu and L A Collins. Imaging Molecular Structures by Electron Diffraction Using an Intense Few-Cycle Pulse. *Physical Review Letters*, 94(7):73004–73008, 2005.

[117] A M Popov, O V Tikhonova, and E A Volkova. Electron-diffraction imaging of nuclear dynamics in molecules. *J. Mod. Op.*, 54(7):1087–1097, May 2007.

[118] Xinhua Xie, Gerald Jordan, Marlene Wickenhauser, and Armin Scrinzi. Time and momentum distributions of rescattering electrons. *J. Mod. Op.*, 54(7):999–1010, May 2007.

[119] C C Chirila and Manfred Lein. Effect of dressing on high-order harmonic generation in vibrating H molecules. *Physical Review A (Atomic, Molecular, and Optical Physics)*, 77(4):43403, 2008.

[120] Misha Yu. Ivanov and Jon P Marangos. Time-resolved imaging of atomic-scale electron and nuclear dynamics. *J. Mod. Op.*, 54(7):899, May 2007.

[121] Zhangjin Chen, Toru Morishita, Anh-Thu Le, and C D Lin. Analysis of two-dimensional high-energy photoelectron momentum distributions in the single ionization of atoms by intense laser pulses. *Physical Review A (Atomic, Molecular, and Optical Physics)*, 76(4):43402–43412, 2007.

[122] Thomas Brabec, Misha Yu. Ivanov, and Paul B Corkum. Coulomb focusing in intense field atomic processes. *Phys. Rev. A*, 54(4):R2551—-R2554, October 1996.

[123] Gennady L Yudin and Misha Yu. Ivanov. Physics of correlated double ionization of atoms in intense laser fields: Quasistatic tunneling limit. *Physical Review A (Atomic, Molecular, and Optical Physics)*, 63(3):33404–33428, February 2001.

[124] Ryan Murray and Misha Yu. Ivanov. Two-color control of laser induced electron diffraction. *Journal of Modern Optics*, 55(16):2513–2525, 2008.

[125] Markus Kitzler and Matthias Lezius. Spatial Control of Recollision Wave Packets with Attosecond Precision. *Physical Review Letters*, 95:253001, 2005.

[126] Markus Kitzler, Kevin O'Keeffe, and Matthias Lezius. Attosecond control of electronic motion using light wave synthesis. *J. Mod. Op.*, 53:1, 2006.

[127] Markus Kitzler, Xinhua Xie, Armin Scrinzi, and Andrius Baltuska. Optical attosecond mapping by polarization selective detection. *Physical Review A (Atomic, Molecular, and Optical Physics)*, 76:11801, 2007.

[128] J Mauritsson, P Johnsson, E Gustafsson, A L'Huillier, K J Schafer, and M B Gaarde. Attosecond Pulse Train Generated Using Two Color Laser Fields. *Physical Review Letters*, 97:13001, 2006.

[129] I J Sola, Zair A., R Lopez-Martens, P Johnsson, K Varj, E Cormier, J Mauritsson, A L'Huillier, V Strelkov, E Mevel, and E Constant. Temporal and spectral studies of high-order harmonics generated by polarization-modulated infrared fields. *Physical Review A (Atomic, Molecular, and Optical Physics)*, 74(1):13810, 2006.

[130] I J Sola, E Mevel, L Elouga, E Constant, V Strelkov, L Poletto, P Villoresi, E Bendetti, J.-P. Caumes, S Stagria, C Vozzi, G Sansone, and M Nisoli. Controlling attosecond electron dynamics by phase-stabilized polarization gating. *Nature Physics*, 2:319, 2006.

[131] M Okunishi, Toru Morishita, G Prümper, K Shimada, C D Lin, S Watanabe, and K Ueda. Experimental Retrieval of Target Structure Information from Laser-Induced Rescattered Photoelectron Momentum Distributions. *Physical Review Letters*, 100 (14):143001, 2008.

[132] N B Delone and Vladimir P Krainov. Energy and angular electron spectra for the tunnel ionization of atoms by strong low-frequency radiation. *Journal of the Optical Society of America*, 8(6):1207–1211, June 1991.

[133] Michael Spanner and Paul Brumer. Entanglement and timing-based mechanisms in the coherent control of scattering processes. *Physical Review A (Atomic, Molecular, and Optical Physics)*, 76(1):13408–13418, July 2007.

[134] D B Milosevic, G G Paulus, and Wilhelm Becker. Ionization by few-cycle pulses: Tracing the electron orbits. *Physical Review A (Atomic, Molecular, and Optical Physics)*, 71(6):61404–61408, June 2005.

[135] Camilo Ruiz-Mendez. qfishbowl.

[136] D B Milošević, G G Paulus, D Bauer, and W Becker. Above-threshold ionization by few-cycle pulses. *Journal of Physics B: Atomic, Molecular and Optical Physics*, 39 (14):R203–R262, July 2006.

[137] Y Mairesse, N Dudovich, J Levesque, Misha Yu. Ivanov, Paul B Corkum, and D M Villeneuve. Electron wavepacket control with elliptically polarized laser light in high harmonic generation from aligned molecules. *New Journal of Physics*, 10(2):25015, 2008.

[138] D Comtois, D Zeidler, H Pépin, J C Kieffer, D M Villeneuve, and P B Corkum. Observation of Coulomb focusing in tunnelling ionization of noble gases. *Journal of Physics B: Atomic, Molecular and Optical Physics*, 38(12):1923–1933, June 2005.

[139] Zhangjin Chen, Anh-Thu Le, Toru Morishita, and C. Lin. Quantitative rescattering theory for laser-induced high-energy plateau photoelectron spectra. *Physical Review A*, 79(3):033409, March 2009.

[140] N Dudovich, Olga Smirnova, J Levesque, Y Mairesse, Misha Yu. Ivanov, D M Villeneuve, and Paul B Corkum. Measuring and controlling the birth of attosecond XUV pulses. *Nat Phys*, 2(11):781–786, November 2006.